

IMPACT OF PROCESSING PARAMETERS ON CONDUCTIVE  
POLYMER ELECTROACTIVITY

by

Jacob Benjamin Frazer, B.S.

A thesis submitted to the Graduate Council of  
Texas State University in partial fulfillment  
of the requirements for the degree of  
Master of Science  
with a Major in Chemistry  
May 2018

Committee Members:

Jennifer Irvin, Chair

Tania Betancourt

Chang Ji

**COPYRIGHT**

by

Jacob Benjamin Frazer

2018

## **FAIR USE AND AUTHOR'S PERMISSION STATEMENT**

### **Fair Use**

This work is protected by the Copyright Laws of the United States (Public Law 94-553, section 107). Consistent with fair use as defined in the Copyright Laws, brief quotations from this material are allowed with proper acknowledgment. Use of this material for financial gain without the author's express written permission is not allowed.

### **Duplication Permission**

As the copyright holder of this work I, Jacob Frazer, refuse permission to copy in excess of the "Fair Use" exemption without my written permission.

## **DEDICATION**

To my mother and father

## ACKNOWLEDGEMENTS

If I was to include all of those who have helped me during the course of this project this section would surely be the length of this manuscript. That aside, without the seemingly endless patient guidance from my research advisor Dr. Jennifer Irvin this project would have quickly ended. Like other lab members, I came into the Irvin Research Group with limited experience. She took me in and helped me grow as a person and scientist. The other members of my committee: Dr. Chang Ji and Dr. Tania Betancourt have been crucial to my progress and completion of this work. Dr. Ji was always very kind and often lent advice on electrochemical experiment design and provided his gas-chromatography/mass spectrometry expertise during the synthetic aspects of these experiments. Dr. Betancourt's willingness to give access to her resources that include: her lab space, water purification system, UV-Vis, optical microscope, and micropipettes were all absolutely essential to my experiments. She also aided me in many of my experimental procedures, and was always patient with my constant inquisitive nature. I want to give thanks to Dr. William Brittain for his mentorship and belief in me as a researcher. He was also pivotal in my project by giving me the use of his goniometer for contact angle measurements.

The faculty and staff in the Texas State Chemistry & Biochemistry department are nothing short of exemplary. I have spoken to almost all of them, and each one in their own way has guided me since my start as an undergraduate chemistry major. Approaching graduation Dr. Christopher Dorsey encouraged me to enter the Masters

program. Without his nudge I would likely not be here. I would like to thank Dr. Christopher Rhodes for his kind and helpful guidance with my project. His creative insights and confidence in my abilities I will never forget. Dr. Ben Martin is a motivating professor and very caring person who pushed me to be a better scientific writer. His insights into my project were also very useful. Dr. Ben Shoulders is an amazing individual with endless wisdom. I am grateful for having met him. Dr. Streusand for his time to talk about pursuits after my time here at Texas State. Dr. Beall for our intriguing conversations. Al Martinez, thank you for all the time and effort you have put into our lab and department. I appreciate you showing me how to be more mechanically inclined. I would like to thank Dr. Alex Zakhidov for the use of his plasma etcher, and helpful advice during my experiments.

It was once said that in science we always are “standing on the shoulders of giants”. I am not an exception to this rule as countless hours of work have gone into the development of this project by my lab-mates before me. I am in great debt to my dear friends Zack Iszard, Joe Garcia, and Sothavy Vong. Zack and Joe are responsible for the synthesis of poly(ProDOT-Bu<sub>2</sub>), and Sothavy for poly(3-hexylthiophene). Zack also was my mentor coming into the Irvin Research Group. Many of his brilliant ideas live on in this work. I would like to thank all my group members who are very close to my heart. They are Marisa Marquez, Xu Wang, Mariana Ocampo, Steven Gralinski, and Kelli Burke. Each possess unique talents as scientists and as people. I am glad to have met all of them.

My mother and father always taught me to follow my heart no matter what happened in life. Words cannot describe how much I love them and the countless sacrifices they have made for me to be here. I thank my brother Stephen and Grace for their constant support during this part of my life. Without them, none of this would be possible. My Grandpa Niño, for our long and meaningful talks of the greater things in life. He is my inspiration, and a prime example of the true meaning of an academic. Both my Grandpa and Grandma Frazer for their love and support over the years. My Nana, you will forever be in my heart. You are an example of persistence and manifestation of love itself. For the love and support of Marissa, Travis, Alex, Grace, Dean, and Toni. You have all helped me through very challenging moments in my life. For the Bastidas and Thompson families, they took me in as their own. I love all of you so much. Keifer, you are my brother. You have helped me through so many things in life and taught me the true definition of existence. My friends Jeff, Anthony, Brad, Emily, Missy, and Ryan. Thank you to my Uncle Michael and his family. I love you Uncle Delbert. You were an amazing man and will always be remembered. To Nikki, my wife $\infty$ , may our love for each other help us grow and guide us as a “True North” even when times are tough. Tim and Terri, thank you so much for all of your selfless support and love. To the Maresch family, for unending love and support over the years.

My children are my heart. I am very excited to welcome my new beautiful baby girl Rowan Isabel Frazer into the world. To my son John (my little scientist). You are an incredible person. You are going to do amazing things. Your daddy loves you very much.

## TABLE OF CONTENTS

	<b>Page</b>
ACKNOWLEDGEMENTS .....	v
LIST OF TABLES .....	x
LIST OF FIGURES .....	xi
ABSTRACT .....	xix
CHAPTER	
1. INTRODUCTION .....	1
1.1 Overview of Conductive Polymer History .....	1
1.2 Conduction Mechanisms in Electroactive Polymers .....	2
1.3 Organic Soluble Polymers .....	12
1.4 Electroactive Polymer Film Performance Parameters .....	14
1.5 Current Techniques for Modifying Polymer Film Morphology .....	20
1.6 Benefits/Applications of Enhanced Electroactive Polymer Films .....	22
1.7 Thesis of This Work.....	23
2. MONOMER SYNTHESIS & POLYMERIZATION.....	25
2.1 Motivation for Research .....	25
2.2 Synthetic Method .....	25
2.3 Experimental .....	28
2.3.1 Materials .....	28
2.3.2 Instrumentation .....	28
2.3.3 Synthesis .....	29
2.4 Results and Discussion .....	31
2.4.1 Poly(3-hexylthiophene) identification and solubility .....	31
2.4.2 Poly(ProDOT-Bu <sub>2</sub> ) identification and solubility .....	32
2.4.3 Molecular Weight and Polydispersity Index.....	34

3. ELECTROACTIVE POLYMER MORPHOLOGY CONTROL.....	35
3.1 Motivation for Research .....	35
3.2 Background.....	35
3.3 Experimental.....	40
3.3.1 Materials .....	40
3.3.2 Surface Treatment of Indium Tin Oxide Coated Glass .....	40
3.3.3 Polymer Film Templating Methodology .....	42
3.3.4 Microscopy .....	47
3.4 Results and Discussion .....	48
3.4.1 Polymer Solution Drying Physics .....	48
3.4.2 Contact Angle Measurements .....	50
3.4.3 Investigation of Polymer Film Morphology .....	52
3.4.4 UV-Vis Analysis of Polymer Solutions and Films .....	63
4. ELECTROCHEMICAL ANALYSIS OF POLYMER FILMS .....	67
4.1 Motivation for Research .....	67
4.2 Cyclic Voltammetry Background .....	67
4.3 Theory of Immobilized Redox Centers.....	69
4.4 Electrochemical Characterization of Polymer Films .....	70
4.4.1 Experimental.....	70
4.4.2 Poly(ProDOT-Bu <sub>2</sub> ) .....	72
4.4.3 Poly(3-hexylthiophene).....	76
5. CONCLUDING REMARKS.....	84
5.1 Monomer Synthesis & Polymerization.....	84
5.2 Electroactive Polymer Morphology Control.....	85
5.3 Electrochemical Analysis of Polymer Films.....	85
5.4 Future Work/Suggested Experiments .....	87
APPENDIX.....	89
REFERENCES .....	121

## LIST OF TABLES

<b>Table</b>	<b>Page</b>
1. Conductivities of Notable Materials .....	22
2. Molecular Weight Data for P3HT and Poly(ProDOT-Bu <sub>2</sub> ).....	34
3. Solvent Systems and Drying Protocols.....	47
4. MALDI-TOF-MS Data (Poly(ProDOT-Bu <sub>2</sub> ) .....	95
5. Linear Regression Data.....	116
6. Normalized Peak Current Response Data for P3HT Experiments .....	120

## LIST OF FIGURES

Figure	Page
1. Common conducting polymers .....	1
2. Reaction scheme for the formation of the TTF-TCNQ complex.....	3
3. Crystal structure of TTF-TCNQ .....	4
4. Energy band visualization in insulators, semiconductors, and conductors.....	5
5. Illustration of the effect of conjugation on conductive polymer electronic properties .....	9
6. Visualization of doping in a conductive polymer .....	9
7. Formation of intermediate energy levels between the valence and conduction bands in doped conductive polymers .....	10
8. Illustration of soliton formation in polyacetylene.....	11
9. Polaronic excitations upon removal or addition of an electron from polythiophene .....	12
10. Oxidative polymerization mechanism of thiophene .....	13
11. Oxidative polymerization mechanism of thiophene with radical recombination mechanisms.....	15
12. Oxidative polymerization mechanism of EDOT(ethylenedioxythiophene) with radical recombination mechanisms .....	16
13. Linkages in a thiophene polymer with asymmetric monomer structure.....	17
14. Head-Head linkage of poly(3-hexlythiophene) .....	18

15. Illustration of conductive polymer film morphologies produced from various techniques .....	22
16. Grignard coupling reaction scheme .....	27
17. Structures of poly(benzimidazobenzophenanthroline) (BBL) ladder polymer & 1-ethyl-3-methyl-imidazolium bis(trifluoromethylsulfonyl)imide (EMI-BTI) ionic liquid .....	36
18. Scanning electron microscope (SEM) images of BBL polymer cast with and without ionic liquid EMI-BTI.....	37
19. Cyclic voltammogram of solution cast films created with and without EMI-BTI .....	38
20. Illustration of different polymer morphologies produced from varying the mole fraction of two different blocks in a block copolymer.....	39
21. Soft templating of conductive polymers using a high-boiling liquid .....	39
22. P3HT/chloroform solution pre and post solvation upon heating .....	43
23. Images of P3HT films templated from a 15% DMSO/chlorobenzene solution on ITO glass with different drying conditions .....	46
24. Experimental setup to enhance film drying rate .....	46
25. Images of templated polymer films .....	48
26. Marangoni flow illustration of polymer and porogen within a solution droplet on a substrate .....	50

27. Contact angle study of poly(ProDOT-Bu <sub>2</sub> )/chloroform droplets on surface treated indium-tin oxide (ITO) glass .....	51
28. Contact angle images of poly(ProDOT-Bu <sub>2</sub> )/chloroform solution on surface treated ITO glass .....	52
29. Poly(ProDOT-Bu <sub>2</sub> ) films created from five different solvent systems.....	53
30. SEM images of DMSO film morphology.....	54
31. SEM images of film overview .....	54
32. SEM image of 28% ethanolamine film with unique “leg-like” structures .....	55
33. SEM images of film cross-sections.....	55
34. SEM image of experimental control (no DMSO present during templating).....	56
35. Optical microscopy image of a 25% DMSO/P3HT film templated from CHCl <sub>3</sub> .....	56
36. SEM images of morphology relationship-(pore formation increase with increase in DMSO percentage in templating solution).....	57
37. SEM image of 0% DMSO/P3HT film failure.....	58
38. Optical microscopy of two P3HT films templated from different solvent systems.....	59
39. SEM image of a P3HT film templated from chlorobenzene (0% DMSO) with no pore formation.....	60

40. SEM images of morphology relationship-(pore formation increase at the internal region of the film with increase in DMSO percentage in templating solution) .....	60
41. SEM images of morphology relationship-(pore formation increase at the edges of the film with increase in DMSO percentage in templating solution) .....	61
42. Optical microscope image of a P3HT film templated from 32% DMSO/chlorobenzene .....	62
43. SEM image of a dramatic “pore gradient” observed in the 38% DMSO/chlorobenzene film.....	62
44. Diluted P3HT/chloroform solution UV-Vis analysis .....	63
45. UV-vis comparison of a 0.025mg/mL and 55% DMSO 0.025mg/mL P3HT/CHCl <sub>3</sub> solution. ....	64
46. UV-vis comparison of solution state P3HT and solid state draw-down film sample templated from heated and unheated solutions.....	65
47. UV-vis analysis of draw-down films templated from increasing DMSO percentage in solution .....	66
48. Experimental set-up for electrochemical analysis of film samples .....	68
49. Scan-rate dependency plot for a P3HT film templated from chloroform.....	72
50. Cyclic voltammogram of poly(ProDOT-Bu <sub>2</sub> ) films templated using three different porogens as compared to a control film prepared without a porogen .....	73

51. Image of poly(ProDOT-Bu <sub>2</sub> ) films submerged in ethanolamine.....	75
52. Comparison of cyclic voltammograms from a control film and one exposed to ethanolamine.....	76
53. Normalized peak current response for P3HT/CHCl <sub>3</sub> films with increasing amounts of DMSO at 500mV/s.....	77
54. 100 mV/s scans at different percentages of DMSO (chloroform-based solvent system).....	78
55. Peak current response of P3HT films annealed using three different experimental conditions.....	79
56. Normalized peak current response of P3HT/chlorobenzene films with increasing DMSO percentage at 500mV/s.....	80
57. Cyclic voltammogram overlay of P3HT/chlorobenzene film behavior (0-55% DMSO) at 100mV/s.....	81
58. Comparison of averaged film current response from chloroform and chlorobenzene solvent systems as a function of DMSO percentage.....	81
59. Comparison of cyclic voltammograms from two films templated from chloroform and chlorobenzene (55% DMSO) at the 100 mV/s scan rate.....	83

## LIST OF EQUATIONS

Equation	Page
1. Electrochemical equation for the formation of TTF-TCNQ (tetrathiafulvalene-tetracyanoquinodimethane) .....	3
2. Equation to find the polydispersity index of a polymer.....	31
3. Equation to find the number average molecular weight of a polymer.....	33
4. Equation to find the weight average molecular weight of a polymer .....	33
5. Equation to find the mass of porogen to be added to a templating solution.....	43
6. Equation to find the mass of polymer from a polymer stock solution.....	44
7. Randles-Sevick equation.....	69
8. Relationship of peak current response to scan rate for a surface-immobilized redox process .....	69

## LIST OF ABBREVIATIONS

Abbreviation	Description
ICP/ECP .....	Inherently/Electrically conducting polymer
EAP .....	Electrically active polymer
TTF-TCNQ .....	Charge transfer complex: (tetrathiafulvalene-tetracyanoquinodimethane)
BCS .....	(Bardeen, Cooper, Schrieffer) theory
HOMO .....	Highest occupied molecular orbital
LUMO .....	Lowest unoccupied molecular orbital
SCE .....	Saturated calomel electrode
UV-Vis .....	Ultraviolet-visible spectroscopy
EDOT .....	Monomer: 3,4-ethylenedioxythiophene
PEDOT .....	Polymer: poly(3,4-ethylenedioxythiophene)
P3HT .....	Polymer: poly(3-hexylthiophene)
XRD .....	X-ray Diffraction
DMSO .....	Dimethylsulfoxide
Poly(ProDOT-Bu <sub>2</sub> ) .....	Polymer: (poly(3,3-dibutyl-3,4-dihydro-2H-thieno[3,4-b][1,4]dioxepine))
GRIM .....	Grignard metathesis
DMF .....	Solvent: dimethylformamide



## ABSTRACT

Soft-templating techniques have been applied to organic soluble polymer systems that produce a large variety of film morphologies. Film morphology is observed to greatly influence the system's electrochemical current response. Thiophene-based conjugated systems are templated from chloroform and chlorobenzene solvent systems that are injected with a high-boiling polymer-immiscible liquid ("porogen") at varying percentages with the intent of creating a highly porous network. The porogen percentages chosen are modeled after literature co-polymeric experiments to find the most continuous pore formation (predicted to be 28-34%). Upon electrochemical analysis via cyclic voltammetry, charges that form across the polymer backbone during doping are balanced by available electrolyte ions from solution. Increased polymer surface area facilitates rapid charge balancing interactions during redox processes. Poly(3-hexylthiophene)/chlorobenzene solvent systems utilizing dimethylsulfoxide as a porogen generate the most reproducible film morphologies upon optimization of polymer solution drying rate. Films templated from this solvent system show the greatest capacitive behavior while generating the most reproducible and largest normalized current responses (400 mA/g improvement on average compared to chloroform-based solvent system templated with DMSO). The increase in electrical performance of polymer films generated from this soft-templating approach provide promise for a wide scope of applications that include environmentally friendly charge storage systems, consumer display technologies, and biomedical sensors.

# 1. INTRODUCTION

## 1.1 Overview of Conductive Polymer History

An excellent starting point when opening a discussion about conductive polymers is to acknowledge the advent of the field with the Nobel Prize winning work of Heeger, MacDiarmid, and Shirakawa on polyacetylene.<sup>1</sup> A turning point for conductive polymer research occurred with the discovery in 1977 that iodine doping of polyacetylene increased conductivity significantly.<sup>2</sup> Even though polyacetylene was an interesting window of research into the expanding field of conductive polymers, it became apparent that the material's practicality in technological applications was severely limited due to solubility and stability issues.<sup>3</sup>

The search for balance between conductivity and processability gave birth to the now well-researched polymers such as polypyrrole, polyaniline, and polythiophene. Polyheterocycles are particularly interesting due to their synthetically modifiable backbone for enhanced solubility, and increased stability in the oxidized state.<sup>4</sup> The structures of common conductive polymers are presented in Figure 1. Today, conductive polymers remain an important research area due to the need for clean energy storage materials as well as more robust chemical sensors in biomedical applications.<sup>5,6</sup>



Figure 1: Common conducting polymers

## 1.2 Conduction Mechanisms in Electroactive Polymers

Due to the diversity of the conductive polymer field, many different definitions have arisen over the years in order to describe and classify these materials. Conductive polymers have been organized into four major classes: filled polymers, ionically conductive polymers, charge transfer polymers, and intrinsically conducting or electrically active conducting polymers (ICPs/ECPs).<sup>7,4</sup> The terms ICP and ECP are often used interchangeably, but they both represent a subset of conductive polymers that are defined to be innately conductive. This is in contrast to filled polymers, which are non-conductive by nature, but are filled with conductive materials to induce conductivity. The polymers studied in this thesis are classified as ECPs.

Early work with charge-transfer salts has undoubtedly contributed to the understanding of conductive polymers. The TTF-TCNQ (tetrathiafulvalene-tetracyanoquinodimethane) complex can be used as a starting point to describe the reason conductive properties are observed in these polymeric systems. The experiments of Ferraris, Cowan, and Heeger combined the non-conductive molecules TTF and TCNQ to form an organic ionic salt capable of metallic conductivity.<sup>8</sup> The synthesis of the organic ionic salt is a straightforward mixing of equal concentrations of TTF and TCNQ to produce a greenish-black solid that can be collected via filtration techniques (Figure 2).<sup>9</sup>

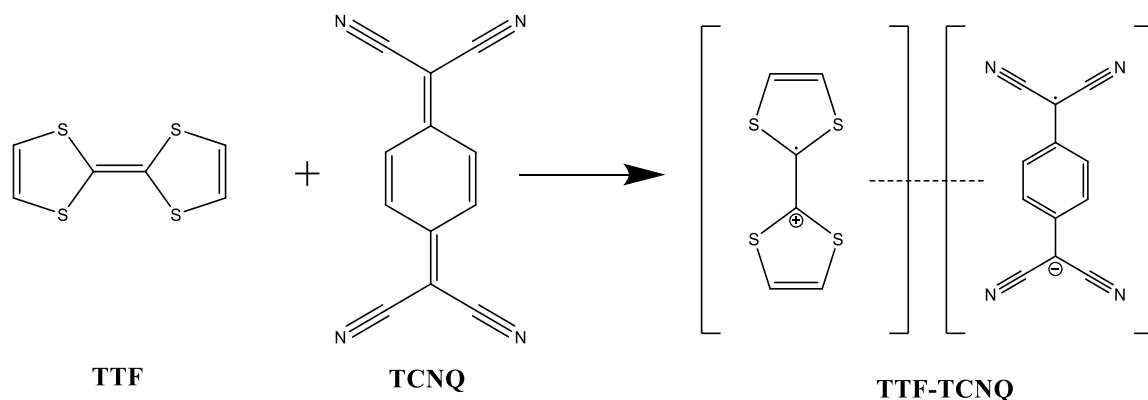
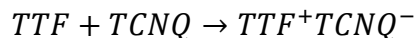


Figure 2: Reaction scheme for the formation of the TTF-TCNQ complex

The reaction of the two organic molecules involves the transfer of one electron from TTF (reducing agent) to TCNQ (oxidizing agent). This is illustrated in equation 1.<sup>9</sup>



Electron transfer at the interface of the two molecules results in the formation of two aromatically stable charged radical species that combine to form the ionic organic complex. Upon redox interactions between the two compounds the TTF radical cation and TCNQ radical anion are both found to be stable due to satisfaction of Hückel's Rule of Aromaticity.<sup>10</sup> An aromatic system allows for charge delocalization through resonance, and therefore displays conductive properties. One resonance structure of the TTF radical cation has one ring with  $6\pi$  electrons (ring with positive charge) and the other with  $7\pi$  electrons (ring with radical). The TCNQ compound forms an aromatically stable  $6\pi$  electron system. In one resonance structure, the negatively charged TCNQ compound has a radical and lone pair of electrons segregated to the benzylic carbon positions of the molecule.

Upon formation of the organic ionic salt, the charged TTF and TCNQ molecules stack into alternating columnar patterns within the crystal structure shown in Figure 3.<sup>9</sup>

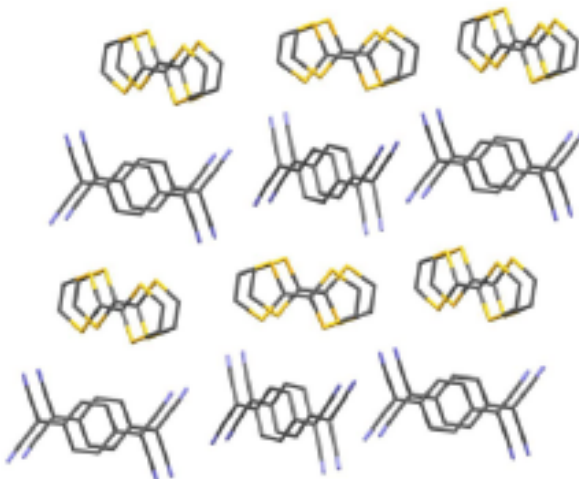


Figure 3: Crystal structure of TTF-TCNQ. Carbon = grey, sulfur = yellow, nitrogen = blue

It has been demonstrated that upon columnar stacking of charged TTF and TCNQ the  $\pi$ -orbital overlap between adjacent molecules primarily occurs in a single dimension in the crystal structure. This results in the delocalization of charges along one vector in the crystal structure.<sup>11</sup>

In order to give contextual understanding to the discovery and importance of the TTF-TCNQ complex, a fundamental understanding of conduction in common materials is needed. Materials can be described as insulators, conductors, or semi-conductors. When two atoms are bonded, their atomic orbitals merge to form molecular orbitals (bonding and anti-bonding). In a bulk solid, there are a large number of atoms that bond together to form molecular orbitals with discrete energy levels. As the number of molecular orbitals increases with the number of bonding atoms in a bulk material, the energy levels of the discrete molecular orbitals are spaced very closely together. Ultimately, the energy levels are so close they are said to form energy “bands”. In a bulk

material the bonding of atoms form two energy bands called the valance and conduction bands. These energy bands can help describe the physical and chemical properties of insulating, conducting, and semi-conducting materials (namely electrical conduction). In an insulator, energy bands are separated by a generally larger gap relative to semiconductors and conductors.<sup>12</sup> A good comparison is between the insulator soda-lime borosilicate glass, and the semiconductor silicon ( $\approx 2.6 > 1.1$  eV respectively).<sup>13,14</sup> In conductors such as metals, the valence band and conduction band energies overlap (Figure 4).

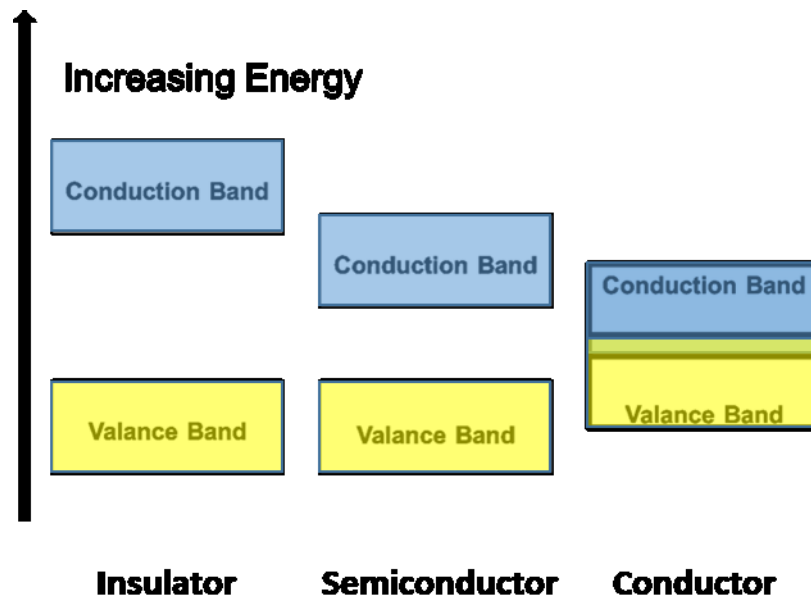


Figure 4: Energy band visualization in insulators, semiconductors, and conductors

In conductors, there are more electrons available for conduction due to the fact the conduction and valance bands overlap. Conversely, for semiconducting materials the Fermi-energy (maximum energy of an electron at 0k) is farther away from the conduction band implying that there are less electrons available for conduction. Inorganic semi-conductors are often doped with electron rich or electron poor materials that alter the

band gap energy. Upon doping, the material can acquire a more insulating or conducting nature. This is due to changes in the density of electronic states within the band gap of the material. In an N-doping semiconductor (addition of an electron-rich dopant) this can reduce the amount of energy required to promote electrons from the valence band to the conduction band increasing the number of free electrons for conduction. This is due to the formation of intermediate energy states close to the conduction band within the band gap of the material.<sup>15</sup>

Superconductivity was a heavily researched topic in the 1900s due to the discovery of mercury's temperature dependent electrical conductivity.<sup>16</sup> Electrical resistivity can be described as the opposition of charge movement within a material. The SI-unit (international system of units) is the Ohm-meter ( $\Omega\text{m}$ ). Consequently, conductivity is the product of reciprocal resistivity given as Siemens per meter (S/m), and can be describe as the ability of a material to allow for charge flow.<sup>4</sup> Superconductivity can be defined as a material's potential to conduct electricity without energy loss. This superconductive transition is induced by a phase transition at a specific temperature in the material called the critical temperature (critical temperature = resistivity of metal drops to zero). Mercury's critical temperature is 4.154 K for the alpha allotrope.<sup>17</sup> This superconducting transition is characterized by the Meissner Effect. As a material is cooled below its critical temperature it excludes magnetic fields within its interior. This is in contrast to perfect diamagnetism, in which a perfect transition to zero resistance occurs with no change in the material's magnetic field.<sup>18</sup>

In discovering mercury's superconductive transition, the question arose as to whether or not superconductivity is possible in organic materials. One of the projected

benefits of an organic superconductor was the possibility of room temperature superconductivity, and eliminating costly liquid helium required for most known existing superconductors.<sup>16</sup> Those materials were postulated to be compounds that displayed certain structural characteristics such as aromaticity.<sup>19</sup> One of those compounds heavily researched was the mentioned TTF-TCNQ complex. The argument for a room temperature superconducting transition was built off the newly developed BCS (Bardeen, Cooper, Schrieffer) theory and the 1-dimensional predicted Peierls electronic system. BCS theory states that fermions (electrons) can form “Cooper-pairs” that display boson-like properties. Cooper pairs are electron pairs that couple through phonon interactions on the order of the system’s crystal lattice spacing (nanometers).<sup>20</sup>

Peierls predicted that a 1-dimensional electronic system would display thermal transitions that had implications on the conductive properties of the system: the superconducting transition is temperature dependent due to lattice distortions often referred to as dimerization. Dimerization results in the lowering of energy states and the creation of new energy band gaps and is directly related to the previously mentioned Cooper pair formation.<sup>20,19,18</sup> The TTF-TCNQ complex has 1-dimensional donor-acceptor stacking in its crystal structure that allows for dimerization during its superconducting transition at 59K. This transition is accompanied by a dramatic increase in conductivity observed by Heeger and coworkers to be on the order of  $10^6 (\Omega\text{cm})^{-1}$  at 60K.<sup>21</sup>

The research conducted with TTF-TCNQ set the foundation for work with conductive polymers like polyacetylene. The major difference between the TTF-TCNQ complex and a conductive polymer is that when dimerization occurs in the polymer it takes the form of changes in bond length between adjacent carbon atoms. The energy cost

when changing bond length is outweighed by that of the lowering of the overall energy state of the electronic system.<sup>22</sup>

A defining structural component of conductive polymer systems is conjugation. Conjugation can be defined as three or more adjacent p-orbitals that overlap to create a system that shares electron density.<sup>23</sup> Many resonance forms showing the “pushing and pulling” electronic distortions (localized charges such as lone pair electrons, radicals, or carbocations) can be drawn to illustrate conduction in a conjugated system. Increasing the number of repeat units in a conductive polymer increases the number of degenerate orbitals that blend together to form non-degenerate energy bands. The energy barrier to promote an electron from the highest occupied molecular orbital (HOMO) in the valence band to the lowest unoccupied molecular orbital (LUMO) in the conduction band is referred to as the polymer’s band gap ( $E_g$ ).<sup>4</sup>

In Figure 5 the formation of energy bands with increased number of polymer repeat units, as well as the relationship between increased conjugation length and lowered

oxidation potential (decreased band gap energy), is presented using polyacetylene as an example.

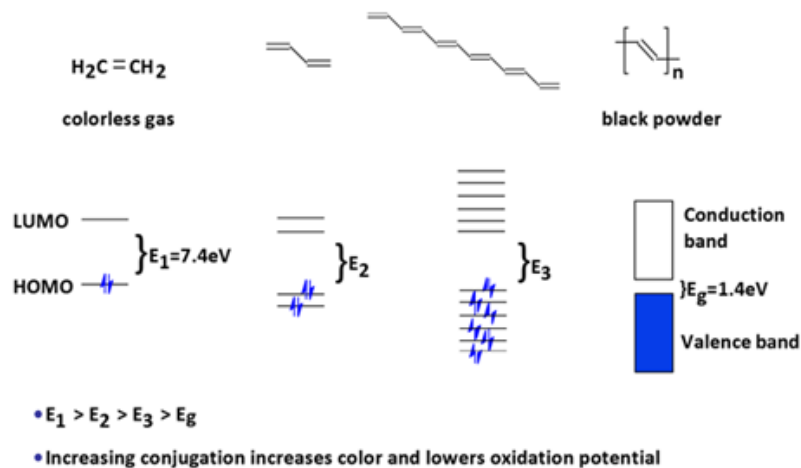


Figure 5: Illustration of the effect of conjugation on conductive polymer electronic properties. ( $E_g$ =band gap)

Doping of conductive polymers is different from that of inorganic semiconductors and metals. The doping process involves the removal (oxidation of a neutral polymer, known as p-doping) of an electron from the polymer or addition (reduction of a neutral polymer, known as n-doping) of an electron to the polymer (Figure 6). This process is fully reversible, and it can occur for thousands of cycles.<sup>24</sup>

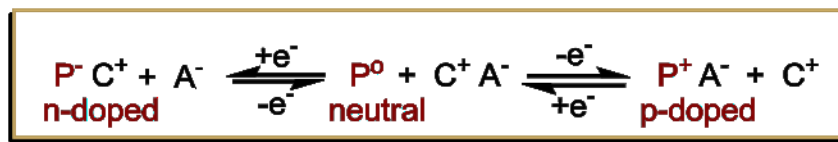


Figure 6: Visualization of doping in a conductive polymer

During doping intermediate energy levels are formed between the valence and conduction bands, decreasing the amount of energy needed to promote electrons from the valence band (Figure 7).

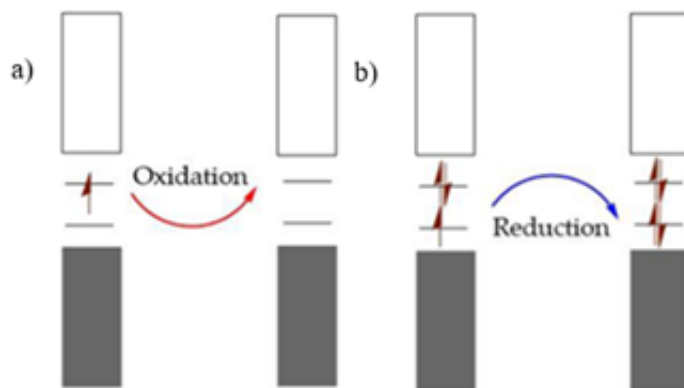


Figure 7: Formation of intermediate energy levels between the valence and conduction bands in doped conductive polymers: a) oxidation b) reduction

These intermediate energy levels can be observed with ultraviolet-visible (UV-vis) spectroscopy.<sup>25</sup> The conduction mechanism in these polymers has been a topic of substantial debate. The most widely accepted theory is that upon oxidation or reduction of symmetrical conductive polymers such as polyacetylene, a localized electronic distortion called a soliton appears in the conjugated network.<sup>26</sup> These solitons can be neutral, positive, or negative depending upon the redox reaction. This electronic distortion in the structure is stabilized through resonance across the polymer backbone. The simplest case is the original *trans*-polyacetylene system. It is the only known conductive polymer to have degenerate resonance structures, due to the symmetry of the system (R-form and L-form) (Figure 8).<sup>27</sup>

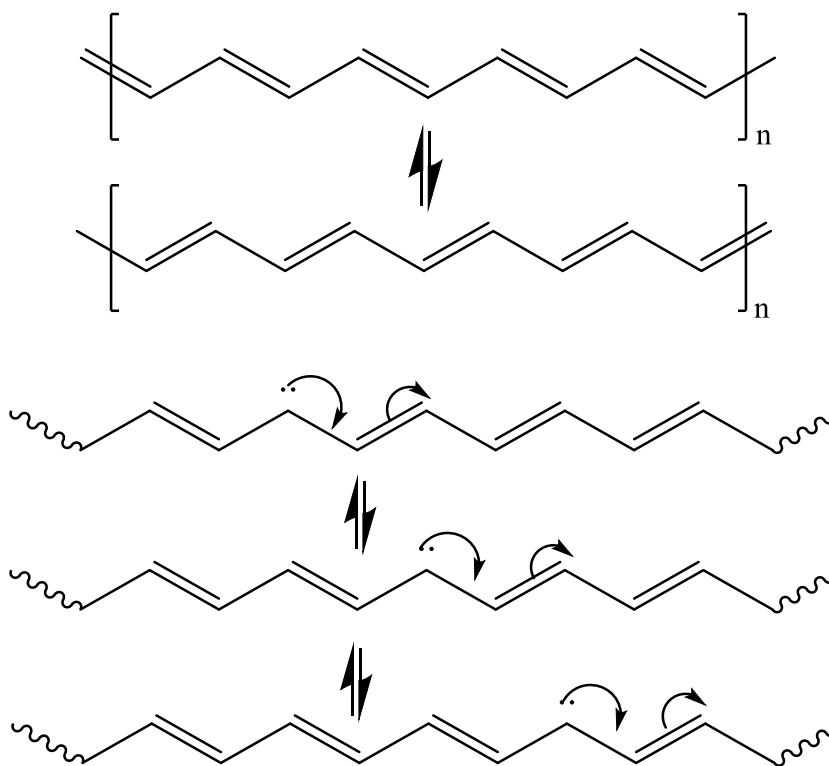


Figure 8: Illustration of soliton formation in polyacetylene. Top structures: degenerate ground states of trans-polyacetylene (R and L form) Bottom structures: resonance forms of degenerate negative solitons of trans-polyacetylene

Conducting polymers with non-degenerate resonance structures, such as polythiophene, follow a different conduction mechanism from that of polyacetylene. In p-doped polythiophene there are a series of electron removals that result in polaronic and bipolaronic electronic states (Figure 9). The initial electron removal involves the oxidation of the neutral polymer to form a resonance-delocalized radical cation, known as a polaron. The polymer is then further oxidized by the removal of a second electron to form a resonance-delocalized dication, known as a bipolaron.<sup>4,22,23,27</sup> As stated previously these redox reactions are fully reversible.

The localized distortions in a bipolaron are typically stabilized across three to five heterocycle rings (depending on polymer structure and amount of dopant used) in order to minimize unfavorable repulsive interactions.<sup>4,26</sup>

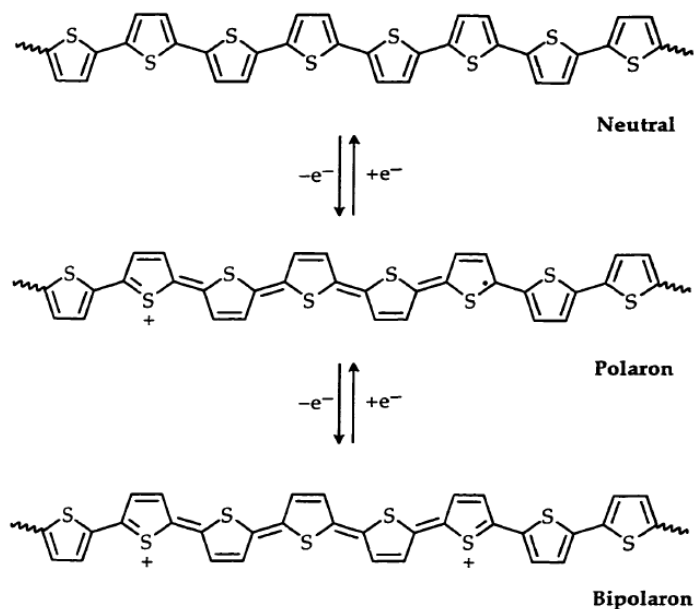


Figure 9: Polaronic excitations upon removal or addition of an electron from polythiophene

### 1.3 Organic Soluble Polymers

Conductive polymers can be synthesized using oxidative or non-oxidative methods.<sup>22,7</sup> The oxidative polymerization of thiophene is shown in Figure 10. First, an electron is removed from a neutral molecule of thiophene to form a resonance-stabilized radical cation. The radical cation then couples with another molecule of thiophene, followed by loss of another electron, or it couples with another radical cation; both pathways form a dicationic dimer, which loses two protons to form a neutral dimer. This process is repeated to form the polymer.

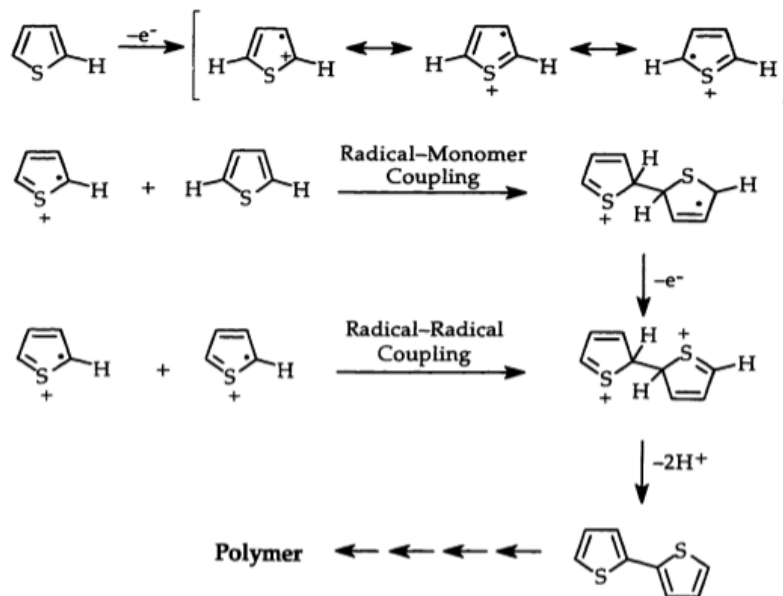


Figure 10: Oxidative polymerization mechanism of thiophene

One of the main advantages of polyheterocycles is the ability to create a variety of structural modifications in order to enhance parameters such as solubility and stability in the oxidized or reduced state.<sup>28,29,4,7</sup> Electron rich monomers have lower oxidation potentials, resulting in fewer side reactions and a more stable doped state.<sup>30,26</sup>

One thiophene derivative that has been extensively studied is (3,4-ethylenedioxythiophene) (EDOT), in which the 3- and 4- positions of the thiophene ring have been substituted to form a cyclic ether. The ether substituents of the monomer reduce the oxidation potential by raising the energy of the HOMO. This fact can be illustrated by comparing the oxidation potentials of the monomers EDOT and thiophene (+2.07V for thiophene monomer compared to +1.43 V for EDOT monomer; oxidation potentials vs. SCE).<sup>31,32</sup>

The ability to solubilize a conductive polymer is of great importance and has many implications on the properties and performance on the materials. As previously mentioned when describing the draw-backs of polyacetylene, the polymer is highly

conductive when doped, but researchers had trouble finding an industrial application due to processing problems related to poor stability as well as lack of solubility.<sup>3</sup>

Polyheterocycles can be modified to have long alkyl chain functional groups to enhance solubility in common organic solvents for greater processability.<sup>33,34</sup>

#### 1.4 Electroactive Polymer Film Performance Parameters

There are a number of factors that influence the electrochemical performance of conductive polymer films. Among the most important are the conditions of polymer synthesis and film processing conditions.<sup>35,36</sup>

##### **Impact of synthetic conditions on conductive polymer film performance:**

The synthetic method used has significant impact on the structural properties of the conductive polymer.<sup>37,38,39</sup> High levels of conjugation require a specific arrangement of repeat units in the backbone of the polymer to maintain resonance stabilization of localized electronic distortions during doping.<sup>40</sup> One issue observed with oxidative polymerization is that when the radical species combine they can create structural defects in the polymer backbone. Polymerization conditions such as oxidant choice, solution temperature, and monomer concentration can affect the formation of structural defects.<sup>41</sup> These defects disrupt conjugation and therefore the ability of the polymer to be doped efficiently.<sup>42</sup> The previously described oxidative mechanism involves the oxidation of a neutral monomer that forms a resonance stabilized radical cation. The positions that the radical can take on the ring are named alpha and beta, so that coupling can occur between two alpha carbons ( $\alpha,\alpha$ -coupling), two beta carbons ( $\beta,\beta$ -coupling) or one alpha and one beta carbon ( $\alpha,\beta$ -coupling), as illustrated in Figure 11.<sup>26,39</sup>

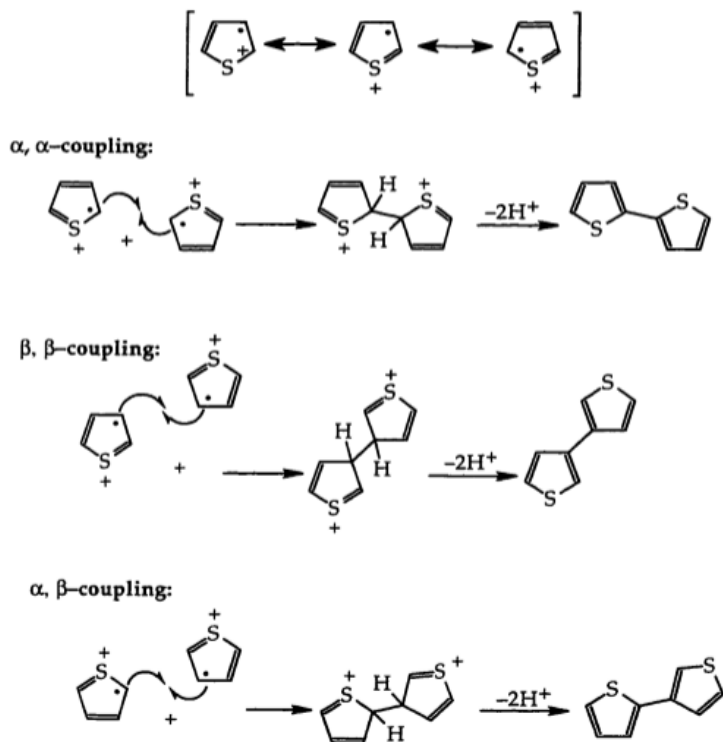


Figure 11: Oxidative polymerization mechanism of thiophene with radical recombination mechanisms

Beta coupling can be prevented by adding substituents to the beta positions of the heterocycle; for example, 3,4-ethylenedioxythiophene (EDOT) cannot undergo beta coupling during oxidative polymerization because the 3- and 4- positions of the thiophene ring are protected by the cyclic ether linkage so that only  $\alpha, \alpha$ -coupling can occur (Figure 12).<sup>43,44</sup>

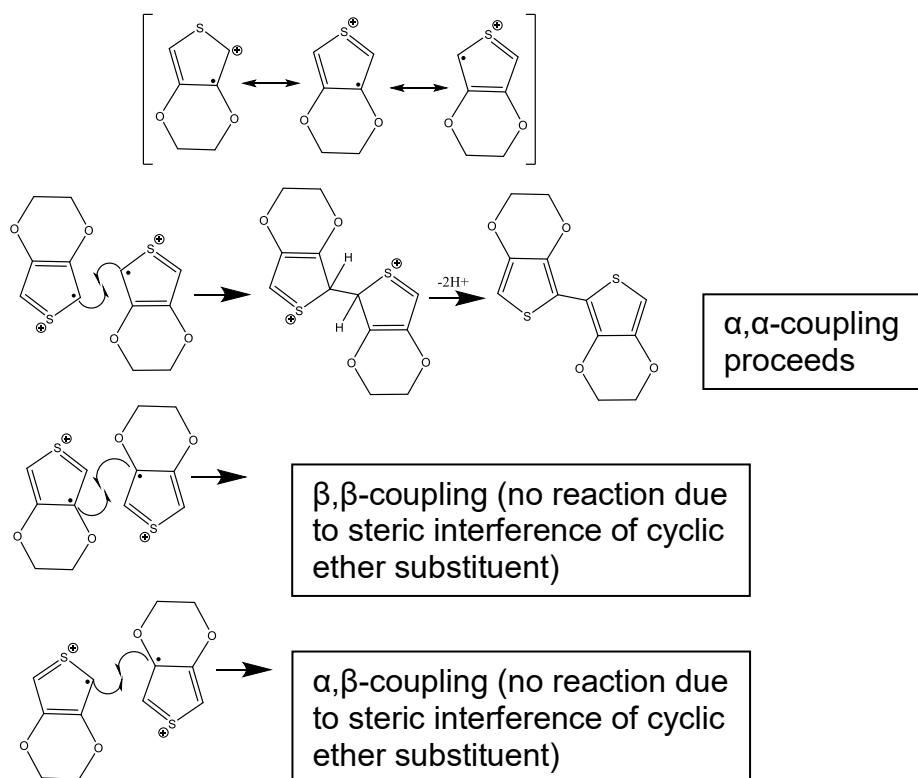


Figure 12: Oxidative polymerization mechanism of EDOT(ethylenedioxythiophene) with radical recombination mechanisms. (only  $\alpha,\alpha$ -coupling occurs due to steric interference of cyclic ether functional group)

In addition to beta-coupling defects, other defects can occur when asymmetrical monomers are employed. The relative orientation of repeat units in an asymmetric polymer is referred to as regioregularity.<sup>45,39,26</sup> An asymmetrical monomer can be assigned a “head” and a “tail”; when two monomer units are bonded together, they can bond “head” to “head”, “tail” to “tail”, or “head” to “tail” (Figure 13). In a regioregular polymer, the type of bonding is consistent throughout the polymer (e.g., all “head” to “tail” linkages.) In Figure 13, the polymer is regioirregular because its repeat units are a random mixture of linkages.

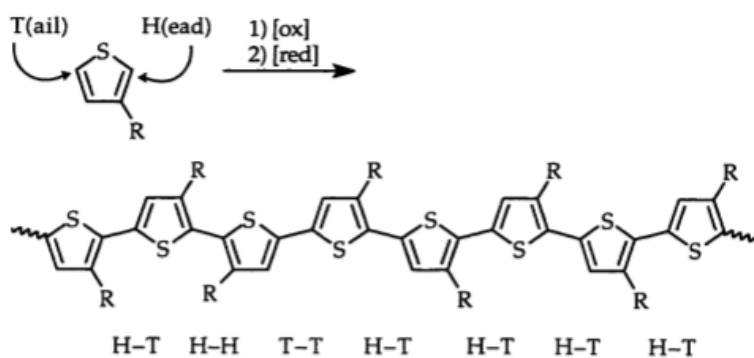


Figure 13: Linkages in a thiophene polymer with asymmetric monomer structure. (Alkyl chain at 3-position) Defects in the polymer chain can occur as a result of oxidative polymerization techniques.

It has been shown that the electroactivity for a polymer is heavily affected by regioregularity.<sup>46</sup> If the linkages produced during polymerization are “head to head”, alkyl chains in the 3- and 4- positions introduce a barrier to free rotation around the carbon-carbon bond linking repeat units (Figure 14). Efficient resonance stabilization of any localized electronic distortions in the backbone of the polymer is highly dependent upon the ability of the heterocycle rings in the structure to become coplanar due to favorable  $\pi$ -orbital overlapping.<sup>47,40,45</sup> Highly regioregular systems have predominantly “head to tail” linkages in polymer structure. These linkages prevent steric interaction of the side chains and preserve planarity in the backbone leading to conserved conjugation.

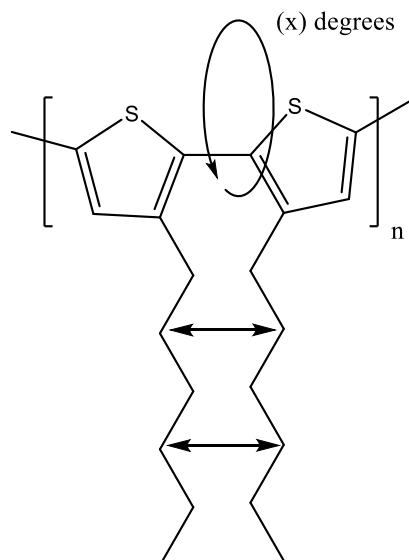


Figure 14: Head-Head linkage of poly(3-hexylthiophene). The van-der waals interactions of the hexyl chains (represented as black arrows) prevent free rotation (x degrees) around adjacent repeat units, disrupting heterocycle ring planarity throughout the polymer chain.

Regioirregularity can be avoided using certain reaction conditions or by using symmetrical monomers.<sup>4,26</sup>

The synthetic protocol can also have a profound effect on polymer molecular weight and molecular weight distribution (polydispersity).<sup>24,38,39</sup> Both molecular weight and polydispersity can have a dramatic impact on film performance.<sup>46,45,39</sup>

### **Implications of conductive polymer film processing conditions:**

The method by which a polymer is processed into a film is another factor that affects performance, and builds off the existing structural characteristics of the polymer that are a consequence of synthetic protocol. Studies of solution cast films of soluble poly(3-alkylthiophene)s such as poly(3-hexylthiophene) (P3HT) show extensive connections between the electrical performance of the film and the choice of solvent, solution additives, drying protocols, and substrate properties.<sup>48,49</sup> The molecular weight, polydispersity, and regioregularity of the polymer influence how the polymer chains orient themselves with respect to adjacent chains and the substrate. P3HT is a

semicrystalline polymer. The polymer chains often orient themselves into three distinct patterns: crystal lamellae, amorphous chains, and local ordered packing.<sup>50</sup> Research suggests that these longer chains in a film can interconnect ordered structures, while lower molecular weight P3HT may have greater ability to organize into stacked structures than does higher molecular weight P3HT, resulting in increased crystallinity and conductivity.<sup>45</sup> Ultimately, there exists a trade-off between longer and shorter chain length with respect to electrical performance for a film sample. Even though shorter chain lengths may allow for increased crystallinity in a film, conductivity for a single polymer chain suffers due to a lower number of repeat units. This is because the conductivity of an electroactive polymer chain generally increases with an increasing number of repeat units.<sup>7,4,26</sup> In general it has been stated that increasing or decreasing the molecular weight by approximately 17,000 gmol<sup>-1</sup> of a P3HT film sample (with controlled regioregularity) varies the charge carrier mobility by four orders of magnitude, and can be attributed mostly to changes in the crystallinity.<sup>51</sup> Increasing polydispersity in a P3HT film is predicted to decrease crystallinity, which can result in a film sample that has lowered charge transport capabilities.<sup>52,50</sup>

A large amount of research for the P3HT system has focused on understanding how the polymer chains  $\pi$ - $\pi$  stack. This stacking of P3HT chains leads to greater order and p-orbital overlapping in a film, resulting in increased conductivity. The stacking of these polymer chains in an organized fashion is referred to as P3HT aggregation.<sup>53</sup> Aggregation of P3HT chains has been shown to have a great impact on film electrical properties.<sup>54</sup> Techniques such as X-ray diffraction (XRD), ultraviolet-visible spectroscopy (UV-Vis), and Raman spectroscopy have all been used to confirm the

presence of aggregates and characterize these aggregates in both solution and in films.<sup>55</sup> Relationships have been found between the use of P3HT non-solvents such as acetonitrile and aggregate formation.<sup>56</sup> Controlled drying of polymer solution droplets has also been used to induce aggregation. Aggregation of polymer chains has been demonstrated to be highly solvent-specific.<sup>57</sup>

### 1.5 Current Techniques for Modifying Polymer Film Morphology

Polymer morphology can be described as the physical form and solid-state structural arrangement of molecules in a film.<sup>58</sup> A polymer film can adopt many different types of morphologies, and each one can be utilized in a variety of applications. One highly studied morphology in polymer science is porosity. There are numerous important applications of porous polymer films. Some of those applications include: gas storage and separation for clean energy technologies, polymer actuators, and antibacterial surfaces.<sup>59,60,61</sup> There are two generalized approaches for creating porous polymer films. Those techniques are appropriately named hard-templating and soft-templating. Both methods are used when templating a polymer film from solution (solution-deposited method). Hard-templating involves the use of nanoparticles or the machining of structures for controlled pore formation. These techniques often create a more uniform pore distribution. The potential drawback of the hard templating approach is that removal of the hard templating material may damage the polymer film. In contrast, soft-templating involves the use of “soft materials” such as ionic liquids, dissolved gasses, and others to introduce pores. Soft-templating also has its own Achilles heel: control of nano-structure sizes is very challenging and is highly dependent upon the material used and methodology employed.<sup>62,63,64</sup>

Solution-deposition is not the only technique that can be used to create unique polymer film morphologies. Electrochemical polymerization methods often utilize a technique called cyclic voltammetry (CV) that results in notable molecular arrangements. Described in Chapter 4, this technique involves the use of a computer-controlled instrument called a potentiostat. The potentiostat is often connected to a three-electrode experimental system (working electrode, counter electrode, and reference electrode). The computer-controlled potentiostat can be programmed to apply electrical waveforms to the electrodes. Depending on the electrical bias of the applied potential (negative or positive), the chemical species at the working electrode is oxidized or reduced.<sup>26</sup> As implied by the name (cyclic voltammetry), one completion of a voltage “scan” within a set voltage window (programmed voltage value limits: eg. -1.5V to +1.5V) constitutes beginning at the initial voltage value (eg. -1.5V), rising to a chosen peak voltage value (eg. +1.5V), and ending back at the initial voltage value (eg. -1.5V). Two experiments that are often used are repeated potential scanning and potentiostatic electropolymerization. In repeated potential scanning electropolymerization the experimental parameters are such that multiple cycles are repeated at a certain scan rate (voltage value over time: eg. mV/s). In potentiostatic electropolymerization, polymerization is conducted at a chosen constant potential value. In both techniques polymer films are grown onto the working electrode that is submerged into a solution of monomer and electrolyte. Depending on multiple experimental parameters such as monomer concentration, electrolyte concentration, and monomer structure, film morphology produced from the two techniques can be strikingly different. It was reported for the 2,2'-bithiophene monomer that potentially dynamic methods (repeated potential scanning) produced amorphous films versus potentially static

methods that produced more crystalline morphologies.<sup>65</sup> An illustration of morphologies produced from various porous film creating techniques as well as electropolymerization is given in Figure 15.

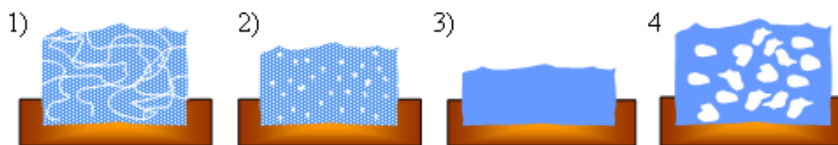


Figure 15: Illustration of morphologies produced from various techniques. 1) repeated potential scanning electropolymerization 2) potentiostatic electropolymerization 3) solution casting 4) templating with porogen

### 1.6 Benefits/Applications of Enhanced Conductive Polymer Films

Modifying film morphology is an important endeavor because conductive polymer properties (such as conductivity) can be enhanced upon changes in molecular arrangement.<sup>7,4,58</sup> Metals, such as copper, have conductivities greater than  $10^4$  S/cm. Common ECP conductivity information is given in Table 1. Inherent conductivities of doped ECPs are much lower than that of copper, so ECPs are not likely to be useful as replacement materials for copper wires.<sup>4</sup>

Table 1: Conductivities of Notable Materials<sup>4,17</sup>

<b>Material</b>	<b>Conductivity (S/cm)</b>
Doped poly(acetylene) (PA)	$10^3$ - $10^5$
Doped poly(pyrrole) (PPy)	$10^2$ - $10^3$
Poly(thiophene) (PT)	$10^2$
Poly(aniline) (PANI)	$10$ - $10^2$
Poly(p-phenylene) (PPP)	$10^2$ - $10^3$
Poly(phenylene vinylene) (PPV)	$10^3$ - $10^4$
Copper	$10^5$

Instead, most potential applications of ECPs are based on their “electroactivity”. Electroactivity is a term used to describe the ability of a material to change electrical properties in response to an external stimulus such as doping. Doping ECPs results in

increased conductivities as well as changes in other useful properties of the polymer such as volume, color, reactivity, and solubility.<sup>66,4,7,22</sup> For the remainder of this thesis the polymers utilized will be referred to as EAPs (electroactive polymers).

EAP property changes (volume, color, etc.) upon doping are highly tunable via alterations in polymer structure through the method of processing.<sup>67</sup> Common applications that utilized these property changes are: drug delivery, energy storage, polymer actuators, and chemical and biochemical sensors.<sup>68,69</sup> The mentioned physical attributes can all be “enhanced” through changes in the polymer film morphology. Some changes in polymer morphology include: polymer chain alignment, sample anisotropy, and porosity.<sup>70,58</sup> Examples of “enhancement” of polymer film properties include more dramatic color change, increased volume change, and higher conductivity. An example of enhancement for a polymer material via a morphology change can be demonstrated with conductive polymer actuators. Actuators that use conductive polymers such as polypyrrole have been shown to benefit from the increased alignment of chains within a device by rolling or stretching processes. Augmented strain or stretch forces were observed for the polypyrrole actuators, and were attributed to increased conductivity of the polymer samples. The explanation for higher observed conductivity was that the organized fibers allowed for greater uniform infiltration of solution electrolyte ions as opposed to bulk polymer films.<sup>71,22</sup>

### 1.7 Thesis of This Work

The focus of this work was to explore the use of the soft-templating approach to enhance the electronic properties of conductive polymer films. Two known polymers poly(3-hexylthiophene) (P3HT) and poly[3,4-(2,2-dibutylpropylenedioxy)thiophene]

(poly(ProDOT-Bu<sub>2</sub>)) were synthesized via a non-oxidative Grignard metathesis polymerization. The polymers were soft-templated using a variety of solvent systems with the intent of creating a network of interconnecting (co-continuous) pores. An attempt was made to predict the extent of porosity for polymer-porogen combinations based upon the amount of porogen used. Cyclic voltammetry experiments were used to evaluate the effect of polymer morphology on conductive polymer electroactivity.

## 2. MONOMER SYNTHESIS & POLYMERIZATION

### 2.1 Motivation for Research

The need for a high molecular weight regioregular polymer is of high importance for the electrical performance of templated films.<sup>45,46,47,50</sup> Oxidative polymerization schemes can produce defects in the polymer backbone and limit the molecular weight due to solubility issues during polymerization.<sup>72,39</sup> Non-oxidative techniques allow for conserved electrical neutrality of the polymer chain during polymerization. The Grignard Metathesis polymerization method was used to synthesize P3HT and poly(ProDOT-Bu<sub>2</sub>) because it has been shown to yield polymers with higher regioregularity and higher molecular weights than those resulting from oxidative chemical polymerization.<sup>73,74</sup>

### 2.2 Synthetic Method

While it has been shown that oxidative polymerization techniques can yield polymers with high molecular weight P3HT (> 10,000 g/mol), even under the proper experimental conditions, there are usually significant defects in the backbone of polymer chains (only 50-80% head to tail linkages).<sup>75</sup> Also, when polymerized through oxidative schemes the polymer is formed in its oxidized state; double bonds between adjacent rings in the oxidized state prevent free rotation, decreasing solubility and thus limiting molecular weight.<sup>76</sup> Oxidative polymerization is poorly controlled; unwanted beta-coupling occurs during radical recombination of monomers or oligomers. These structural defects limit the ability of the backbone to become coplanar, compromising the electrical properties of the polymer. Experiments have shown this relationship between regioregularity of the polymer and its doping efficiency. Electron paramagnetic resonance spectroscopy was used to detect delocalized charges in regioregular samples of

P3HT as opposed to regiorandom upon doping with 2,3,5,6-tetrafluoro-7,7,8,8-tetracyanoquinodimethane. The ability of the regioregular sample to stabilize delocalized charges was attributed to its ability to form ordered aggregates (a quality that is unobserved for regiorandom P3HT samples).<sup>77</sup>

In order to avoid backbone defects commonly encountered with oxidative polymerization methods, non-oxidative synthetic techniques were used to produce both P3HT and poly(ProDOT-Bu<sub>2</sub>). Like oxidative polymerization, transition metal-mediated coupling reactions can be used to produce polymers via carbon-carbon bond formation. A common non-oxidative polymerization scheme utilizes the well-known Yamamoto aryl-aryl coupling reaction in the presence of a nickel (II) catalyst.<sup>78</sup> When this reaction is used to produce polyheterocycles, it is known as a Grignard Metathesis (GRIM) polymerization. In the GRIM polymerization, organometallic Grignard reagents react with an aryl halide, undergoing a transition metal-mediated coupling reaction to form carbon-carbon bonds.<sup>79</sup> As shown in Figure 16, a brominated alkyl thiophene (1) when reacted with a tert-butylmagnesium chloride (Grignard reagent) forms a magnesium chloride functionalized monomer at the “head” or “tail” position (2,3). Through oxidative addition, the brominated monomer (1) adds to the neutral metal center, and a transmetallation step follows with the reaction of the magnesium chloride functionalized monomer (2). Dibrominated neutral dimer is then formed via reductive elimination. The metal center again becomes neutral. This process is repeated many times, forming a neutral polymer.<sup>73</sup>

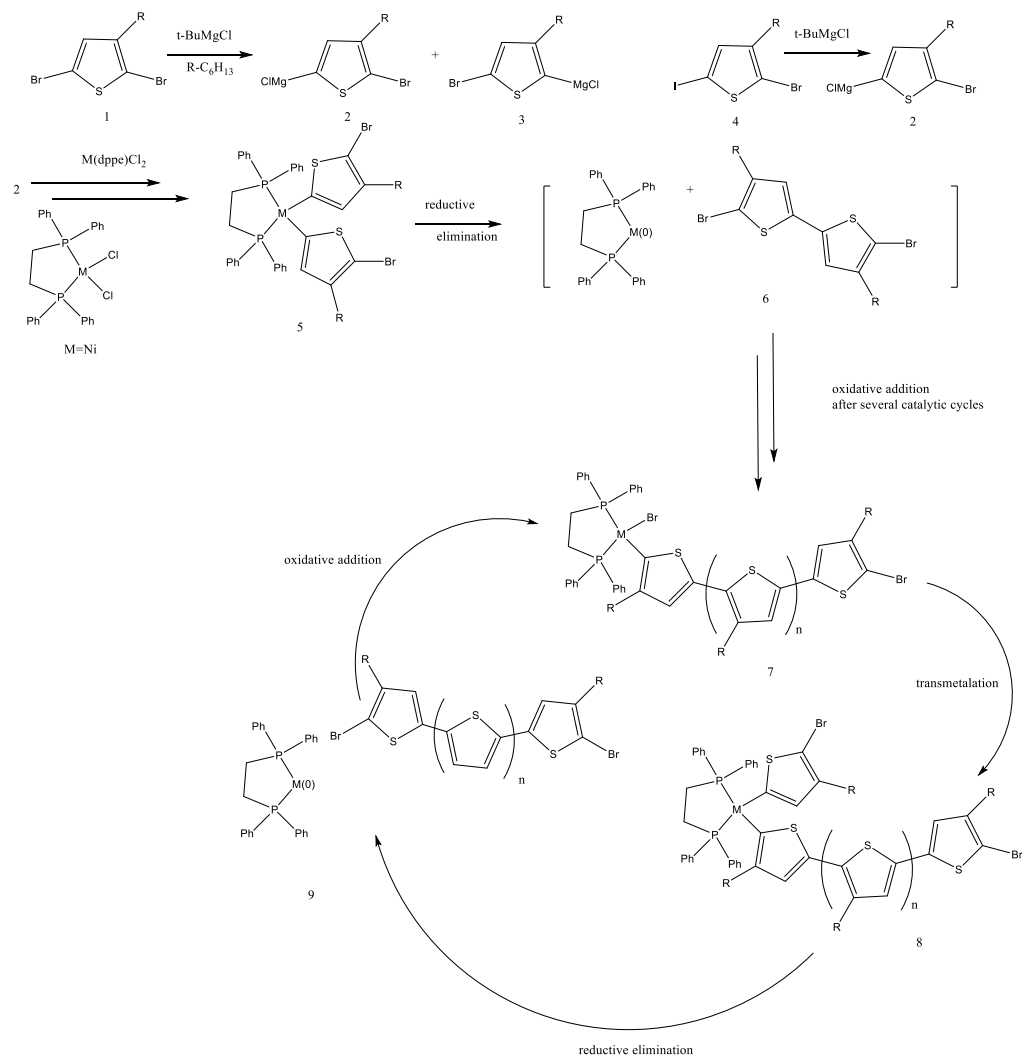


Figure 16: Grignard coupling reaction scheme

The Grignard metathesis polymerization (GRIM) can produce reasonable molecular weight, highly regioregular conductive thiophene polymers such as P3HT ( $>30,000 \text{ gmol}^{-1}$ ),<sup>73</sup> which is much higher than typical molecular weights obtained via chemical oxidative polymerization (ca.  $10,000 \text{ gmol}^{-1}$ ).<sup>75</sup> Molecular weight often is lower for oxidative techniques as opposed to non-oxidative techniques due to the fact that the polymer remains in the oxidized state throughout the reaction. The oxidized state increases polymer chain rigidity which lowers solubility, and limits obtainable molecular weight.<sup>26</sup> One explanation for higher molecular weight in the Grignard reaction is the

high conversion rate of the nickel(II)-based catalysis: up to 98% conversion has been observed in some cases.<sup>73</sup> In addition, it has been shown that the ligands chosen that are attached to the catalytic metal center highly affect the regiospecificity of the reaction.<sup>80</sup> Carefully chosen ligands strategically create steric crowding close to the metal center. This allows for the directional approach of the monomer to be highly controllable. 3-Hexylthiophene has an alkyl chain at the 3-position on the thiophene ring as its chemical name implies. The presence of this alkyl chain controls how the monomer approaches a sterically crowded catalytic center. Ideally, the center is crowded in such a way that controls the approach of the 3-hexylthiophene monomer to allow for consistent H-T-H-T linkages. Most nickel(II) catalysts that are designed for this application give such results.<sup>81</sup> One last aspect that gives non-oxidative syntheses an advantage over oxidative techniques is that the polymer chain stays in the aromatic, neutral state throughout the reaction, allowing free rotation about the sigma bonds between adjacent rings, resulting in higher solubilities and ultimately, higher molecular weights.<sup>4,26</sup>

## 2.3 Experimental

### 2.3.1 Materials

3-Hexylthiophene and 1.0M methymagnesium bromide in tetrahydrofuran (THF) were purchased from Aldrich and used as received. N-bromosuccinimide (NBS) was purchased from Fisher Scientific and recrystallized from water. Dimethylformamide (DMF), (THF), hexane, methanol, dichloromethane, dichloro[1,3-bis(diphenylphosphino)propane]nickel, 3,4-dimethoxythiophene, 2,2-dibutyl-1,3-propanediol, p-toluenesulfonic acid, were also used as received from VWR.

### 2.3.2 Instrumentation

Molecular weight determination for P3HT was accomplished using a Viscotec GPC with a triple detector (polystyrene standard). Poly(ProDOT-Bu<sub>2</sub>) molecular weight was determined using a Bruker Autoflex MALDI/TOF/TOF. A Bruker Avance 400 MHz FT NMR and Bruker Tensor II FT-IR were used in characterization of each synthesized polymer. Proton NMR spectra were collected using deuterated chloroform as the solvent with the number of scans at 16. FT-IR samples were prepared by placing multiple droplets of diluted stock solution (1 mg/mL) onto polyethylene sample cards. Spectra were collected using the wavelength range of 400-4000 cm<sup>-1</sup>.

### 2.3.3 Synthesis

The synthesis of both polymers (P3HT and poly(ProDOT-Bu<sub>2</sub>)) was implemented using the GRIM polymerization technique. Before polymerization, monomers were synthesized and then subsequently brominated. The syntheses of P3HT and 2,5-dibromo-3-hexylthiophene were modified from literature procedures.<sup>82</sup> The syntheses of 3,3-dibutyl-3,4-dihydro-2H-thieno[3,4-b][1,4]dioxepine ((ProDOT-Bu<sub>2</sub>)), 6,8-dibromo-3,3-dibutyl-3,4-dihydro-2H-thieno[3,4-b][1,4]dioxepine ((ProDOT-Bu<sub>2</sub>-Br<sub>2</sub>)), and poly(3,3-dibutyl-3,4-dihydro-2H-thieno[3,4-b][1,4]dioxepine) (poly(ProDOT-Bu<sub>2</sub>)), 3,3-dibutyl-3,4-dihydro-2H-thieno[3,4-b][1,4]dioxepine ((ProDOT-Bu<sub>2</sub>)) were modified from literature procedures.<sup>83</sup>

#### **Poly(3-hexylthiophene)<sup>1</sup>:**

Pure 2,5-dibromo-3-hexylthiophene (0.99 g, 3.03x10<sup>-3</sup> mol) was added in THF (15 mL) to a flamed dried flask that was blanketed under argon. Methylmagnesium bromide (2.5 mL, 2.5x10<sup>-3</sup> mol) was added dropwise, and the solution was slowly stirred

---

<sup>1</sup> Synthesized by Sothavy Vong

while refluxing at 60°C. Dichloro[1,3-bis(diphenylphosphino)propane]nickel (15.3 mg, 28.2 μmol) was added, causing the solution to turn dark orange. The solution was further refluxed for 2 hours and allowed to cool to room temperature. The product was added dropwise to rapidly stirring methanol (turning purple upon addition), and the dark purple powder was collected via vacuum filtration. The collected product was purified further via soxhlet extraction in a cellulose thimble: first with methanol at 60°C to remove salts, then with hexane at 60°C to remove oligomers. A final extraction with chloroform dissolved the polymer, leaving behind a colorless cellulose thimble. Evaporation of chloroform yielded P3HT as a brownish-gold, freestanding film (0.623g, 63% yield). <sup>1</sup>H NMR (CDCl<sub>3</sub>, 400 MHz) 6.98 (s-1H), 2.80 (t-2H), 1.69 (m), 1.35 (m), 0.91 (t). FT-IR (cm<sup>-1</sup>): 3054.90, 2916.56, 2850.30, 1509.11, 1472.47, 1462.69, 1377.27, 1261.52, 1094.48, 1020.03, 819.07, 802.16.

**Poly(3,3-dibutyl-3,4-dihydro-2H-thieno[3,4-b][1,4]dioxepine) (poly(ProDOT-Bu<sub>2</sub>))<sup>2</sup>:**

Polymerization of the brominated product was accomplished by addition of methylmagnesium bromide (4.7 mL, 4.7x10<sup>-3</sup> mol) to a mixture of THF (155 mL) and the brominated monomer (1.4048 g, 3.2960x10<sup>-3</sup> mol) (yellow colored solution).

Dichloro[1,3-bis(diphenylphosphino)propane]nickel catalyst (1.90x10<sup>-2</sup> g, 3.50x10<sup>-5</sup> mol) was added, causing the reaction mixture to turn a dark violet color. After 24 hours, the reaction mixture was precipitated from methanol. The precipitate was collected in a Büchner funnel. The collected polymer was further purified via soxhlet extraction: 48 hours in hexane, 24 hours in methanol, and 24 hours in chloroform. Evaporation of chloroform yielded poly(ProDOT-Bu<sub>2</sub>) as a reddish-purple/metallic gold, freestanding

---

<sup>2</sup> Synthesized by Joe Garcia

film. <sup>1</sup>H NMR (CDCl<sub>3</sub>, 400 MHz) 3.97 (bm-≈4H), 1.38 (bm-≈12H), 0.96 (t-6H). FT-IR (cm<sup>-1</sup>): 2918.02, 2850.23, 1472.67, 1462.87, 1433.96, 1369.45, 1040.36.

## 2.4 Results and Discussion

Both polymers that were synthesized (P3HT and poly(ProDOT-Bu<sub>2</sub>)) have been identified on the basis of FT-IR and NMR spectroscopy. Molecular weights of the polymers were determined using gel permeation chromatography (GPC) and matrix assisted laser desorption time of flight mass spectrometry (MALDI/TOF/MS).

### 2.4.1 Poly(3-hexylthiophene) identification and solubility

FT-IR results for P3HT align with literature-recorded peaks. Namely, the peak at 1509 cm<sup>-1</sup> corresponds to a C=C asymmetric stretching vibration characteristic of P3HT (Appendix A.1).<sup>84</sup> Proton NMR signals also agree well with literature values-<sup>1</sup>H NMR (CDCl<sub>3</sub>): 6.96 (s, 1H), 2.79 (t, 2H), 1.69 (m, 2H), 1.25 (m, 18H), 0.86 (t, 3H).<sup>39</sup> The most identifiable signal is the singlet peak at approximately 6.98 ppm that corresponds to the single hydrogen attached to the thiophene ring (Appendix B.1).

GPC results show that the  $\bar{M}_n$  and  $\bar{M}_w$  of the polymer are approximately 38,713 and 55,436 g/mol respectively. This indicates around 230 repeat units ( $X_n$ ) (Appendix C.3). Polydispersity index:

$$PDI = \left( \frac{\bar{M}_w}{\bar{M}_n} \right) \quad (\text{Equation 2})$$

for the polymer was approximately 1.432.

P3HT is most soluble in chlorinated solvents such as chloroform and chlorobenzene (50 mg/mL). The polymer displays some solubility in xylene, toluene, and THF. The solubility of P3HT is highly dependent on molecular weight, with higher molecular weight polymer being more soluble in the chlorinated solvents and lower

molecular weight chains being more soluble in solvents like toluene.<sup>85</sup> A discernable way of predicting P3HT solubility is currently being developed by using Hansen Solubility parameters and Flory-Huggins models.<sup>85</sup> It was experimentally determined that typical “non-solvents” of the P3HT used in this research include: dimethylsulfoxide, dimethylformamide, ethanolamine, 1,4-dioxane, and methanol. Non-solvents were identified by placing milligram amounts of P3HT into a clean dry test-tube and introducing the solvent in question. The test-tube (with solvent and P3HT present) was agitated with a vortex mixer for approximately 5 minutes. If any dissolution occurred, the solvent was not considered a non-solvent of P3HT.

#### 2.4.2 Poly(ProDOT-Bu<sub>2</sub>) identification and solubility

The FT-IR spectrum for poly(ProDOT-Bu<sub>2</sub>) is consistent with the spectrum reported in literature<sup>83</sup> (Appendix A.2). Literature peaks include: (neat, cm<sup>-1</sup>): 2957, 2931, 2863, 1468, 1430, 1370, 1041. Notice the absence of a peak at 1509 cm<sup>-1</sup> (C=C asymmetrical stretching vibration in the P3HT spectrum) highlighting the symmetrical nature of the poly(ProDOT-Bu<sub>2</sub>) repeat unit. Proton NMR resonance values are in good agreement with literature values with the exception of the signals that indicate protons next to the oxygens in the cyclic ether ring ( $\approx$  3.98 ppm) (Appendix B.2).<sup>83</sup> The spectrum was obtained using deuterated chloroform as a solvent. Upon later inspection of the reference article, it was observed that deuterated chloroform may react with the polymer. The solution to this problem presented was to use deuterated benzene.<sup>83</sup> This could most likely explain the difference in peak shape when comparing the literature spectrum with the spectrum provided in the Appendix section.

Poly(ProDOT-Bu<sub>2</sub>) molecular weight was determined using MALDI-TOF-MS. The spectrum is presented in Appendix C.1. Interpretation of the spectrum involved the use of two equations. Equation 3 describes the calculation of number average molecular weight ( $\bar{M}_n$ ):

$$\bar{M}_n = \frac{\sum N_i M_i}{\sum N_i} \quad (\text{Equation 3})$$

with  $N_i$  representing the number of moles of molecules having the molecular weight  $M_i$ . Equation 4 indicates the calculation of weight average molecular weight ( $\bar{M}_w$ ):

$$\bar{M}_w = \frac{\sum N_i M_i^2}{\sum N_i M_i} \quad (\text{Equation 4})$$

that involves taking the summation of the product of  $N_i$  and square of  $M_i$  divided by the summation of product  $N_i$  and  $M_i$ . The number of moles of molecules ( $N_i$ ) was found by printing out the spectrum and measuring each peak (14 peaks total) in cm. The intensity axis spans from 100-800 intensity units. A conversion factor was created in order to convert peak height (cm) to intensity units. The conversion factor was found to be approximately 100 intensity units (iu) per 2.90 cm ( $\approx 34.48$  iu/cm). M/z ( $M_i$ ) values for each peak were calculated by adding or subtracting the value 266.90 (approximate repeat unit m/z) from peak number five in the spectrum. Tabulated calculation results for this method are given in Appendix C.2. Using the values in Appendix C.2,  $\bar{M}_n$  and  $\bar{M}_w$  for the polymer were found to be 3,974 and 4,174 g/mol respectively. The average number of repeat units for the polymer was found to be about 15. Polydispersity index was calculated to have a value of approximately 1.05.

Solubility of poly(ProDOT-Bu<sub>2</sub>) was slightly different from that of P3HT in chlorinated solvents. Homogenous chloroform-based solutions of the polymer were produced at approximately 20 mg/mL, but upon increasing to higher mass amounts the

polymer started to precipitate out of solution. Poly(ProDOT-Bu<sub>2</sub>) shares common non-solvents with P3HT. Most notably the polymer is not soluble at all in dimethylsulfoxide. Dimethylformamide, ethanolamine, 1,4-dioxane, and methanol were also found to be non-solvents using the method described in 2.4.1.

### 2.4.3 Molecular Weight and Polydispersity Index

Table 2 presents calculated  $\bar{M}_n$ ,  $\bar{M}_w$ , PDI, and  $X_n$  (number of repeat units) values for P3HT and poly(ProDOT-Bu<sub>2</sub>).

Table 2: Molecular Weight Data for P3HT and Poly(ProDOT-Bu<sub>2</sub>)

Polymer	$\bar{M}_w$ (g/mol)	$\bar{M}_n$ (g/mol)	PDI	$X_n$
P3HT	55,436	38,713	1.432	230
poly(ProDOT-Bu <sub>2</sub> )	4,174	3,974	1.05	15

The dramatic difference in molecular weight between polymers can be possibly attributed to the electron rich nature of the ProDOT-Bu<sub>2</sub> monomer (presence of oxygen atoms).<sup>86</sup> The nickel catalyst used in the GRIM polymerization procedure may interact with the ProDOT-Bu<sub>2</sub> monomer differently than the 3-hexylthiophene monomer, affecting rate of conversion of monomer to polymer, thus lowering the degree of polymerization. The PDI calculated for P3HT is consistent with that reported in the literature method (1.20-1.47).<sup>83</sup> The higher PDI (when compared to poly(ProDOT-Bu<sub>2</sub>)) could be explained on the basis of large P3HT chains (> 30,000 g/mol) having limited solubility, thus affecting chain termination and re-initiation during polymerization.

### **3. ELECTROACTIVE POLYMER MORPHOLOGY CONTROL**

#### 3.1 Motivation for Research

The drawback to electrochemically deposited films is that the methods used to produce them may not be practical or economical from an industrial viewpoint. Solution-processable polymers are therefore desirable for commercial applications of EAPs. However, the electrochemical performance of solution-cast films is often inferior to that of electrochemically prepared films.<sup>87,88</sup> Methods of improving electrochemical performance of solution-cast films are needed.

#### 3.2 Background

If EAP technology is going to be practical in application, then an industrially scalable method of producing processable films is desirable, likely involving deposition of the polymer from solution. Unfortunately, the electrochemical performance of solution-templated films is typically inferior to that of electrochemically deposited films.<sup>88</sup> This may be due to non-uniform doping of the polymer film during electrochemical oxidation. During electrochemical analysis (eg. cyclic voltammetry), charges that form along the backbone of a polymer are balanced by the available electrolyte in solution.<sup>4,22,24,26,27</sup> Therefore, uniform doping of an EAP is highly dependent upon the availability of the electrolyte and its close proximity to localized charge formation along the backbone of the polymer. If a polymer's morphology is such that electrolyte is blocked from entering the bulk of the film, then only surface doping will occur, resulting in lowered current response, decreased capacitance, or poor electrochromic performance. When a polymer is deposited from solution, it is possible

for a dense polymer film to be produced. The dense film most likely can only be charge balanced at the surface during doping, limiting electroactivity.<sup>89</sup>

Inferior performance was observed previously for the solution-deposited ladder polymer poly(benzimidazobenzophenanthroline)(BBL, Figure 17).<sup>90</sup> In order to combat the problem, it was suggested that creating a porous network within an EAP might allow for electrolyte infiltration and ultimately uniform doping. The hypothesis was that templating with an ionic liquid such as 1-ethyl-3-methyl-imidazolium bis(trifluoromethylsulfonyl)imide (EMI-BTI) would result in pore formation. EMI-BTI was a desirable pore creating agent “porogen” due to the liquid being relatively high boiling, unreactive, a non-solvent for BBL, and similar in density to BBL. The use of a high-boiling liquid can be identified as a “soft-templating” approach to induce porous morphology in a polymer film. The basis of this idea was derived from previous experiments involving the use of co-polymers to induce unique phase separation within a sample.<sup>91</sup> With BBL, instead of using a co-polymer to induce phase separation, a high boiling solvent was utilized. It was predicted based upon the co-polymer studies that with specifically chosen percentages of porogen, desired co-continuous porous networks within the BBL polymer film could be achieved.

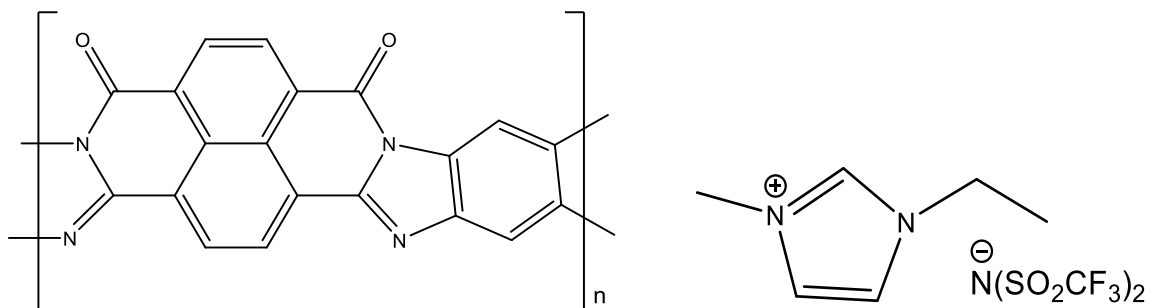


Figure 17: Structures of poly(benzimidazobenzophenanthroline) (BBL) ladder polymer (left) & 1-ethyl-3-methyl-imidazolium bis(trifluoromethylsulfonyl)imide (EMI-BTI) ionic liquid (right).

Templating with and without the ionic liquid present showed a dramatic increase in surface roughness of the polymer film. The dramatic morphology change in the SEM image of the film cast with the ionic liquid suggests the possibility of co-continuous pore formation within the bulk of the film (Figure 18). This possibility is strengthened by the fact that removal of the porogen EMIBTI, with a subsequent methanol wash during templating, is demonstrated by the absence of a fluorine signal during EDX analysis.<sup>90</sup>

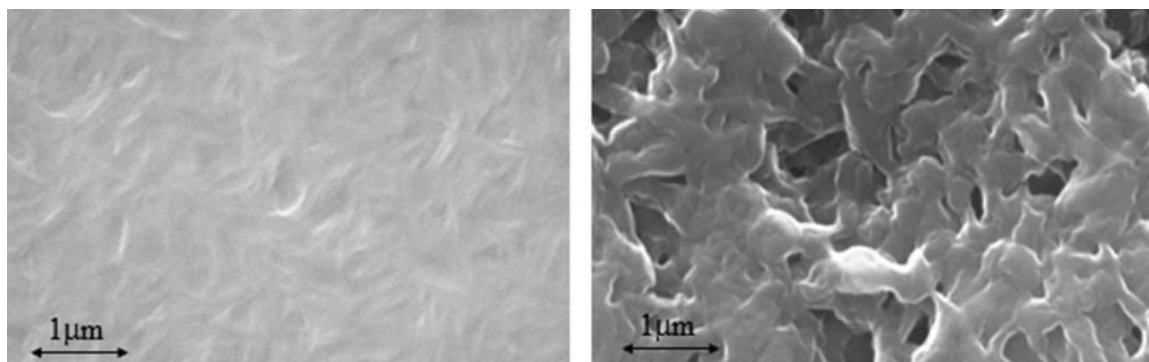


Figure 18: Scanning electron microscope (SEM) images of BBL polymer cast with and without ionic liquid EMIBTI. SEM images of left: BBL neat film (no ionic liquid) right: BBL co-cast with ionic liquid EMIBTI

Theoretically, an increase in accessible surface area of the polymer film should allow the polymer to be doped to a greater extent during electrochemical measurements. If pores in the polymer film are co-continuous, the accessible surface area of the polymer film will increase, allowing the electrolyte present in solution to freely migrate into and out of the film, stabilizing charge formation on the polymer backbone. This phenomenon is demonstrated in Figure 19. Films cast with the porogen EMIBTI demonstrate a thirty-fold increase in current response when compared to the BBL films cast without EMIBTI. In addition, the BBL films cast with EMIBTI demonstrate a more capacitive response when compared to the films cast without. This suggests that an increase in surface area due to increased porosity of the film sample may allow for more electrolyte to infiltrate the BBL film, leading to larger current response and capacitive behavior.

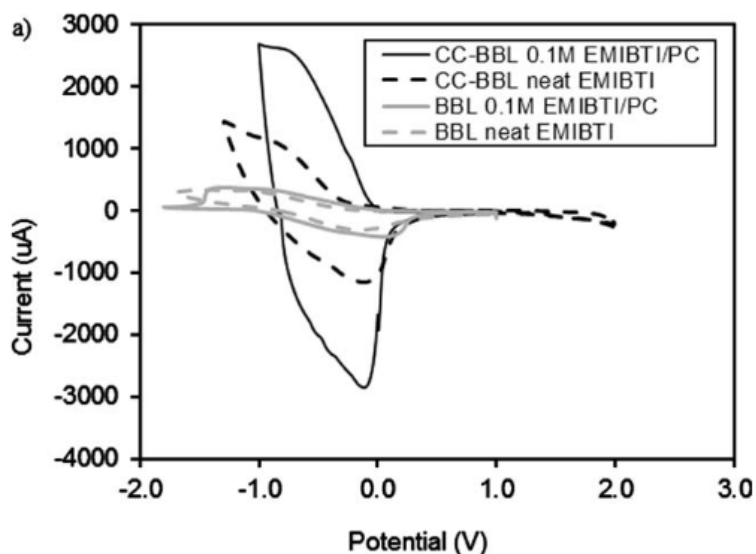


Figure 19: Cyclic voltammogram of solution cast films created with and without EMIBTI. PC = propylene carbonate (supporting electrolyte). CC-BBL= BBL cast with EMIBTI, BBL= BBL without EMIBTI as a porogen. Reference = Ag wire at 50 mV/s.

It has been shown that changing the mole fractions of two different blocks in a block copolymer can result in significant changes in block copolymer morphology. In Figure 20, below, block A is blue, and block B is red. As the mole fraction of A ( $f_A$ ) increases (from left to right), the morphology of the polymer transitions from isolated regions of A (labeled S), to columns of A (labeled C), to co-continuous regions of A (labeled G), to alternating layers of A and B (labeled L). These morphologies result from minimization of the overall Gibbs free energy of thermodynamic mixing. The mole fraction that was theorized to create co-continuous regions of A was predicted to be in a range of 28-34% A.<sup>91</sup>

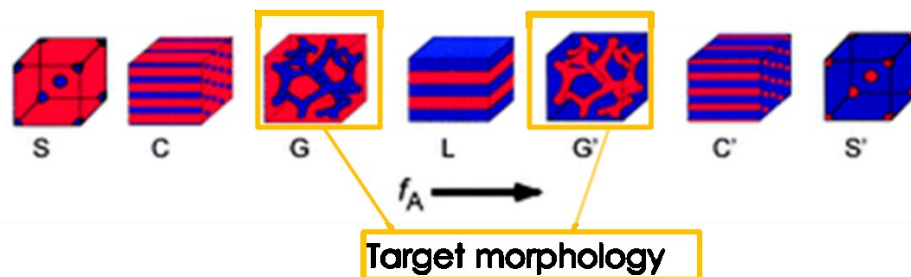


Figure 20: Illustration of different morphologies produced from varying the mole fraction of two different blocks in a block copolymer

In this study, a soft-templating approach was applied with the intention to create a co-continuous network of pores. The block copolymer study discussed above was applied to the soft-templating approach; instead of controlling mole fractions in a block copolymer, the method was applied to a mixture of polymer and liquid porogen (Figure 21).

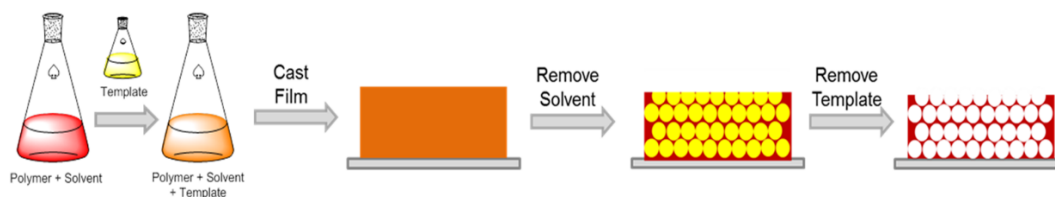


Figure 21: Soft templating of conductive polymers using a high-boiling liquid

The hypothesis was that the same minimization of Gibbs free energy would occur if a polymer solution and a non-solvent were used instead of two blocks in a block copolymer. The non-solvent would be a high-boiling liquid that did not dissolve the polymer, allowing the liquid to remain in the polymer matrix upon solvent removal. This high boiling solvent would generate pores in the polymer; thus, it is referred to as a “porogen”. Porogens for this study were chosen based upon several parameters: 1) The porogen must not be reactive with or dissolve the polymer; 2) The porogen must have a similar density to that of the polymer so that density-driven phase separation is not

encountered; 3) The template must have a high enough boiling point to remain in the polymer matrix during solvent removal.

### 3.3 Experimental

#### 3.3.1 Materials

ITO (indium-tin oxide) coated glass slides (surface resistance 8-12  $\Omega$ /sq.) were purchased from Delta Technologies. The two polymers P3HT and poly(ProDOT-Bu<sub>2</sub>) prepared as described in Chapter 2, were stored in sealed vials under argon until use in templating experiments. Chloroform purchased from VWR was neutralized before use in templating experiments by washing in a separatory funnel three times with saturated sodium bicarbonate. Acetone, chlorobenzene, dimethylsulfoxide, dimethylformamide, 1,4-dioxane, and ethanolamine were used as received from VWR. All deionized (DI) H<sub>2</sub>O used in these studies was 18 M $\Omega$  ultrapure water.

#### 3.3.2 Surface Treatment of Indium Tin Oxide Coated Glass

ITO glass slides were subjected to variety of different surface treatment methods. The surface treatment procedural details are provided below with contact angle measurement methods.

##### **Contact Angle Measurement Sample Preparation:**

The neat polymer solutions (poly(ProDOT-Bu<sub>2</sub>) in chloroform (no porogen present in solution) were deposited using a micropipette (10 microliter droplets) and contact angles were measured. A series of 30 measurements were taken of the droplet using the image software. Contact angle measurements on surface treated substrates were collected using a ramé-hart Model 200 Standard Goniometer with Dropimage Standard

v2.4 software (Windows operating system). Optical images were calibrated using spherical and cylindrical standards provided with the goniometer.

### **Surface Treatment Methods:**

#### ***1M HCl procedure:***

ITO glass slides were rinsed three times with H<sub>2</sub>O, wiped with an acetone dampened low lint paper wipe (KIMWIPE), dipped into 1M HCl, rinsed three more times with H<sub>2</sub>O, and stored in acetone prior to templating.

#### ***20% ethanolamine procedure (Delta Technologies)<sup>92</sup>:***

ITO glass slides were rinsed three times with H<sub>2</sub>O, wiped with an acetone dampened KIMWIPE, sonicated in a 20% (w/v) ethanolamine solution for 15 minutes, rinsed three more times with H<sub>2</sub>O, and stored in acetone prior to templating.

#### ***Oxygen-Plasma treatment:***

Prior to oxygen-plasma treatment, ITO glass slides were rinsed three times with H<sub>2</sub>O and wiped with an acetone dampened KIMWIPE. The procedure for operating the Harrick Plasma Cleaner was as follows:

1. ITO glass slides were placed into the plasma chamber. The chamber was allowed to evacuate for approximately two minutes by opening the needle valve to the connected vacuum pump.
2. The needle valve to the plasma chamber was opened to the outside room, and atmosphere was allowed to enter the chamber. The needle valve was then closed.

3. The plasma cleaner switch was then turned to the ON position while setting the RF (radio frequency) level to a low enough setting to generate a purplish-glow in the chamber.
4. ITO slides were allowed to plasma clean for about 10 minutes.
5. Upon completion, the plasma cleaner was turned off. The vacuum pump was switched to the off position. The needle valve to the chamber was opened to allow for atmosphere to enter the chamber and establish equilibrated pressure.
6. The door to the plasma chamber was opened, and the ITO glass slides were removed.
7. ITO glass slides were stored in acetone prior to templating.

### 3.3.3 Polymer Film Templating Methodology

#### **P3HT & poly(ProDOT-Bu<sub>2</sub>) Stock Solution Preparation:**

A stock solution of P3HT (20 mg/mL) was prepared using chloroform or chlorobenzene as the solvent. The mass of the polymer was measured using a 5-place balance. The polymer solution was stirred with heating at 50°C until bright orange; this generally occurred within 10 minutes.

Note: poly(ProDOT-Bu<sub>2</sub>) is deep violet/purple and does not change colors upon heating at 50°C.

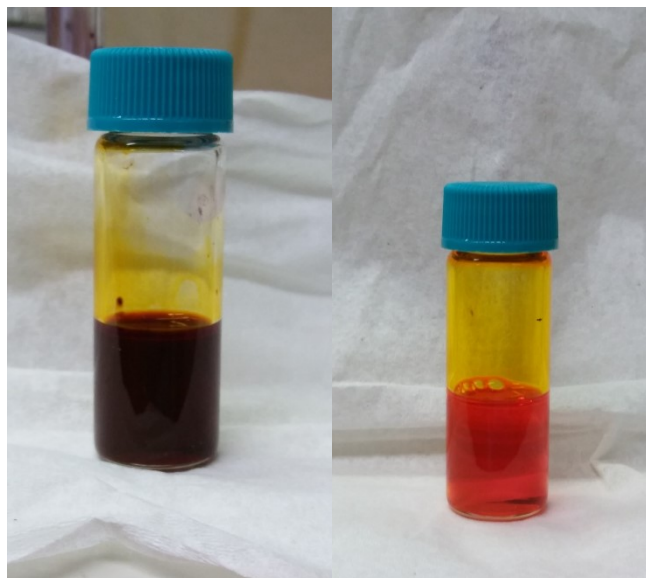


Figure 22: P3HT/chloroform solution pre and post solvation upon heating. P3HT solution left: pre-solvation, and right: post-solvation via heating and stirring at 50°C.

### **Templating Solution Preparation:**

Using a micropipette an aliquot of previously prepared stock solution was introduced into a clean, pre-weighed vial. A GC syringe was used to inject the desired amount of pore creating agent (porogen) into the pre-weighed vial. The solution was stirred for 24 h, in the dark, and in a sealed container at 50°C under argon.

The amount of porogen added to the templating solution was calculated as follows:

$$X = W * \frac{Y}{1-W} \text{ (Equation 5)}$$

X = mass of porogen (mg)

Y = mass of polymer (mg)

T= total mass (X + Y) (mg)

W= weight fraction of porogen desired (X/T)

The mass of the polymer (Y) found in the aliquot was calculated as shown below:

concentration of stock solution  $\left(\frac{\text{mg}}{\text{mL}}\right) * \text{aliquot volume (mL)} = Y(\text{mg})$  (Equation 6)

The volume of porogen needed was found using equation 5 and the solvent's mass and density at room temperature.

*Templating of Polymer Solutions:*

1. A leveled stage was created inside the annealing chamber (with a clean small glass sheet) using molding clay.
2. The annealing chamber was equilibrated by introducing an open 40 mL vial filled about halfway with the either chloroform or chlorobenzene.. The chamber was sealed, allowing solvent vapors to reach equilibrium for approximately 10 minutes.
3. The masses of the dry surface treated ITO slides were measured in triplicate using the 5-place balance. Care was taken not scratch or drop the ITO slides (small changes in mass of the slide dramatically impact the apparent mass of the films post templating). Slide mass changes would invalidate normalization of the film mass necessary for sample comparison.
4. The resistances of previously weighed ITO glass slides were measured using an Ohm meter keeping the distance between probes constant. The conductive side of the ITO is what is necessary to make electrical contact with the film during electrochemical analysis, and therefore MUST be facing upwards during templating. The general conductive side resistance was on the order of 26  $\Omega$ , while the non-conductive side generally did not register a resistance reading (OL).
5. The slides were introduced into the annealing chamber conductive side up, and placed onto the leveled stage. The chamber was sealed with slides inside and allowed to re-equilibrate for 5 minutes.

6. Aliquots of the desired template solution were withdrawn using a micropipette, and the chamber was opened. With the pipette perpendicular to the ITO glass, 15  $\mu$ L droplets were deposited onto the surface of each slide. The chamber was then closed.

7. The droplets were allowed to dry for a specified time depending upon the solvent system.

8. The chamber was then opened, and the ITO slides were withdrawn. The slides were stored in a clean dry container that would not damage the ITO glass.

#### **Removal of liquid porogen from films:**

The polymer-coated slide(s) were placed onto a clean glass sheet that would not damage the ITO glass and put into a vacuum oven. The samples were dried under vacuum over night at room temperature followed by drying at 20°C above the porogen boiling point for 24 hours. The slide(s) were removed from the oven and allowed to cool. The slides were then weighed carefully in triplicate using the 5-place balance.

#### **Modified Drying Protocols:**

Depending upon the solvent system chosen, the drying protocols can be modified to change the morphology of the film produced. The image shown in Figure 23 helps to visualize the importance of drying protocols on the film characteristics by showing that the same polymer solution and substrate combination can produce dramatically different results with a change in the drying protocol.

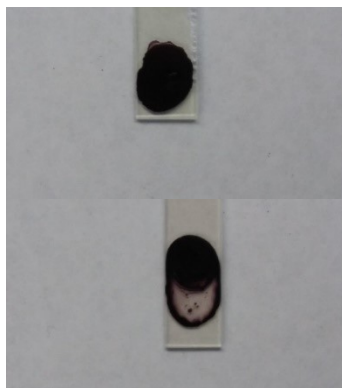


Figure 23: Images of P3HT films templated from a 15% DMSO/chlorobenzene solution on ITO glass with different drying conditions. Top image: P3HT film templated from 15% DMSO/chlorobenzene on ITO glass with enhanced drying rate. Bottom image: P3HT film templated from 15% DMSO/chlorobenzene on ITO glass, but dried in open air

The film dried with an “enhanced drying rate” has a completely different appearance from the film dried in open air. The “enhanced drying rate” is induced by a heat gun set to the “cold air” option and to the low airflow rate setting. This experimental set-up is shown in Figure 24.



Figure 24: Experimental setup to enhance film drying rate. Heat gun has hot and cold settings as well as two airflow settings (High and Low)

A unique set of polymer film morphologies was produced from a set of differing experimental conditions. The parameters that were modified included polymer type, solvent, porogen, and drying protocol. Table 3 presents the experimental conditions below. Solution concentrations of polymer were kept constant at approximately 20 mg/mL.

Table 3: Solvent Systems and Drying Protocols

Polymer	Solvent	Porogen	Drying Protocol
P3HT	chloroform	None	Solvent annealing
P3HT	chloroform	DMSO	Solvent annealing
P3HT	chloroform	DMSO	Open air
P3HT	chlorobenzene	None	Solvent annealing
P3HT	chlorobenzene	None	Open air
P3HT	chlorobenzene	None	Enhanced drying
P3HT	chlorobenzene	DMSO	Solvent annealing
P3HT	chlorobenzene	DMSO	Open air
P3HT	chlorobenzene	DMSO	Enhanced drying
poly(ProDOT-Bu <sub>2</sub> )	chloroform	None	Solvent annealing
poly(ProDOT-Bu <sub>2</sub> )	chloroform	DMSO	Solvent annealing
poly(ProDOT-Bu <sub>2</sub> )	chloroform	1,4-dioxane	Solvent annealing
poly(ProDOT-Bu <sub>2</sub> )	chloroform	ethanolamine	Solvent annealing

### 3.3.4 Microscopy

Electronically neutral polymer films templated onto surface treated ITO glass slides were freeze fractured by submerging into liquid nitrogen for 1 min and then cleaved for SEM (scanning electron microscopy) cross-sectional analysis. The samples were then coated with a layer of iridium using vapor deposition to inhibit surface

charging. Images were acquired with an FEI Helios NanoLab 400 DualBeam system using the charge reduction detector under high vacuum. Instrument parameters include an accelerating voltage of 5-10 kV and a beam current of 21 pico-amperes.

Optical images of films were collected using an Olympus BX60M optical microscope in “Simple Polarized Light Mode” along with the U-A/V360 Analyzer, and U-LBD-2 Filter.

### 3.4 Results and Discussion

#### 3.4.1 Polymer Solution Drying Physics

The differences in film quality are apparent with the images of the varying experimental systems presented below.

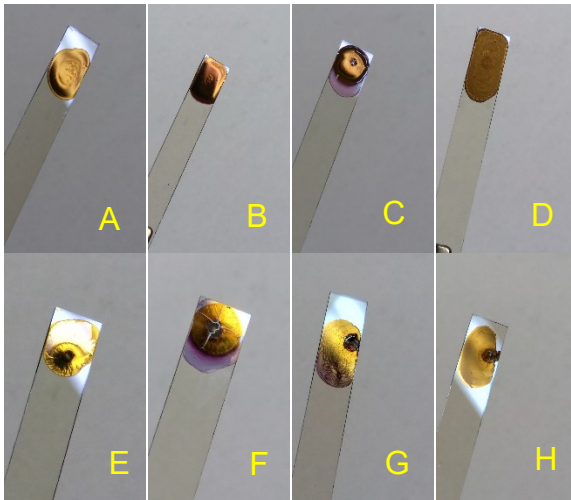


Figure 25: Images of templated polymer films. “A”: poly(ProDOT-Bu<sub>2</sub>)/CHCl<sub>3</sub>/solvent annealing, “B”): poly(ProDOT-Bu<sub>2</sub>)/CHCl<sub>3</sub>/1,4-dioxane/solvent annealing, “C”): poly(ProDOT-Bu<sub>2</sub>)/CHCl<sub>3</sub>/DMSO, “D”): poly(ProDOT-Bu<sub>2</sub>)/CHCl<sub>3</sub>/ethanolamine/solvent annealing, Film “E”): P3HT/CHCl<sub>3</sub>/solvent annealing, “F”): P3HT/CHCl<sub>3</sub>/DMSO/solvent annealing, “G”): P3HT/chlorobenzene/enhanced drying, “H”): P3HT/chlorobenzene/DMSO/enhanced drying

Macroscopic as well as microstructural film morphology changes occur with modifications in the drying protocol, as described in later sections. Each solvent system has a unique behavior when it comes to film drying. Consequently, this approach to creating porous polymer is not trivial. What is observed is that film characteristics

heavily depend on polymer structure, drying protocol, polymer rheology, solution parameters, and surface treatment of the substrate of choice. Even though this approach to soft templating is laborious, reproducibility is achievable with careful consideration of the system's important physical parameters.

It is crucial to understand the underlying physical parameters that determine unique droplet drying patterns. These patterns in droplet drying help predict the resultant polymer film morphology.<sup>93</sup> Ideally, film morphology should be predictable for a given solvent/substrate system.

The unique experimental conditions give rise to sample-specific drying behaviors. These drying behaviors can be predicted using droplet drying physics. Polymer solution drying is an abstract area of research that is also heavily influenced by yet another set of complex physical parameters that include: solubility parameters of the polymer, solution analyte concentrations, and interfacial interactions between the polymer solution droplet and the substrate.<sup>94</sup>

Flory Huggins theory is used to describe polymer dissolution. The polymer-solvent interaction is described as a statistical “random-walk” of the polymer molecule through a 2-dimensional lattice of solvent molecules. The polymer chain interaction with the solvent varies greatly with polymer structure.<sup>95</sup> The interaction of polymer chain with solvent is often a predictable and experimentally testable phenomenon. A physical parameter often used experimentally to determine polymer chain-solvent interactions is the hydrodynamic radius. The hydrodynamic radius of a dissolved polymer describes its size in the solution state. Dynamic light scattering measurements of P3HT in chloroform with varying amounts of DMSO have been used to measure parameters such as the

hydrodynamic radius and demonstrate the presence of solution state aggregation of polymer chains.<sup>48</sup> The changes in polymer solubility behavior in solution and the influence of solution drying environment constitute a complex mosaic of variables in predicting film morphologies. What is known is that the factors that influence film morphology can be influenced by a phenomenon called the Marangoni effect, which is described as a mass transfer along a surface tension gradient.<sup>94</sup> A surface tension gradient can be induced by yet another set of factors that include: solute shape, concentration gradients and solvent viscosity.<sup>96</sup> An illustration of this effect is presented in Figure 26.

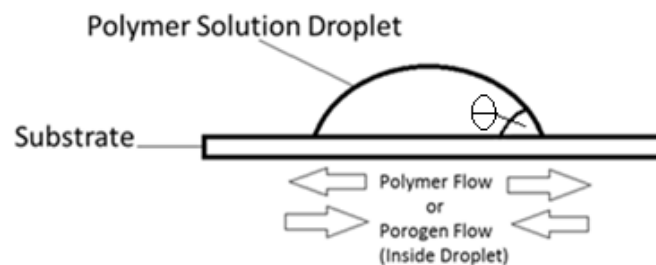


Figure 26: Marangoni flow illustration of polymer and porogen within a solution droplet on a substrate;  $\theta$  is the contact angle between the droplet and the substrate.

The influence of the Marangoni effect on polymer droplet drying will help elucidate the complex and seeming unrelated morphologies observed in the following section. The phenomenon can be used to explain the observed trends in film drying.

### 3.4.2 Contact Angle Measurements

It was observed that greater wettability of the substrate often lead to promoted film adhesion. In general, lower contact angle of a liquid on a surface implies greater wettability. Lower contact angle is a result of the adhesive force between the liquid droplet molecules being greater in magnitude than the cohesive force between the liquid molecules.<sup>98</sup> Surface treatment methodology was found to be of the utmost importance in

order to prevent polymer film delamination. The contact angles given in Figure 27 are the averages of the right and left angles of the droplet-substrate interface.

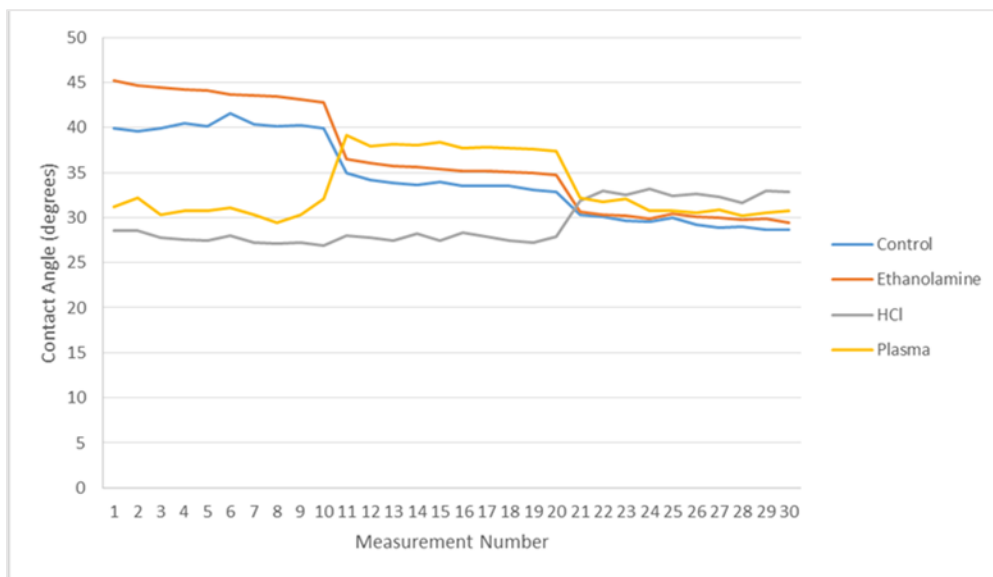


Figure 27: Contact angle study of poly(ProDOT-Bu<sub>2</sub>)/CHCl<sub>3</sub> droplets on surface treated ITO glass. Four different surface treatment methods were employed: control (no surface treatment), 10% ethanolamine with sonication, 1M HCl dip, and oxygen-plasma treatment

The contact angles converge by measurement number 30. This is due to the volatile nature of CHCl<sub>3</sub>. As the solvent evaporates the contact angle decreases due to less liquid available to create a droplet and the beginning of film formation. Initial contact measurements (measurements 1-10) show that the HCl surface treatment procedure produced the lowest contact angle of the various techniques employed. Contact angle images of the polymer solution can be observed in Figure 28. It has been experimentally determined that the treatment of a surface can affect the morphology of P3HT films.<sup>97</sup>

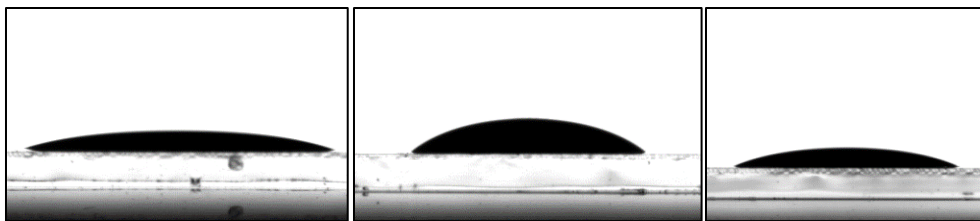


Figure 28: Contact angle images of poly(ProDOT-Bu<sub>2</sub>)/CHCl<sub>3</sub> solution on surface treated ITO glass. From the left: 1 M HCl, oxygen plasma, 20% ethanolamine

### 3.4.3 Investigation of Polymer Film Morphology

#### **Poly(ProDOT-Bu<sub>2</sub>)/CHCl<sub>3</sub>:**

Each film studied was templated from four separate solutions of poly(ProDOT-Bu<sub>2</sub>) dissolved in chloroform to which 28% (weight percent of porogen = [mass porogen/total mass] \* 100) of a uniquely chosen pore creating agent was added. The porogens chosen were DMSO, 1,4-dioxane, and ethanolamine. The fourth solution contained no porogen and was used to create a set of “control” films. All films were templated in an annealing chamber containing 40 mL of chloroform to reduce the rate of solvent evaporation from the film. The differing morphologies can be observed in SEM images presented in Figure 29. Additional images can be observed in Appendix (D.1-D.4).

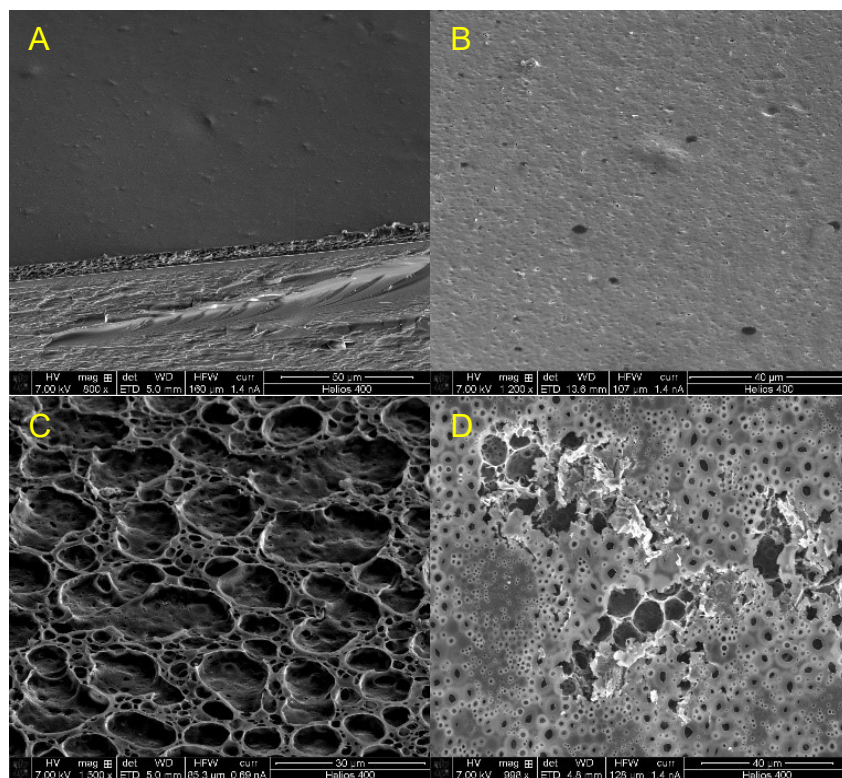


Figure 29: Poly(ProDOT-Bu<sub>2</sub>) films created from five different solvent systems. A) control film (no porogen), B) 28% 1,4-dioxane, C) 28% DMSO, D) 28% ethanoloamine

The 28% DMSO film is the only film that displays inhomogeneous film characteristics. Figure 30 shows that pore formation in the DMSO film is not consistent throughout the film. The central regions of the film display a control-like film morphology. This can be seen by comparing image “A” in Figure 30 with that of image “A” in Figure 29. Pore formation is isolated to the periphery of the film. There is an intermediate surface rough region in the DMSO film that is observed in image “B” of Figure 30. This could imply that the drying physics for the DMSO film during solution drying were not optimal. The DMSO film is also the only film in this experiment to have partial delamination towards the central region of the film (see Figure 30 image “A”). Porosity, as well as delamination of the central film region, is consistent across all four films templated using 28% DMSO solution. More studies are needed in order to

determine if delamination of the central region is directly correlated with the presence of DMSO in solution or other experimental factors. Solution wettability, polymer concentration, and surface defects in the ITO glass may also be potential causes of film delamination.

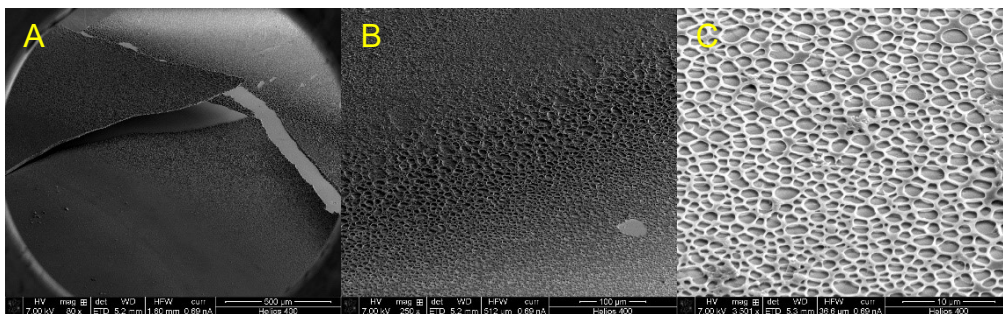


Figure 30: SEM images of DMSO film morphology: A) film overview, B) intermediate surface rough film region, C) film periphery showing unique pore formation

The control, 1,4-dioxane, and ethanolamine films all show consistent features throughout the film, as can be seen in Figure 31.

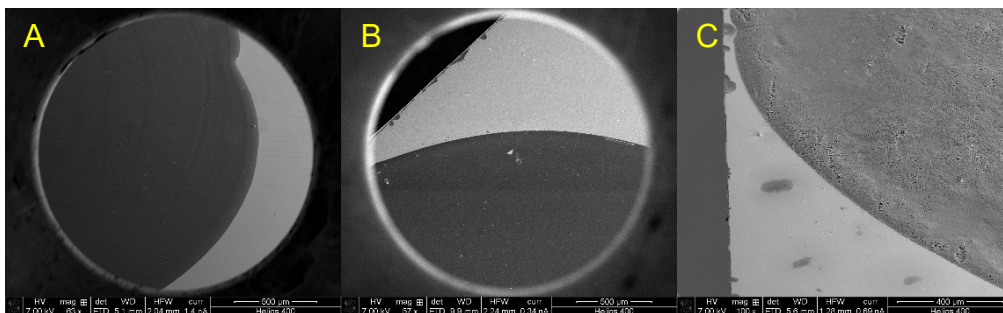


Figure 31: SEM images of film overview: A) control film, B) 1,4-dioxane, C) ethanolamine

The solutions containing 28% ethanolamine exhibited the most consistent pore features (Figure 32). Most pore features are smaller than 10 micrometers with some macro-pores larger than 10 micrometers. Unique film adhesion is present with leg-like polymer fibrils attached at the film edges; these fibrils were not observed with any of the other porogens or the control films.

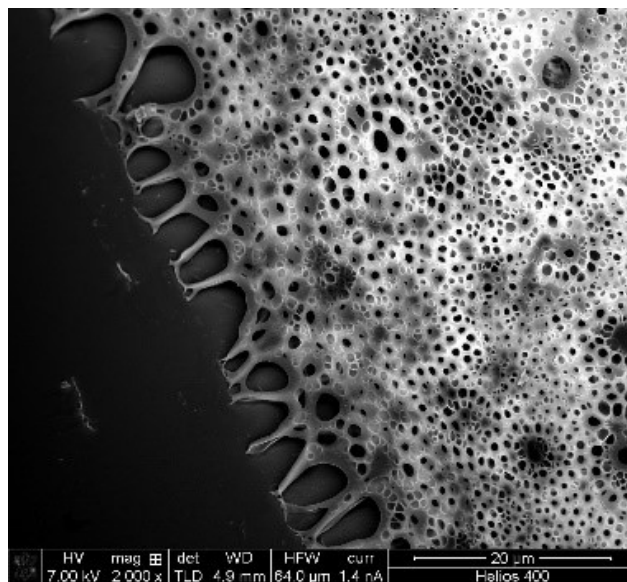


Figure 32: SEM image of 28% ethanolamine film with unique “leg-like” structures

Film thickness varies from film to film and with specific regions within a film.

Figure 33 shows the film cross-section of the four unique film morphologies. Film thicknesses are approximately as follows: control film-8  $\mu\text{m}$ , DMSO film (central region)- 28  $\mu\text{m}$  1,4-dioxane film-14  $\mu\text{m}$ , ethanolamine film- 28  $\mu\text{m}$ .

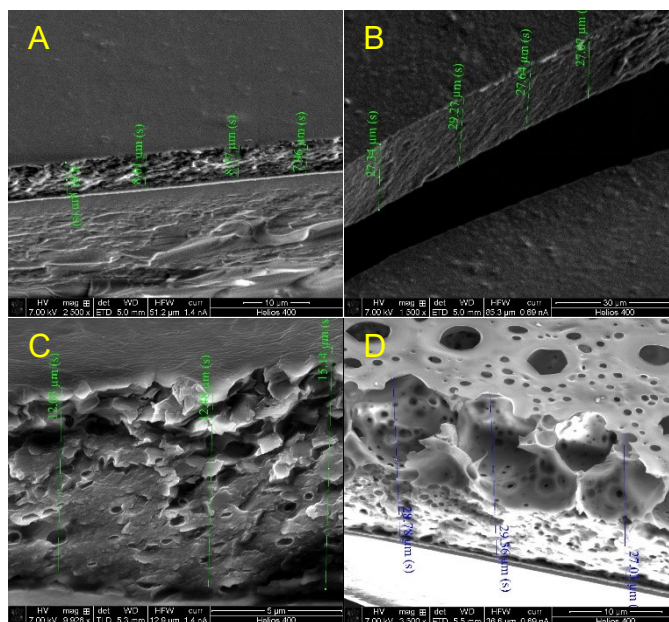


Figure 33: SEM images of film cross-sections: A) control film, B) DMSO film (central region of film), C) 1,4-dioxane film, D) ethanolamine film

### **P3HT/CHCl<sub>3</sub>/DMSO Porogen Percentage Spread:**

In order to investigate the effect of porogen concentration on film morphology, the amount of DMSO present in a P3HT/chloroform solution was varied from 0% to 55%. These samples utilized a solvent annealing protocol in which an annealing chamber containing 40 mL of chloroform was allowed to equilibrate prior to templating. No pore formation is present as expected for the control film (0% DMSO). This can be observed in Figure 34. Additional images for this experiment are available in Appendix (D.5-D.11).

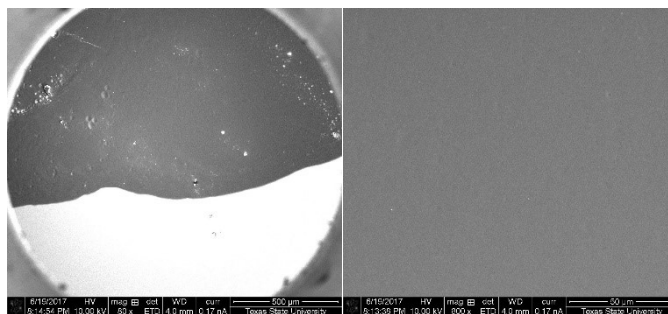


Figure 34: SEM image of experimental control (no DMSO present during templating)

The film morphology seems to follow a common drying pattern in which the polymer ends up depositing towards the center of the film. Pore formation ends up along the periphery of the polymer “rich” regions. Overall film morphology can be observed with the optical microscopy images provided in Figure 35. This observation may imply

the DMSO follows a surface tension gradient towards the edges of the solution droplet during drying. Pore formation is not interconnecting and very sparse.

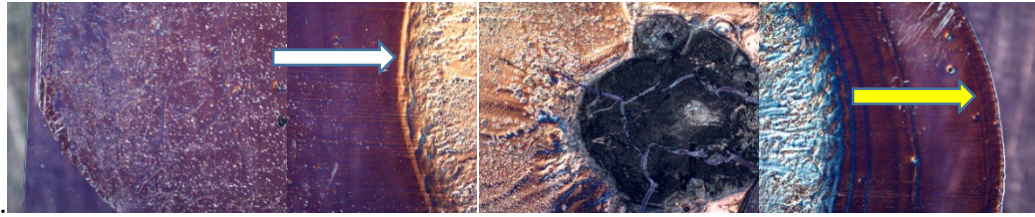


Figure 35: Optical microscopy images of a 25% DMSO/P3HT film templated from  $\text{CHCl}_3$ ; the white arrow points to a polymer “rich” region of the film where pore formation occurs, while the yellow arrow points to a region where the polymer film is thin and not as much polymer has deposited.

Although overall pore formation increases with increasing DMSO content, as previously described, it does not increase uniformly throughout the film. As can be seen in Figure 36, increasing DMSO percentage is accompanied by an increasing amount of pores present in the film on the edge of polymer “rich” regions.

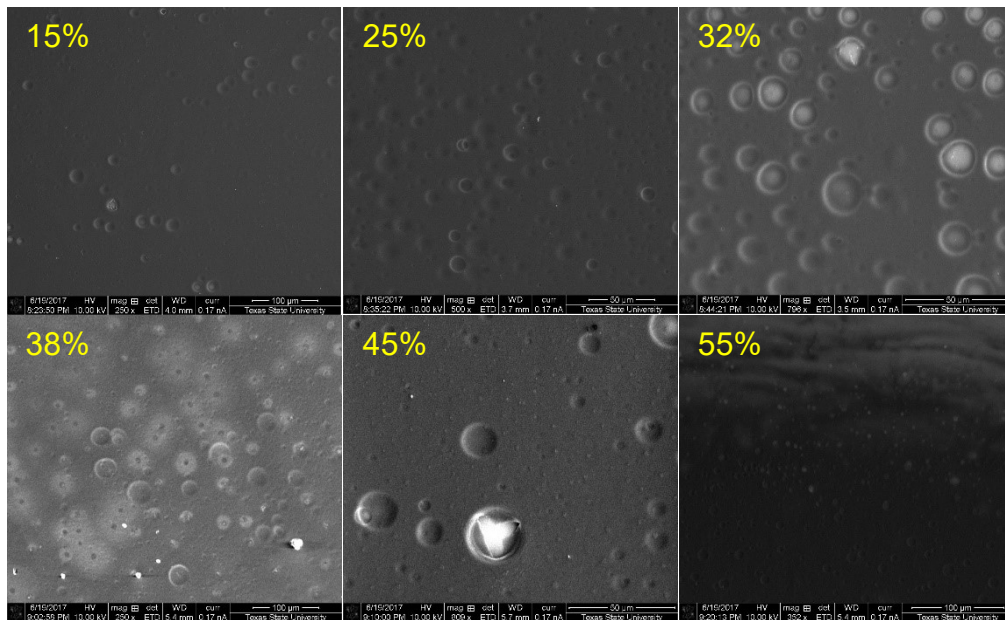


Figure 36: SEM images of morphology relationship-(pore formation increase with increase in DMSO percentage in templating solution): 15%, 25%, 32%, 38%, 45%, and 55%

Film failure at the center of the films is consistent all the way up to 55% DMSO films. A film failure is present at the center of the 0% DMSO film as shown in Figure 37.

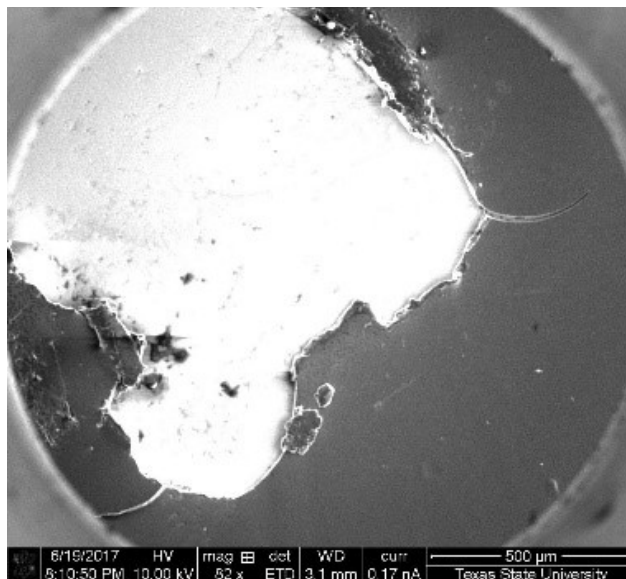


Figure 37: SEM image of 0% DMSO P3HT film failure

Film failure is a common feature in most polymer films. Some factors that affect the formation of film failures include: delamination from the substrate, polymer drying rate, polymer  $T_g$ , and the extent of film crystallinity.<sup>98</sup>

#### **P3HT/Chlorobenzene/DMSO Porogen Percentage Spread:**

After witnessing the morphology produced by the chloroform-based solvent system, the experiments were repeated using chlorobenzene as the solvent in an attempt to homogenize polymer deposition within the templated film. Chlorobenzene has a much lower vapor pressure than that of chloroform (1.6 kPa and 26 kPa respectively at 25°C)<sup>99,17</sup>, which was expected to result in reduced evaporation rate. This difference in evaporation rate could allow for more control over polymer solution drying rate, resulting in a more distinct trend in pore formation with varying DMSO percentage.

The chlorobenzene solutions produced with varying amounts of DMSO (0%-55%) were all subjected to an enhanced drying rate using the experimental set-up shown previously in Figure 24. The heat gun, set to the “cold” and “low” airflow rate settings, was positioned at a set distance above the open annealing chamber. Films were templated on a level glass stage and dried using the heat gun.

This approach to film drying has created some unique film morphologies. Polymer deposition seems to be more consistent than that of the chloroform system. This can be observed in Figure 38. Additional images for this experiment are presented in Appendix (D.12-D.18). The polymer film is more homogenous when templated from the chlorobenzene-based solvent systems. There are no polymer “rich” regions that are segregated from thinner polymer film regions.

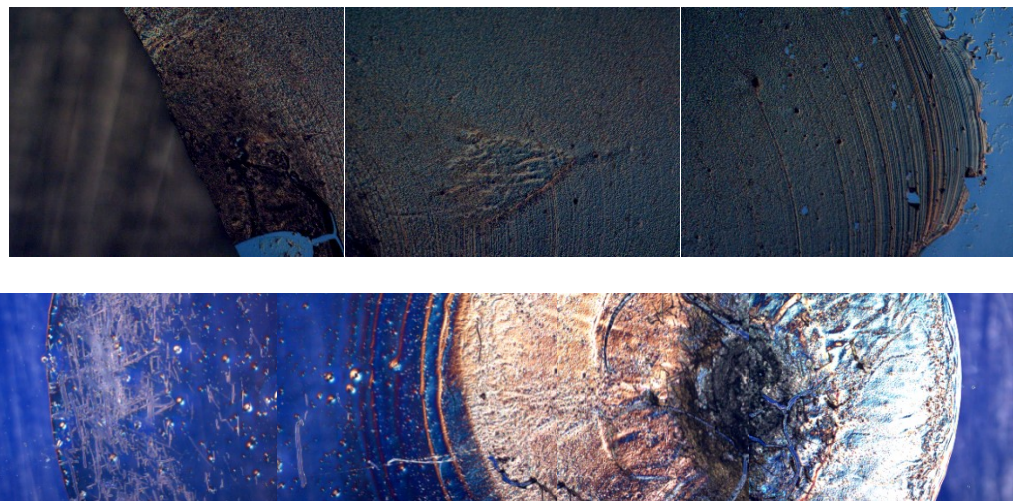


Figure 38: Optical microscopy of two P3HT films templated from different solvent systems: Top film image displays a film templated from a 15% DMSO/chlorobenzene solution. Bottom image displays a film templated from a 15% DMSO/CHCl<sub>3</sub> solution.

As expected, the 0% DMSO control film displays no apparent pore formation. This is shown in Figure 39. The 0% DMSO film displays unique drying features. The lines observed in the film are most likely a consequence of film drying and the pinning of the polymer solution droplet and the ITO glass substrate.<sup>100</sup>

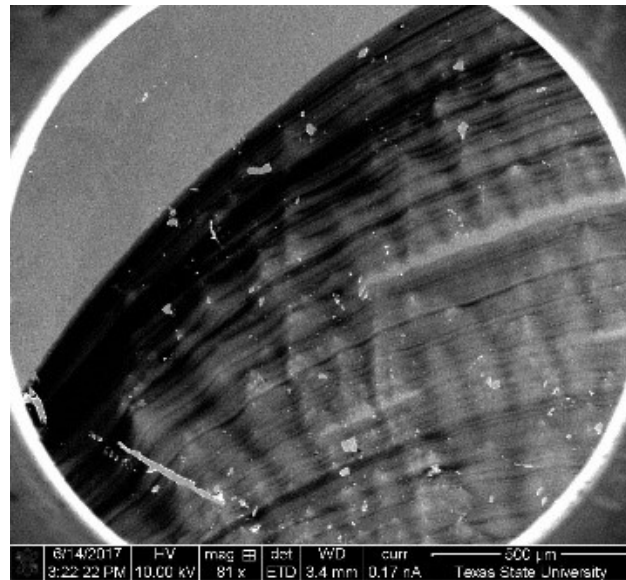


Figure 39: SEM image of a P3HT film templated from chlorobenzene (0% DMSO) with no pore formation

There is also noticeably more pore formation, and a somewhat distinct trend to the number and location of the pores formed as DMSO concentration is increased. This observation is shown in Figure 40.

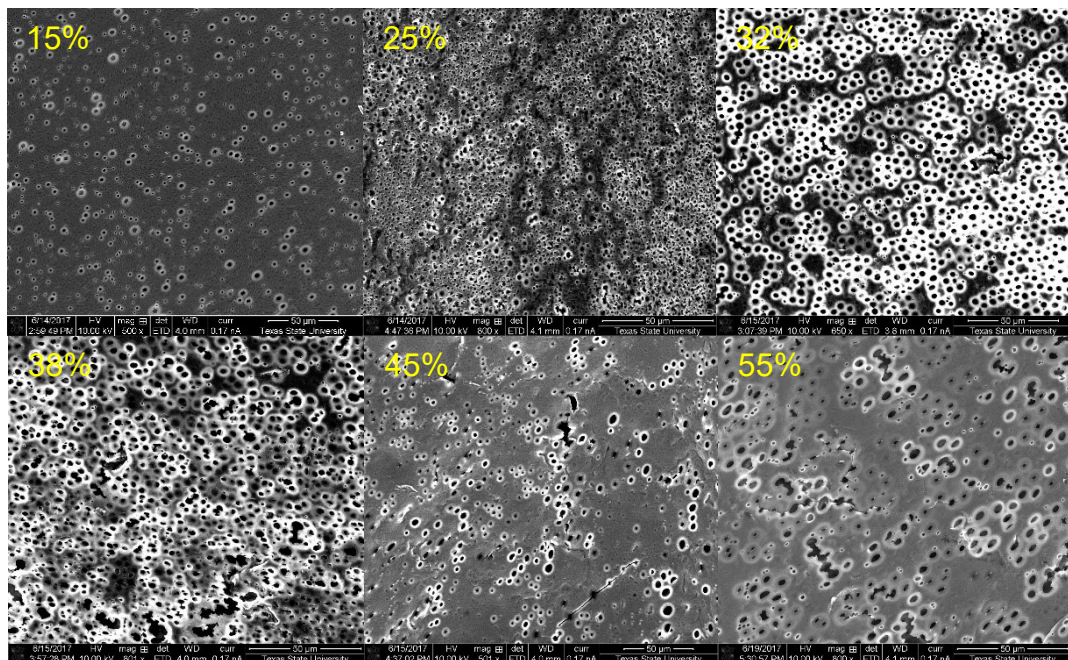


Figure 40: SEM images of morphology relationship-(pore formation increase at the internal region of the film with increase in DMSO percentage in templating solution): 15%, 25%, 32%, 38%, 45%, and 55%

In Figure 41, pore formation can be seen to migrate towards the edges of the film with higher percentages of DMSO. The drying physics of the system could be changing introducing a difference in concentration of DMSO within certain regions of the film. Much like the poly(ProDOT-Bu<sub>2</sub>)/CHCl<sub>3</sub>/ 28% DMSO system, the DMSO tends to migrate to the periphery of the droplet. A Marangoni-like effect seems to be driving pore formation at different percentages of DMSO in solution. At lower percentages of DMSO the pore formation seems to accumulate internally at the center of the film. This implies a reversal of the surface tension gradient described by the Marangoni effect.

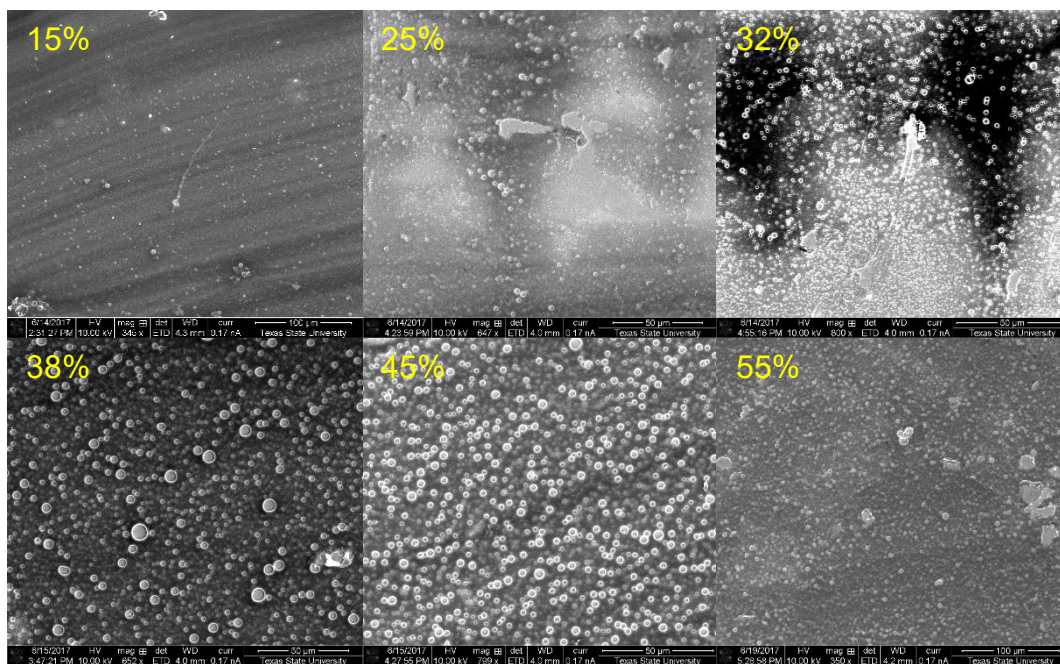


Figure 41: SEM images of morphology relationship-(pore formation increase at the edges of the film with increase in DMSO percentage in templating solution): 15%, 25%, 32%, 38%, 45%, and 55%

An optical microscope image showing the regions where pore formation accumulates at differing percentages is presented in Figure 42.



Figure 42: Optical microscope image of a P3HT film templated from 32% DMSO/chlorobenzene. The white arrow indicates where pore formation accumulates at lower DMSO percentages (left film edge), and the yellow arrow shows where pore formation accumulates at the higher DMSO percentages (right film edge)

Some film failure persists throughout the films, but not on the same scale as the chloroform-based films. The chlorobenzene films all have very distinct regions within the films. Each film has a heavily porous region, a “pore gradient” region, and a thin, lightly porous region. The pore gradient can be observed in Figure 43.

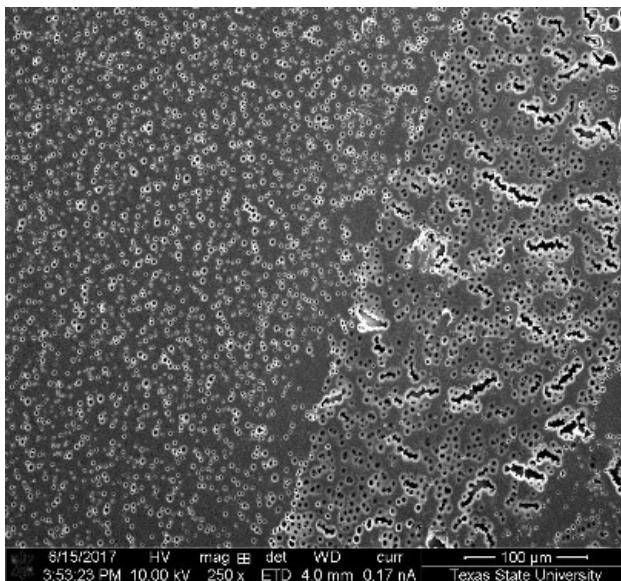


Figure 43: SEM image of a dramatic “pore gradient” observed in the 38% DMSO/chlorobenzene film

The trend in pore formation seems to imply that the system is highly dependent upon the percentage of DMSO present in the templating solution. Marangoni drying effects dictate where and how many pores accumulate in a specific film region.

### 3.4.4 UV-Vis Analysis of Polymer Solutions and Films

#### Motivation for Research:

A number of electronic transitions that occur for P3HT film samples as a consequence of film morphology characteristics can be observed using UV-Vis spectroscopy. The transitions that are of high interest are of those electronic states that correspond to P3HT aggregates ( $\pi$ - $\pi$  stacking).<sup>49</sup> The confirmation of aggregation in a P3HT film helps characterize a film's electronic properties and may imply some structural characteristics such as molecular ordering within a particular film sample.<sup>45,46,48</sup>

#### Solution-State Experimental:

A series of P3HT/CHCl<sub>3</sub> solutions was prepared by diluting 20 mg/mL stock solution with CHCl<sub>3</sub>. Resulting polymer concentrations studied were 5, 1, 0.05, 0.025, and 0.01 mg/mL. In order to determine the optimal concentration for further solution-state UV-Vis experiments with P3HT, each diluted solution was analyzed from 300-700 nm using a Perkin Elmer Lambda 365. The results are presented in Figure 44.

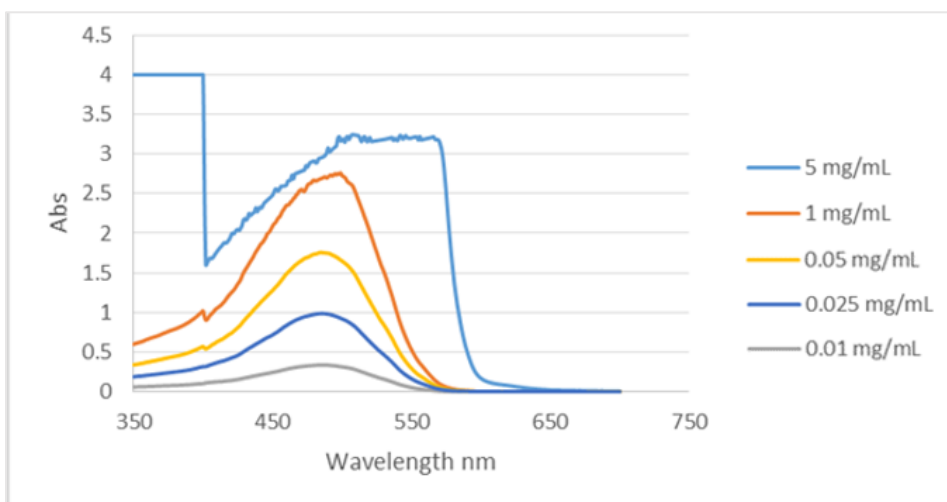


Figure 44: Diluted P3HT/chloroform solution UV-Vis analysis: 5 different polymer concentrations were scanned from 300-700 nm. 0.025 mg/mL produced a solution absorbance closest to 1 abs unit.

Based on the absorption spectra shown in Figure 44, further P3HT solution studies were conducted using 0.025 mg/mL, because this concentration produced a solution absorbance closest to 1 absorbance unit. A 55% DMSO solution was produced (using Equation 5, pg. 42). The amount of DMSO was added to a 20 mg/mL P3HT/CHCl<sub>3</sub> stock solution so the weight percent of DMSO ( $X/T = 0.55$ , where X is DMSO mass in mg and T is total mass (DMSO + P3HT mass in mg) is equal to 55% (volume of CHCl<sub>3</sub> is excluded from calculation). Once the 55% DMSO 20 mg/mL P3HT/CHCl<sub>3</sub> was produced, the solution was diluted further with CHCl<sub>3</sub> to a final concentration of 0.025 mg/mL P3HT/CHCl<sub>3</sub>. The diluted solution was scanned from 300-700nm and compared to the diluted stock solution (0.025 mg/mL P3HT/CHCl<sub>3</sub> with no DMSO present as a control solution). The purpose of this experiment was to identify whether or not solution state aggregation was detectable upon addition of DMSO to solution. The results are presented in Figure 45.

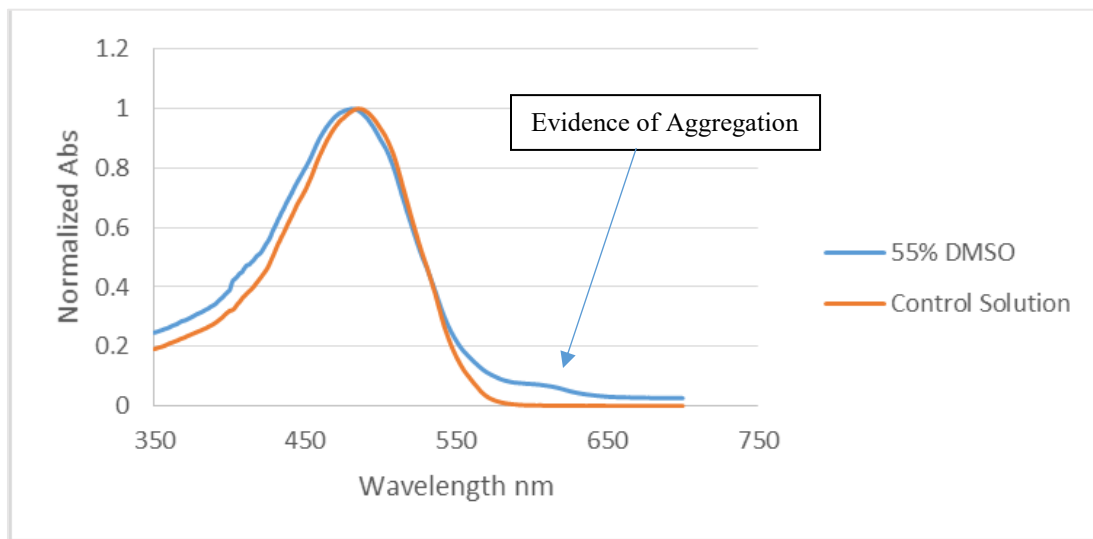


Figure 45: UV-vis comparison of a 0.025mg/mL P3HT/CHCl<sub>3</sub> stock solution (control solution) and 55% DMSO 0.025mg/mL P3HT/CHCl<sub>3</sub> solution. Both spectra presented are normalized for comparison. Notice the increased absorbance from approximately 600-650nm.

Addition of DMSO to the solution results in an additional absorption occurring around 600 nm. This feature is consistent with literature P3HT aggregation wavelengths that correspond to interchain excitations that evolve out of  $\pi$ - $\pi$  stacking. The feature at 455 nm is consistent with the  $\pi$ - $\pi^*$  excitation of P3HT.<sup>49</sup>

### Solid-State Experimental:

Solutions of P3HT (20 mg/mL, the same as those used in templating experiments) with varying DMSO percentages were templated onto borosilicate glass slides (no ITO coating), and thin films were created using a drawdown bar purchased from GARDCO. Wire #3 was used in the drawdown experiments because it is known to produce films approximately 7.7  $\mu\text{m}$  thick. The films were dried under vacuum overnight at 50°C. After cooling, UV-Vis spectra of the films were acquired from 300-700nm using a BioTek sample plate. Differences between solution and solid-state film spectra can be seen in Figure 46.

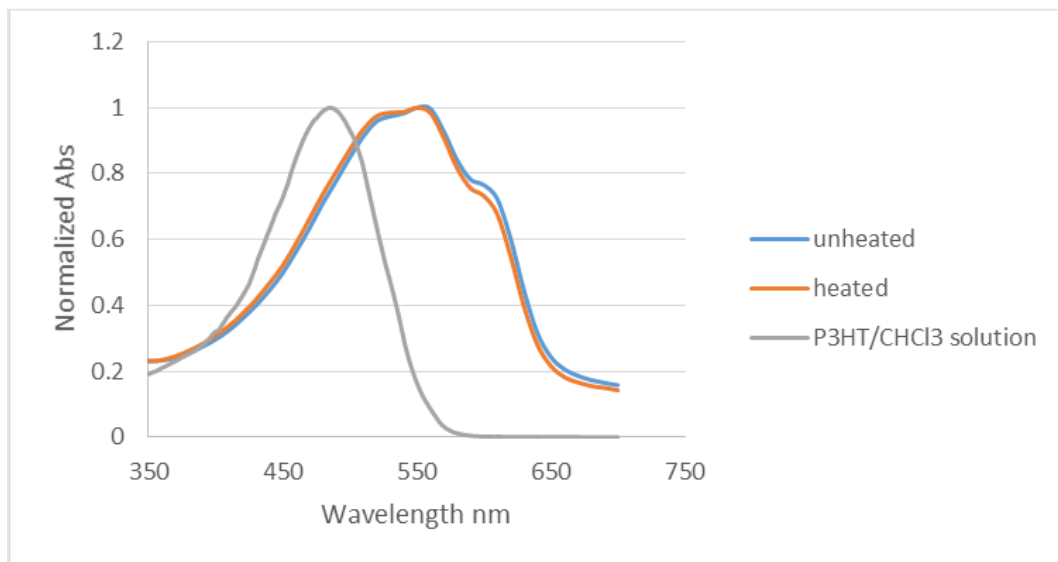


Figure 46: UV-vis comparison of solution P3HT solution and solid state draw-down film sample templated from heated and unheated solutions.

As can be seen in Figures 45 and 46, solution state spectra do not contain any evidence of aggregation present in solution unless DMSO is present. Not surprisingly, all solid state P3HT samples show the aggregation peak at 600nm. The presence of a red-shift in the spectrum going from solution state to solid state P3HT samples implies different orientation of chains and the formation of intra-chain excitations.<sup>49</sup> Changing DMSO concentration during drawdown casting did not produce any trends in the UV/Vis spectra of dried films (Figure 47).

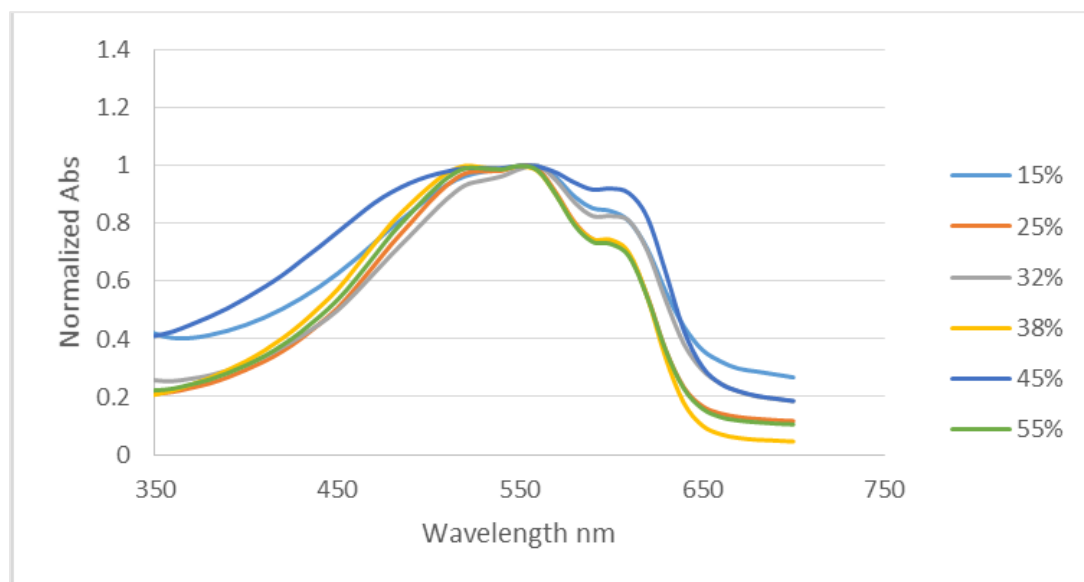


Figure 47: UV-vis analysis of draw-down films templated from increasing DMSO percentage in solution

## 4. ELECTROCHEMICAL ANALYSIS OF POLYMER FILMS

### 4.1 Motivation for Research

Conductive polymers can be chemically and electrochemically doped. Cyclic voltammetry (CV) allows for careful control of the voltage window and for other experimental parameters such as the scan rate. The conductive polymer films templated in Chapter 3 have a unique set of morphologies that have a dramatic impact on the electrochemical properties of the polymers. Cyclic voltammetry experiments were conducted in order to understand the morphology dependency of electrochemical behavior.

### 4.2 Cyclic Voltammetry Background

An indispensable tool used for studying the electrochemical behavior of many different chemical species is cyclic voltammetry. What makes this analytical technique so useful is that the electrical parameters, such as voltage window or scan rate of an experiment, can be well controlled and tailored to the specific conditions needed for the analyte. A large variety of properties (examples: redox potentials, diffusion kinetics, capacitance values, etc.) of a system can be quickly evaluated with reasonable sample sizes.

In the three-electrode cell configuration commonly utilized in cyclic voltammetry, three separate electrodes are immersed in an electrolyte solution (Figure 48). Probing the system electrochemically involves application of a potential difference across two electrodes, the working electrode (WE) and the counter electrode (CE), while referencing the potential to a known redox couple at the reference electrode (RE).<sup>101,26</sup> The working electrode can have a variety of different shapes and material compositions; in this study

the working electrode is an indium tin oxide (ITO) coated glass slide. The counter electrode is usually an inert metal (platinum) with high surface area to act as a source and sink of electrons. The reference electrode maintains a constant reference voltage in order to measure the voltages of the redox processes occurring at the working electrode; the Ag/AgCl reference electrode was used for these studies.<sup>101,26</sup> A waveform generator called a potentiostat (usually controlled using a computer) applies a potential difference across the working and counter electrodes. This waveform generator can control the voltage window and the rate at which the voltage change is applied. During this process the reference electrode maintains a very low input impedance to measure the voltage of the system. Depending on the voltage applied, the analyte at the working electrode becomes oxidized or reduced. Cations or anions supplied by the electrolyte are necessary to aid in charge balancing at the surface of the electrodes and maintain solution conductivity.

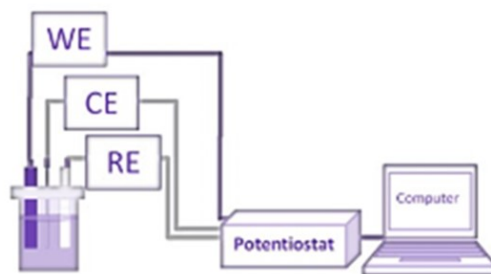


Figure 48: Experimental set-up for electrochemical analysis of film samples. (WE=working electrode, CE= counter electrode, RE= reference electrode)

### 4.3 Theory of Immobilized Redox Centers

During a CV experiment, when a potential is applied the species present in solution readily diffuse to and from the working electrode surface. Depending on the voltage bias, the species present at the surface of the working electrode are either oxidized or reduced. Current response of the system is dependent upon the amount of analyte present at the surface of the electrode. As an electrochemical process occurs, the current response initially rises with increasing amount of analyte (being reduced or oxidized) diffusing to the surface of the electrode.<sup>101,26</sup> Conversely, the current response decreases as the concentration of the redox active species decreases at the electrode surface. The Randles-Sevcik equation<sup>26</sup> captures this relationship:

$$i_p = (2.69 \times 10^5) n^{3/2} A D^{1/2} C^b v^{1/2} \text{ (Equation 7)}$$

where  $n$  is the number of electrons transferred,  $A$  is the electrode surface area ( $\text{cm}^2$ ),  $D$  is the diffusional constant ( $\text{cm}^2\text{s}^{-1}$ ),  $C^b$  is the bulk concentration ( $\text{molcm}^{-3}$ ) and  $v$  is the scan rate ( $\text{Vs}^{-1}$ ). In a diffusion-controlled electrochemical system the peak current is proportional to the square root of the scan rate.<sup>101,26</sup>

In this study, the conductive polymer films are immobilized on the surface of the working electrode, so their electrochemical behavior is not expected to be diffusion controlled, and the Randles-Sevcik equation does not apply. Instead, the electrochemical behavior of the polymer films is described by the theory of surface immobilized redox centers.<sup>101,26</sup> Assuming the analyte in question is immobilized on the electrode surface, then the relationship of peak current to scan rate should follow this equation:

$$i_p = \frac{n^2 F^2 \Gamma v}{4RT} \text{ (Equation 8)}$$

Here,  $n$  is the number of electrons transferred,  $v$  is the scan rate,  $F$  is Faraday's constant ( $C\ mol^{-1}$ ),  $R$  is the gas constant ( $J\ K^{-1}\ mol^{-1}$ ),  $T$  is the temperature (K), and  $\Gamma$  represents the total amount of reactant initially present at the electrode surface. An important aspect of this equation is that for an analyte that is adhered to the electrode surface, the graph of peak current response versus scan rate will produce a linear relationship.

The importance of the linear relationship for this study comes into play when determining if a particular film that is scanned electrochemically behaves according to the theory of immobilized redox centers. If a linear relationship between current response and scan rate is observed, it is implied that a film is well adhered to the working electrode. This is crucial to the experiment because if the process was diffusion controlled then the relationship between film electrochemistry and morphology could not be determined.

#### 4.4 Electrochemical Characterization of Polymer Films

##### 4.4.1 Experimental

###### **Instrumentation:**

The potentiostat-software combination used was a Pine Wavenow system supported by the Windows-based AfterMath Pine research program (Version 1.2.483). The three-electrode configuration was used, and the electrode types are as follows: ITO coated glass working electrode, platinum flag counter electrode, and Basi Ag/AgCl reference electrode.

**Materials:**

All electrochemical experiments in this study were conducted in aqueous solutions (18 M $\Omega$  ultrapure water). The supporting electrolyte used was a 0.1M aqueous solution of tetra n-butylammonium tetrafluoroborate (TBABF<sub>4</sub>). TBABF<sub>4</sub> was recrystallized from a 1,2-dichloroethane/hexane mixed solvent system. Crystals were washed with chilled hexane, dried in vacuum at 50°C, sealed in a vial under argon, and stored in a dark desiccator prior to use. ITO (indium-tin oxide) coated glass slides (surface resistance 8-12  $\Omega$ /sq.) were purchased from Delta Technologies. Prior to use, ITO slides for electrochemical studies were surface treated according to the *IM HCl procedure* discussed in Chapter 3 section 3.3.2.

**Cyclic Voltammetry Experimental Parameters:**

A 1.4 V window (-0.2 - +1.2V) was used for all electrochemical experiments. The electrolyte solution was bubbled with argon to remove any dissolved gasses prior to the experiment. All films (electrochemical analyte) were scanned from 100 mV/s to 500 mV/s (five different experiments per film). The resulting linear regression coefficients of each scan-rate dependency plot for each film studied are provided in Appendix E (Table 5). An example scan-rate dependency plot is shown in Figure 49.

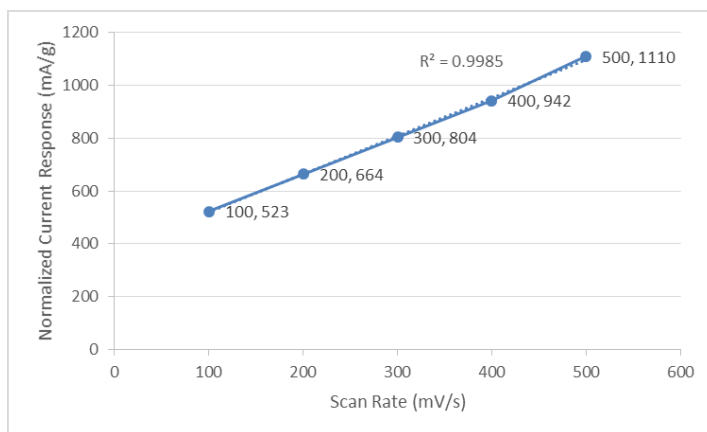


Figure 49: Scan-rate dependency plot for a P3HT film templated from chloroform. Linear regression coefficient close to 1 implies that the polymer film is well-adhered to the ITO working electrode.

### Gravimetric analysis:

Post-templating, the ITO glass slides were weighed in triplicate using an analytical balance accurate to the fifth decimal place. The film masses were calculated by subtracting the mass of the ITO slide from the combined mass of the ITO slide and polymer film. Variation in film mass is accounted for in the electrochemical results by mass normalization (division of sample current response at each voltage value by the film mass in grams). The corresponding current responses in the following cyclic voltammetry experiments are presented in milliamperes per gram. Film mass data is provided in Appendix F.

#### 4.4.2 Poly(ProDOT-Bu<sub>2</sub>):

The films templated from the poly(ProDOT-Bu<sub>2</sub>)/CHCl<sub>3</sub> solvent system with porogens (28%) DMSO, 1,4-dioxane, and ethanolamine were electrochemically analyzed at five different scan rates. The data from those experiments are collected in Figure 50 comparing the electrochemical responses of the films at the 300 mV/s scan rate.

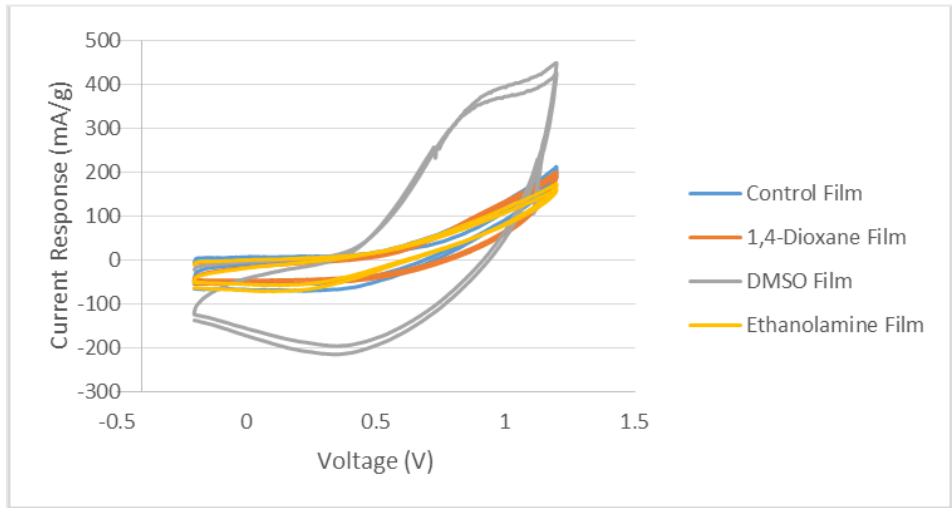


Figure 50: Cyclic voltammograms of poly(ProDOT-Bu<sub>2</sub>) films templated using three different porogens as compared to a control film prepared without a porogen.

Onset of polymer oxidation occurs around +0.5V relative to the Ag/AgCl redox couple. This is consistent for all four films studied. The 1,4-dioxane, ethanolamine, and control films (no porogen) all display similar electrochemical responses. Peak current for these films approaches approximately 200 mA/g. The DMSO film significantly outperforms the other films by at least two-fold in terms of current response.

The lack of performance by the ethanolamine film is notable. As can be seen in Chapter 3, the ethanolamine-templated films are highly porous. Theoretically, this film should display electrochemistry similar to that of the DMSO film. Higher film surface area implies greater access to the charge-balancing electrolyte in solution during electrochemical doping. While this should allow for increased electroactivity, the electrochemical performance of the ethanolamine-templated film is comparable to that of the control film.

These results imply there is an unseen factor that inhibits electroactivity of ethanolamine-templated films. There are a few possible explanations for the lack of

performance in these films. One explanation could be minimal contact of the polymer with the ITO substrate. This would generate higher series resistance in the electrochemical cell thus lowering observed current response. A second explanation is that during templating the incorporation of ethanolamine as a porogen has disrupted the aggregation formation during droplet drying. It is possible that ethanolamine behaves differently than DMSO as an aggregate forming solvent. There is significant evidence in the literature of non-solvent incorporation into P3HT solutions introducing aggregation.<sup>102</sup> Due to differing alkyl chain functionality (two butyl groups attached to the cyclic ether), poly(ProDOT-Bu<sub>2</sub>) most likely behaves differently in terms of aggregation in the presence of a non-solvent. More data that shows the formation of aggregates in poly(ProDOT-Bu<sub>2</sub>) is needed before solid conclusions are made for this system in terms of the connection between electrochemical behavior and chain orientation in the solid state. Cyclic voltammograms of films templated with each porogen (ethanolamine, DMSO, 1,4-dioxane) and the experimental control film are presented in Appendix G.

#### **Testing the chemical reactivity of poly(ProDOT-Bu<sub>2</sub>) with ethanolamine:**

Another possibility for the low ethanolamine film performance is that the solvent may be chemically reacting with the polymer. One of the parameters of porogen choice during the pre-screening stage is that the solvent must not chemically react or dissolve the polymer. Before ethanolamine was chosen as a porogen a small mass of poly(ProDOT-Bu<sub>2</sub>) was placed into a test tube filled with ethanolamine. Ethanolamine was not observed to dissolve the polymer.

Chemical reactivity was tested by exposing a set of templated poly(ProDOT-Bu<sub>2</sub>) films (DMSO as a porogen) to ethanolamine. Exposure of the films was accomplished by submerging in ethanolamine. This can be visualized in Figure 51 below.



Figure 51: Image of poly(ProDOT-Bu<sub>2</sub>) films submerged in ethanolamine

The ethanolamine-exposed films were then rinsed three times with ultrapure deionized water, dried in a vacuum oven overnight at 50°C, cooled to room temperature, then electrochemically analyzed using the same cyclic voltammetry techniques employed with the previously studied films in this chapter.

As can be seen in Figure 52, there is a significant drop in current response (almost 200 mV/g) when comparing a control film that has not been exposed to ethanolamine with a film that has been exposed to ethanolamine. This may be due to a chemical reaction occurring between the polymer and ethanolamine. The exact nature of this reaction is unclear, but it may involve an electrochemically irreversible reaction of the polarons and/or bipolarons formed during oxidation with the lone pair of the

ethanolamine nitrogen. If the product formed was electrochemically inactive, overall polymer electroactivity would decrease.

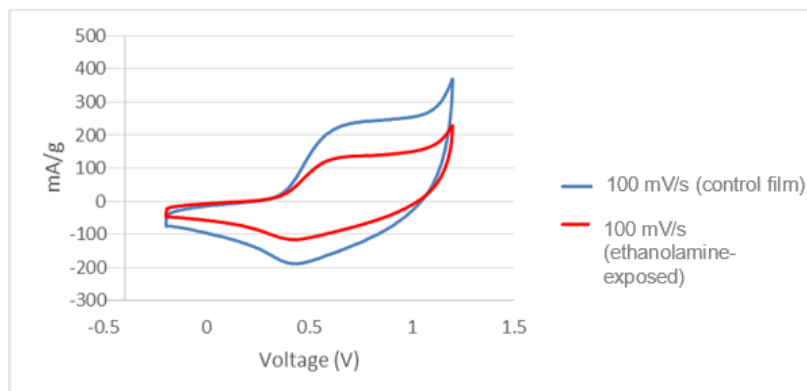


Figure 52: Comparison of cyclic voltammograms from a control film and one exposed to ethanolamine

The existence of a chemical reaction occurring between ethanolamine and poly(ProDOT-Bu<sub>2</sub>) could be confirmed by experimentation using NMR and/or FT-IR.

#### 4.4.3 Poly(3-hexylthiophene)

##### **Chloroform as Solvent (DMSO percentage spread 0%-55%):**

Presented in Figure 53 below is the normalized peak current response of the previously investigated porogen spread film study in Chapter 3 using CHCl<sub>3</sub> as the primary solvent and DMSO as the porogen (0-55 weight percent). As DMSO percentage in the graph increases there does not appear to be a significant dependence of current response on DMSO percentage.

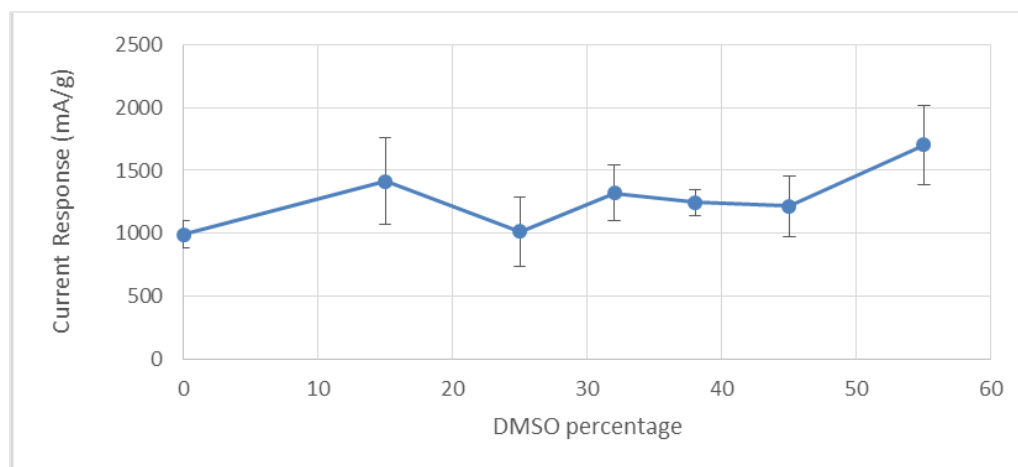


Figure 53: Normalized peak current response for P3HT/ $\text{CHCl}_3$  films with increasing amounts of DMSO at 500mV/s. Curve given represents the averaged current response for three tested films at each DMSO percentage.

The poor quality of templated P3HT/ $\text{CHCl}_3$  films may be the reason for the lack of apparent trends in performance; film failures may result in inhomogeneous doping across samples, making film comparison difficult.

The CV showing the cycled electrochemical data tells a slightly different story (Figure 54). There seems to be a slight trend in the area underneath each CV. This will be shown more vividly in the chlorobenzene solvent studies. The morphology investigation revealed a relationship between the amount of pores and DMSO percentage. It is possible there is a slight increase in surface area when going to higher percentage of DMSO samples. This can translate into electrochemical behavior that is more capacitive in nature, which can be observed by an increase in area under a CV curve.

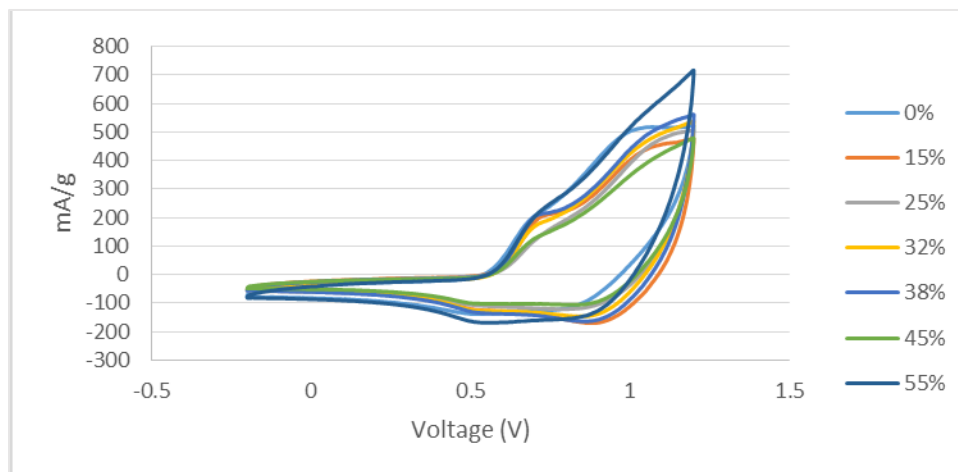


Figure 54: 100 mV/s scans at different percentages of DMSO (chloroform-based solvent system)

### Control Film Drying Experiment:

In the control film drying experiment, the P3HT/ $\text{CHCl}_3$  stock solution (approximately 20 mg/mL) used in the previous templating experiments was deposited onto 1M HCl treated ITO glass. Each sample was subjected to a varied drying time by modifying the surrounding experimental environment. Film set 1 (each film set is three slides) was templated in open air. Film set 2 was templated in the closed annealing chamber with no  $\text{CHCl}_3$  in the chamber. The third film set was annealed in a chamber with 40 mL of  $\text{CHCl}_3$ . The films were then electrochemically tested using the same experimental parameters as described in the above sections. Each film's drying time was timed. The drying time versus average peak current response at 500 mV/s is presented below in Figure 55. Peak current response can be seen to increase with solution drying time when solutions are allowed to drying from 1-5 minutes. This is plausible due to the time-dependent nature of aggregate formation in P3HT solutions. Additional experiments are needed to establish a trend (or lack of trend) between film current response and the presence of aggregates in film samples. More data points are needed to establish the true

current response range for films that are allowed to dry for 0.5 minutes. There is a distinct outlier in the data-set for the 0.5 minute films (approximately 33 mA/g) adding to large error in the calculated average current response. It is hard to say for certain whether or not this outlier is an experimental artifact or a real physical phenomenon.

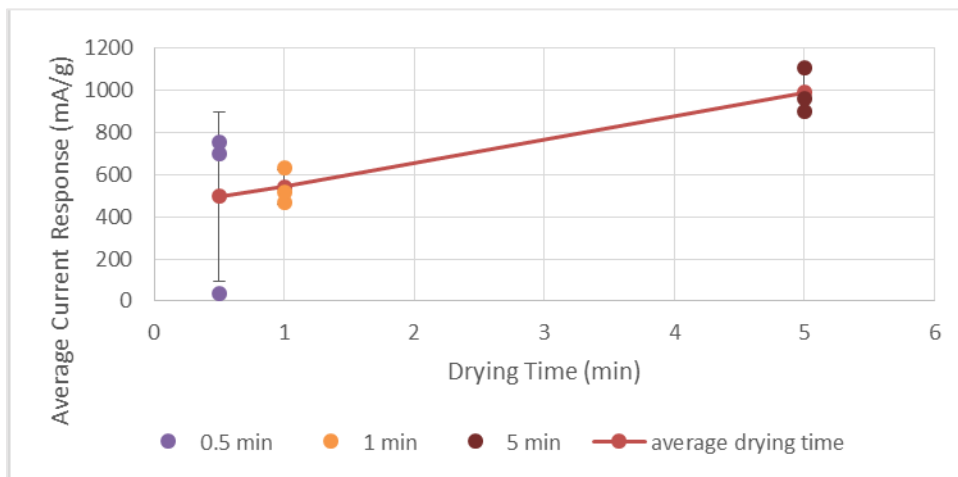


Figure 55: Peak current response of films annealed using three different experimental conditions. From the left of the curve (green) represent the open air trial, (blue) is the “in chamber” trial, and (yellow) is the “annealed in 40 mL  $\text{CHCl}_3$ ” trial. The averaged drying time is shown as a curve with error bars.

### Chlorobenzene as Solvent (DMSO percentage spread 0%-55%):

Revisiting the chlorobenzene morphology studies in Chapter 3 shows that these films follow a much more distinct trend in pore formation relative to the  $\text{CHCl}_3$  trials. Even though pore formation shifts to different regions of the film with increasing DMSO concentration, there is a clear change in film morphology. There is a possibly a co-continuous aspect to pore formation at certain percentages in these films. Normalized peak current responses at 500 mV/s (Figure 56) show that the electrochemical responses of the chlorobenzene films are much more reproducible than those of the  $\text{CHCl}_3$  films. There is still not a very strong trend in current response with respect to DMSO percentage. There seems to be an initial increase in current response going from 0%-15% DMSO, and a maximum current response at 38%. Increasing current response as porogen

concentration is increased, followed by decreasing current response, could be indicative of reaching the optimal, co-continuous morphology as porogen concentration increased, followed by transitions on to less ideal morphologies at higher concentrations as shown in Figure 20.

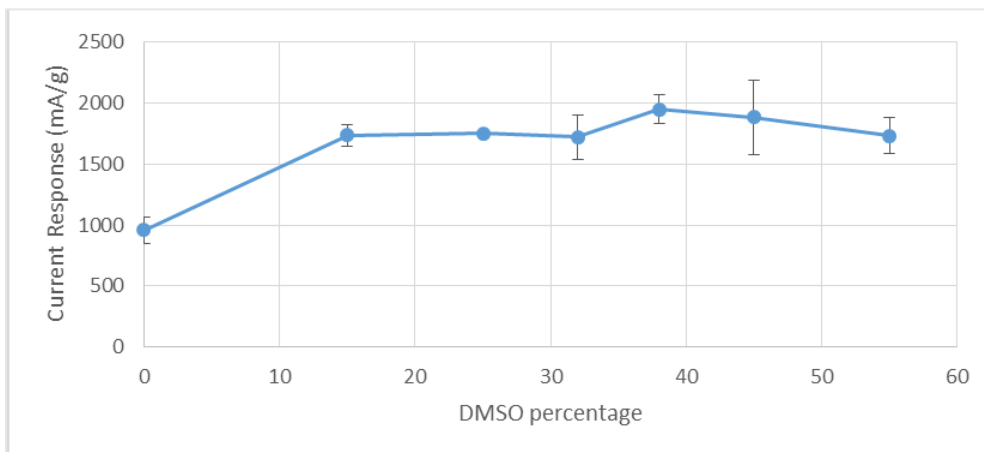


Figure 56: Normalized peak current response of chlorobenzene films with increasing DMSO percentage at 500mV/s. Curve given represents the average current response from three tested films.

The CV overlay showing different electrochemical responses of films templated from increasing percentages of DMSO is shown in Figure 56. The CV data show that with an increase in DMSO percentage going from 0%-15% DMSO there is an increase in the area under the CV (capacitive behavior) between the cycle data. This can most likely be attributed to the increase in porosity going from the 0% to 15% film. Electrolyte can most likely only dope the surface of the control (0%) film. With the introduction of porosity in the 15% film comes the increased surface area and availability of P3HT chains for doping. More experimentation is needed to confirm an increase in film surface area with increasing DMSO percentage in the templating solution.

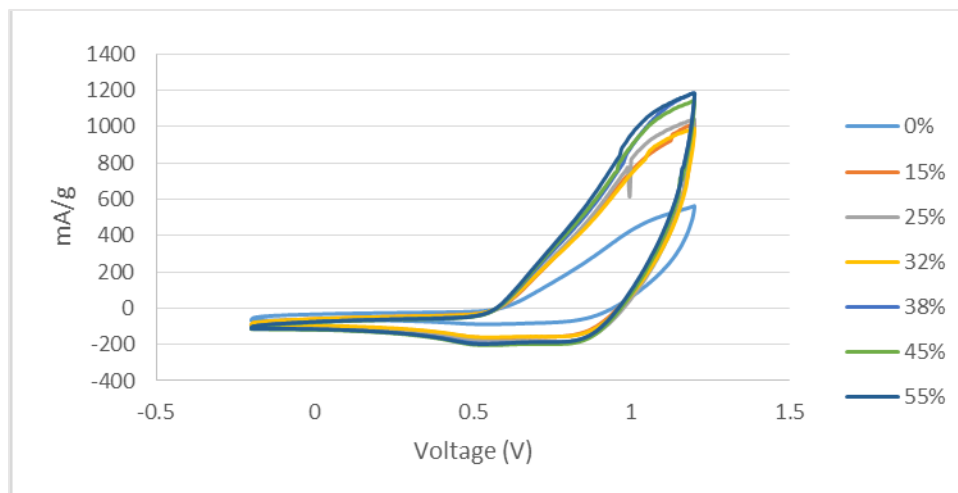


Figure 57: Cyclic voltammogram overlay of P3HT/chlorobenzene film behavior (0-55% DMSO) at 100 mV/s. Notice the large increase in surface area underneath the CV going from 0% DMSO to 15% DMSO

### Comparison of Solvent Systems:

There is an interesting observation when comparing the averaged film current responses for both chloroform and chlorobenzene solvent systems across 10 to 45 percent DMSO; the chlorobenzene solvent system produces films that significantly outperform films templated from a chloroform-based system by approximately 400 mA/g on average (Figure 58).

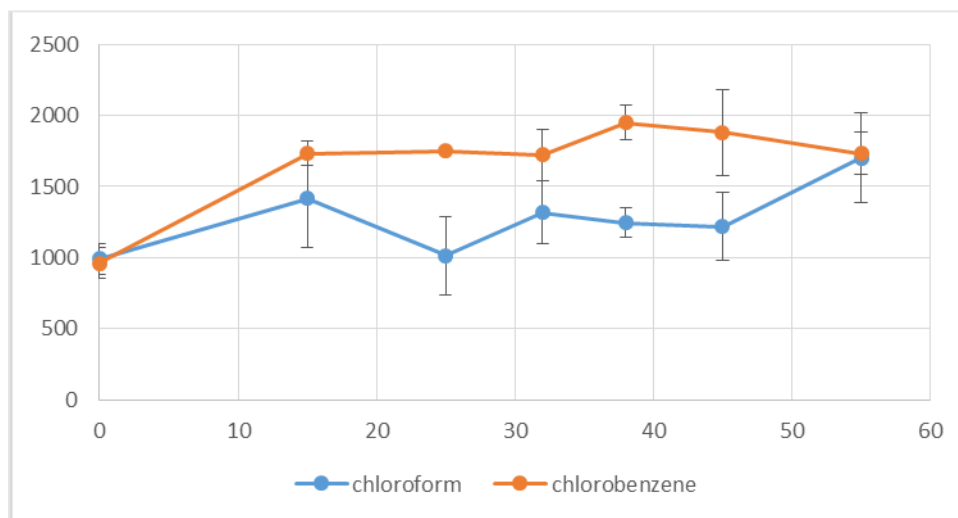


Figure 58: Comparison of averaged film current response from chloroform and chlorobenzene solvent systems as a function of DMSO percentage.

In addition to greater overall current response at each percentage of DMSO (with the exception of 0% and 55%), the chlorobenzene-based solvent system films are statistically more reproducible. This reproducibility can be observed by looking at the error associated with each data point in the comparison graph. The one data point that displays large error in the chlorobenzene system is that of the 45% DMSO trial. The normalized current response data for each percentage of DMSO used to calculate the film current response averages is available in Appendix H along with corresponding relative standard deviation values. It is worthwhile to note that experimentally more data points are needed (possibly upwards to 10 separate trials) at each DMSO percentage (for both solvent systems) in order to draw stronger conclusions. While it can be seen that the relative standard deviation of the data points at each DMSO percentage drops going from the chloroform-based solvent system to that of chlorobenzene, deviations in the chlorobenzene experiment are still relatively high.

Another noteworthy observation is that at 55% DMSO the area under the CV for the chlorobenzene film is significantly larger than that of the chloroform film. As stated before in Chapter 3, the chlorobenzene films show a larger amount of pore formation that may constitute a larger surface area available for electrochemical doping that result in a more capacitive behavior (Figure 59).

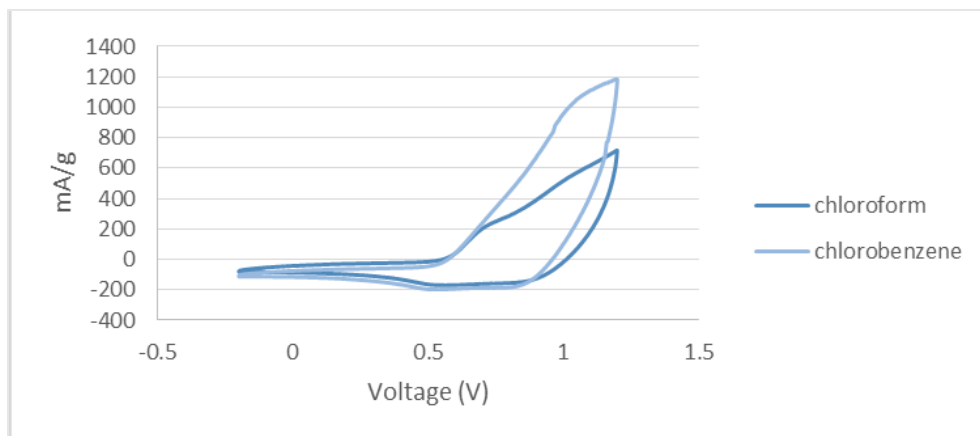


Figure 59: Comparison of cyclic voltammograms from two films templated from chloroform and chlorobenzene (55% DMSO) at the 100 mV/s scan rate.

## 5. CONCLUDING REMARKS

### 5.1 Monomer Synthesis & Polymerization

Characterization of both polymers (P3HT and poly(ProDOT-Bu<sub>2</sub>)) using FT-IR and NMR show good agreement with the spectra reported in the literature. The only discrepancy found is in the poly(ProDOT-Bu<sub>2</sub>) NMR spectrum. The assumed peak at approximately 3.98 ppm (protons adjacent to oxygens in cyclic ether ring) is very broad and not reflective of the sharp peak identified in the literature. It was argued in the literature reference that deuterated chloroform reacts with the polymer. The solution to the problem of reactivity with deuterated chloroform was to use deuterated benzene instead.

P3HT molecular weight determination utilizing the GPC technique show that the  $\bar{M}_n$  and  $\bar{M}_w$  of the polymer are approximately 38,713 and 55,436 g/mol respectively. This indicates around 230 repeat units ( $X_n$ ). Polydispersity index for the polymer was calculated to be 1.432.

Molecular weight determination for poly(ProDOT-Bu<sub>2</sub>) using MALDI-TOF-MS indicates  $\bar{M}_n$  and  $\bar{M}_w$  values for the polymer to be 3,974 and 4,174 g/mol respectively. The average number of repeat units for the polymer was found to be about 15. Polydispersity index was calculated to have a value of approximately 1.05.

Notable differences in molecular weight between P3HT and poly(ProDOT-Bu<sub>2</sub>) can be explained by the possible difference in coordination with the nickel catalyst for each monomer (electron rich nature of ProDOT-Bu<sub>2</sub>). The larger PDI for P3HT is most likely a result of the low solubility of larger chains in solution during polymerization (>30,000 g/mol).

## 5.2 Electroactive Polymer Morphology Control

It is observed that the relationship between percentage of DMSO and pore formation predicted from block-copolymer models does not exist unless the polymer solution drying physics are well controlled. Even with carefully controlled experimental parameters, the structural relationship is still not directly comparable to copolymer percentage experiments. Polymer films produced via templating protocols give way to a variety of unique morphologies that are highly dependent on the solvent system used, surface treatment of the substrate, and experimental drying conditions. Marangoni drying effects dictate where polymer and porogen migrate in the droplet. This places a crucial role in final film morphology. Aggregation of P3HT chains is evident in all  $\text{CHCl}_3$  templated film samples as observed by UV-vis experiments. Solution state aggregation is also present in  $\text{CHCl}_3/\text{DMSO}$  systems. The P3HT/chlorobenzene/DMSO system that has shortened drying time produces the most uniform and predictable film morphologies. Pore formation tends to accumulate in the central regions of the film at lower percentages of DMSO, and near the edges at higher percentages. Even though pore formation is segregated to specific regions of the film, there is a trend in the localization and number of pores that indicate the potential ability to control where and how pores form.

## 5.3 Electrochemical Analysis of Polymer Films

P3HT films templated from a chlorobenzene/DMSO solvent system generate films that have statistically more predictable and reproducible current responses as compared to films templated from the chloroform/DMSO solvent system. There is a notable increase in area under the CV for films templated with porogen as compared to films templated without porogen (example: 0% DMSO to 15%

DMSO/P3HT/chlorobenzene system). In addition, films templated using chlorobenzene also display larger areas under the CV when comparing to chloroform templated counterparts (example: 55% DMSO/P3HT/chlorobenzene versus 55% DMSO/P3HT/chloroform). This may indicate that chlorobenzene films have larger surface area present for charge balancing interactions with the electrolyte.

The poly(ProDOT-Bu<sub>2</sub>) films templated with 28% ethanolamine may provide some explanation as to why some films are enhanced electrochemically upon templating with a porogen and some are not. Ethanolamine templating did not result in the expected enhanced electrochemical response due to increased film porosity. Chemical reaction between ethanolamine and poly(ProDOT-Bu<sub>2</sub>) may be occurring, and this may contribute to the lack of film performance when templated with ethanolamine. It is also possible that there exists a balance between the charge transport characteristics of the film and the morphology.

It was observed that electrochemical response could be increased by approximately 2-fold with the presence of the porogen DMSO for both polymer systems. The first example of this observation is with the poly(ProDOT-Bu<sub>2</sub>) experiments. Control films (no porogen) performed in the 150-200 mA/g range, while post-templating with 28% DMSO saw an increase in the current response to around 400-450 mA/g. The P3HT experiment example of this current response increase can be shown with the chlorobenzene solvent system (0-55% DMSO). Control films performed around 900-1000 mA/g, while films templated with DMSO saw a consistent current response increase to about 1700-2000 mA/g. This is not as significant an increase seen in the initial

BBL/EMI-BTI experiments (30-fold increase in current response with porogen), but it is still notable.

#### 5.4 Future Work/Suggested Experiments

Chlorobenzene seems to be a promising solvent for P3HT, and fine tuning of the drying conditions could lead to more consistent co-continuous pore formation and statistically more reproducible current response data. Spectroscopic studies are needed to probe the nature of the interaction between ethanolamine and poly(ProDOT-Bu<sub>2</sub>).

A problem with the experimental design in this thesis was the need to carefully template on a limited surface area of ITO glass (smaller films could be completely submerged in electrolyte solution). Two problems are created from having to template on a limited surface area. One problem is that film masses had to be large enough to measure and use in normalization during CV experiments. A balance had to be found between film size and the ability of the film to be submerged completely in electrolyte solution. Problem two was that in limiting film mass, this ultimately limited the number of templating techniques and film characterization methods that could be employed. For example, one major drawback of this body of work is that film porosity quantification was a major challenge. Common porosity measurement techniques such as gas isotherm analysis require a larger sample size than possible in our approach with smaller ITO glass. If film mass is limited due to the available surface area of the ITO glass, then characterization using these instruments that require larger sample sizes is not possible.

The solution to the ITO surface area problem is fairly simple. Using ITO glass with larger dimensions would allow for more polymer to be deposited during templating. If the mass deposited from solution could be approximated with the amount of surface

area available during templating, then film masses could be calculated to allow for characterization of porosity in those instruments that require larger sample sizes.

Experiments that allow for better quantification and characterization of polymer aggregation are needed in order for more connections to be made with film electrical performance (polarimetry, differential scanning calorimetry, tunneling electron microscopy, atomic force microscopy). It is possible that aggregates present in the film have an effect on electrochemical performance, but at this time all that can be stated is that aggregation is present in all P3HT films with no strong connection to CV data. A good experiment would be to quantify the P3HT aggregation (Using UV-vis or other techniques) in a situation similar to that of the “Control Film Drying” study (Chapter 4, page 74). The goal would be to produce films that had controllable levels of aggregation. The films could then be electrochemically tested to find current response. The current response would then be plotted versus aggregation level in the films.

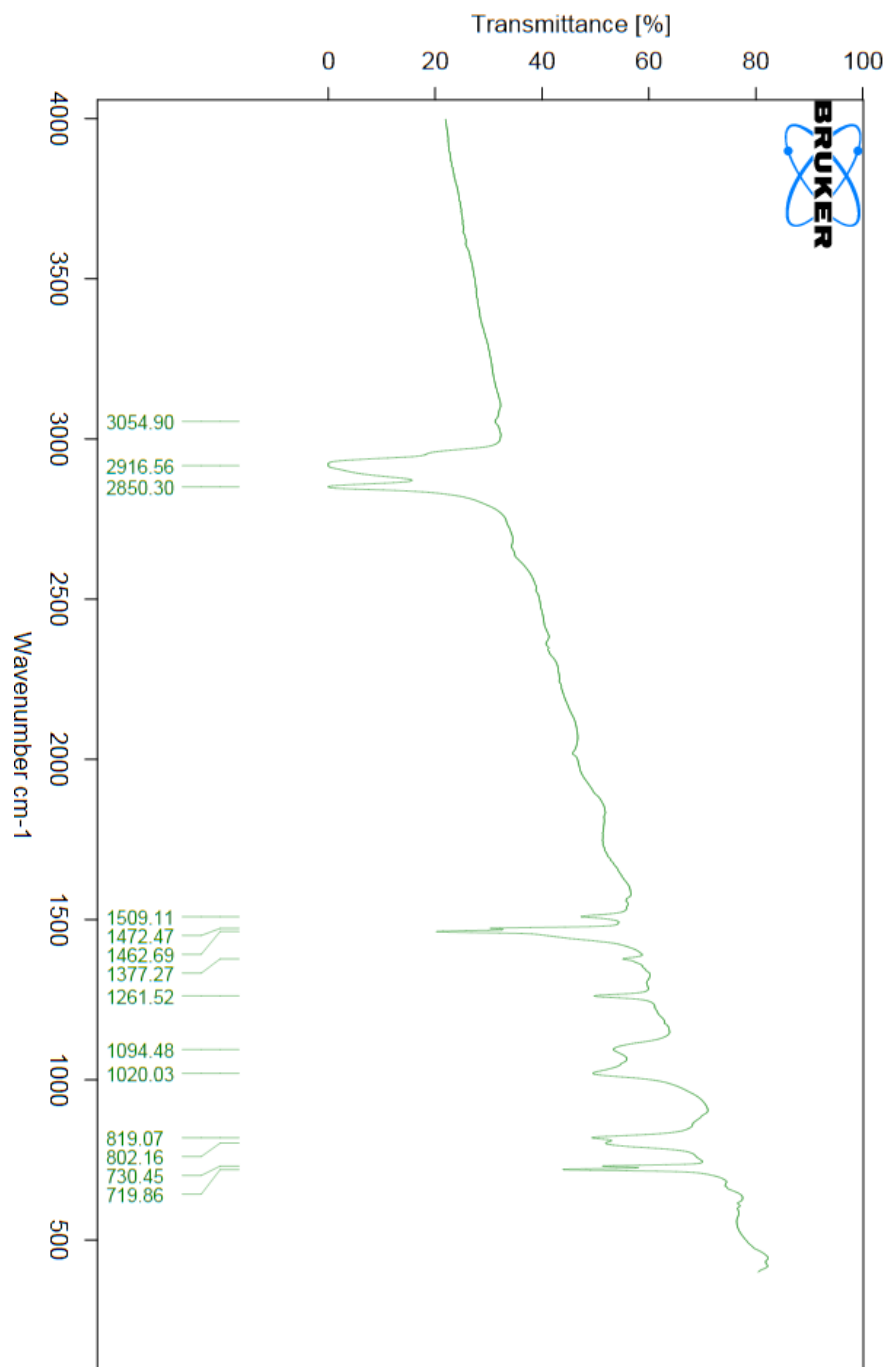
Finally, additional studies are needed to probe the use of GRIM polymerization with ether-substituted monomers. Identification of any undesirable interactions between the catalyst and the monomers is necessary. Alternative coupling reactions should be investigated to improve polymer chain lengths of these desirable electron-rich polymers.

## APPENDIX

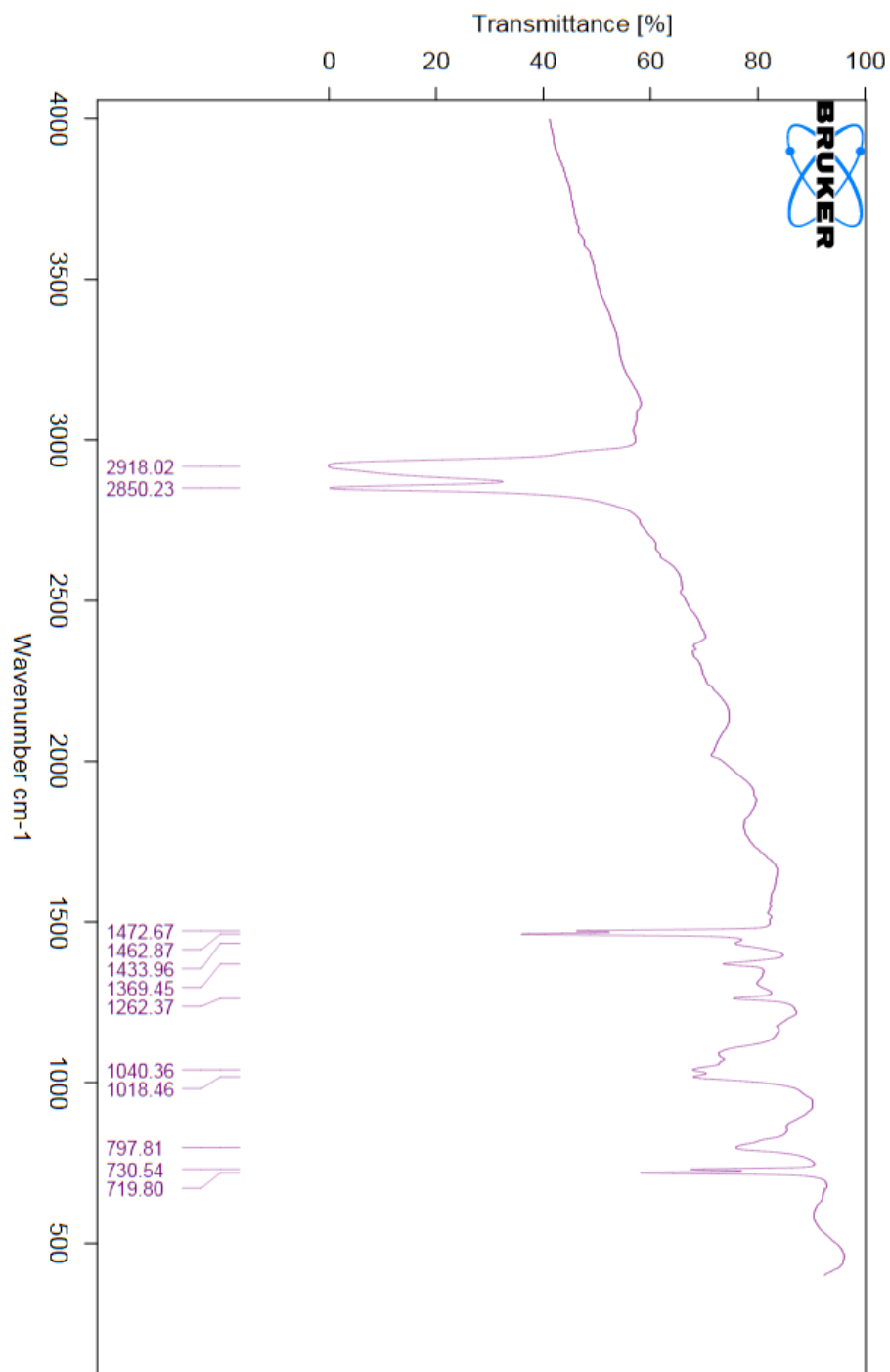
A. FI-IR Spectra for P3HT and poly(ProDOT-Bu <sub>2</sub> ).....	90
B. <sup>1</sup> H NMR Spectra for P3HT and poly(ProDOT-Bu <sub>2</sub> ).....	92
C. Molecular Weight Determination Data for P3HT and poly(ProDOT-Bu <sub>2</sub> ).....	94
D. Microscopy of Templated Films .....	97
E. Linear Regression Data .....	116
F. Gravimetric Analysis Data .....	117
G. Poly(ProDOT-Bu <sub>2</sub> ) Experimental CV Data.....	118
H. Normalized Peak Current Response Data for P3HT Experiments .....	120

## APPENDIX A: FT-IR SPECTRA FOR P3HT AND POLY(PRODOT-BU<sub>2</sub>)

### A.1 FT-IR spectrum of synthesized P3HT

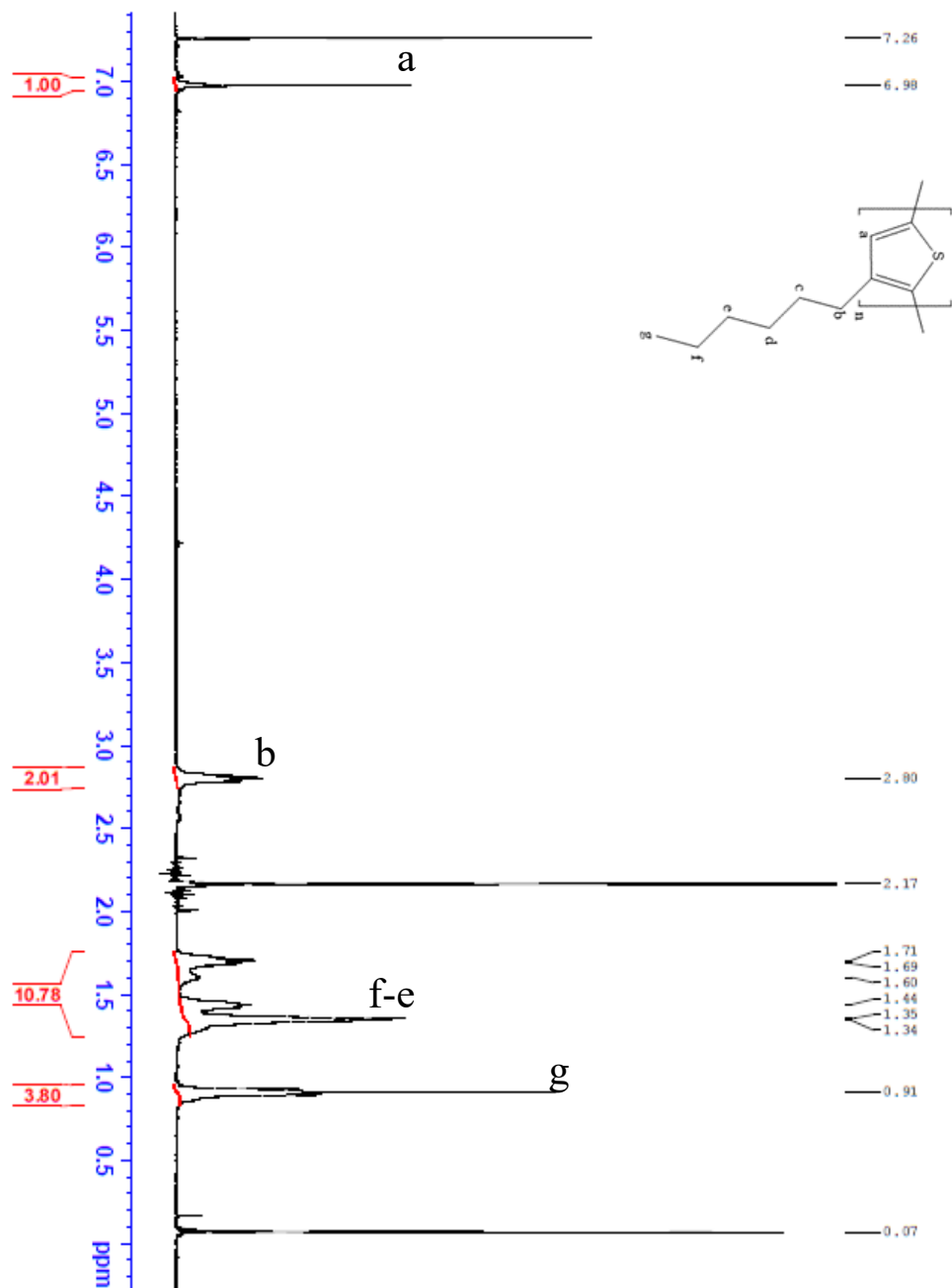


## A.2 FT-IR spectrum of synthesized poly(ProDOT-Bu<sub>2</sub>)

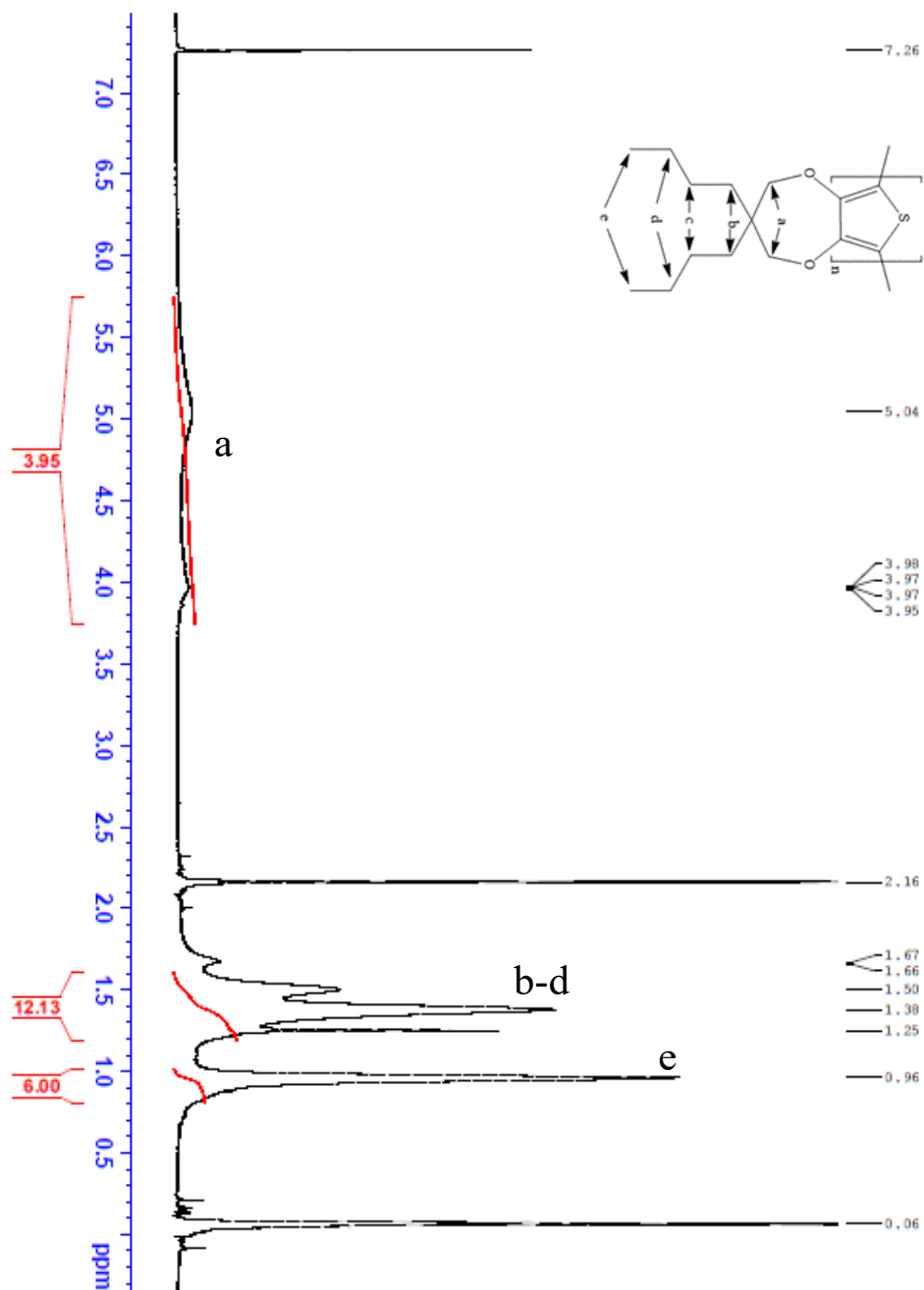


## APPENDIX B: $^1\text{H}$ NMR SPECTRA FOR P3HT AND POLY(PRODOT-BU<sub>2</sub>)

### B.1 $^1\text{H}$ NMR spectrum of synthesized P3HT

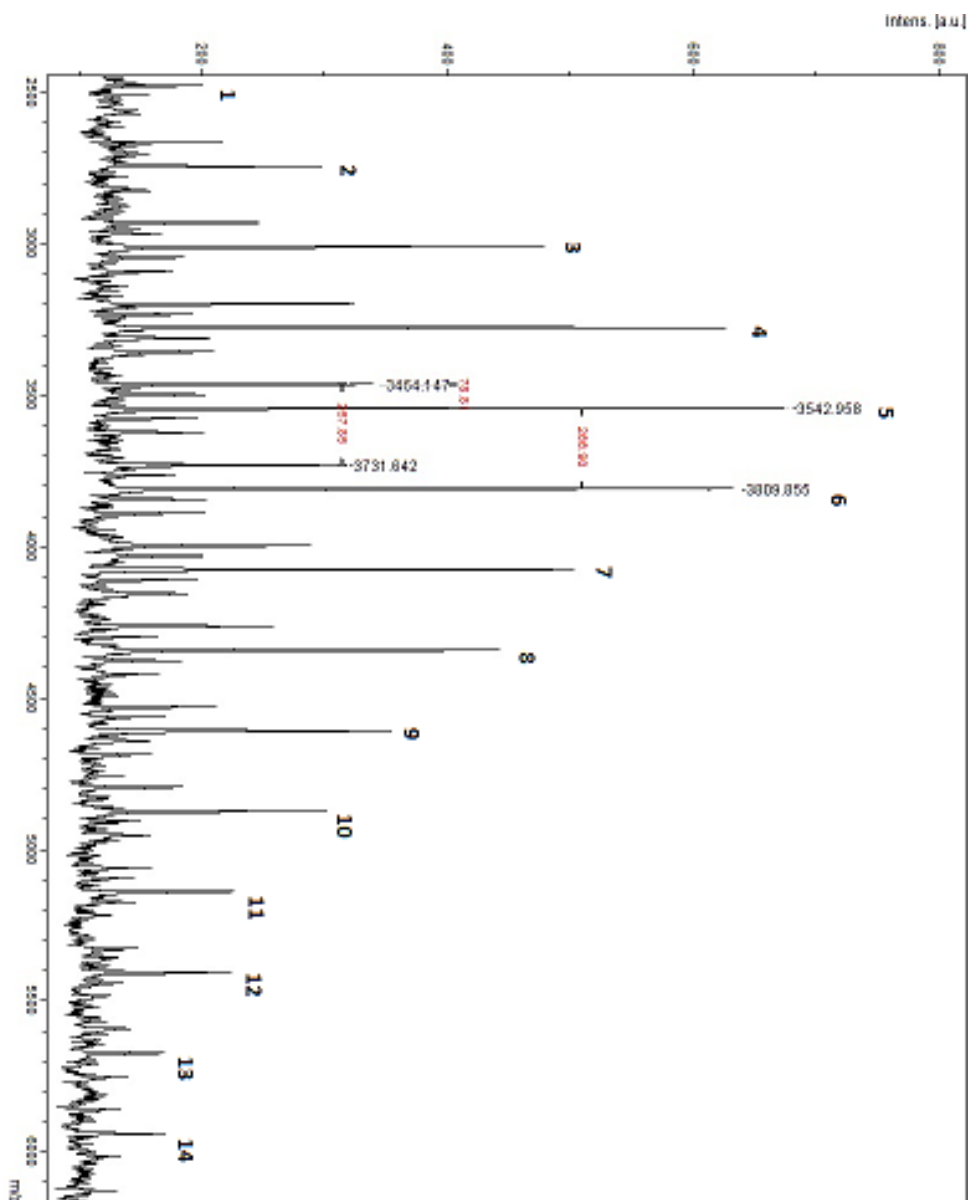


B.2  $^1\text{H}$  NMR spectrum of synthesized poly(ProDOT-Bu<sub>2</sub>)



**APPENDIX C: MOLECULAR WEIGHT DETERMINATION DATA FOR P3HT  
AND POLY(PRODOT-BU<sub>2</sub>)**

C.1 MALDI-TOF-MS data for synthesized poly(ProDOT-Bu<sub>2</sub>). Peaks are labeled in the spectrum (peaks: #1-14)



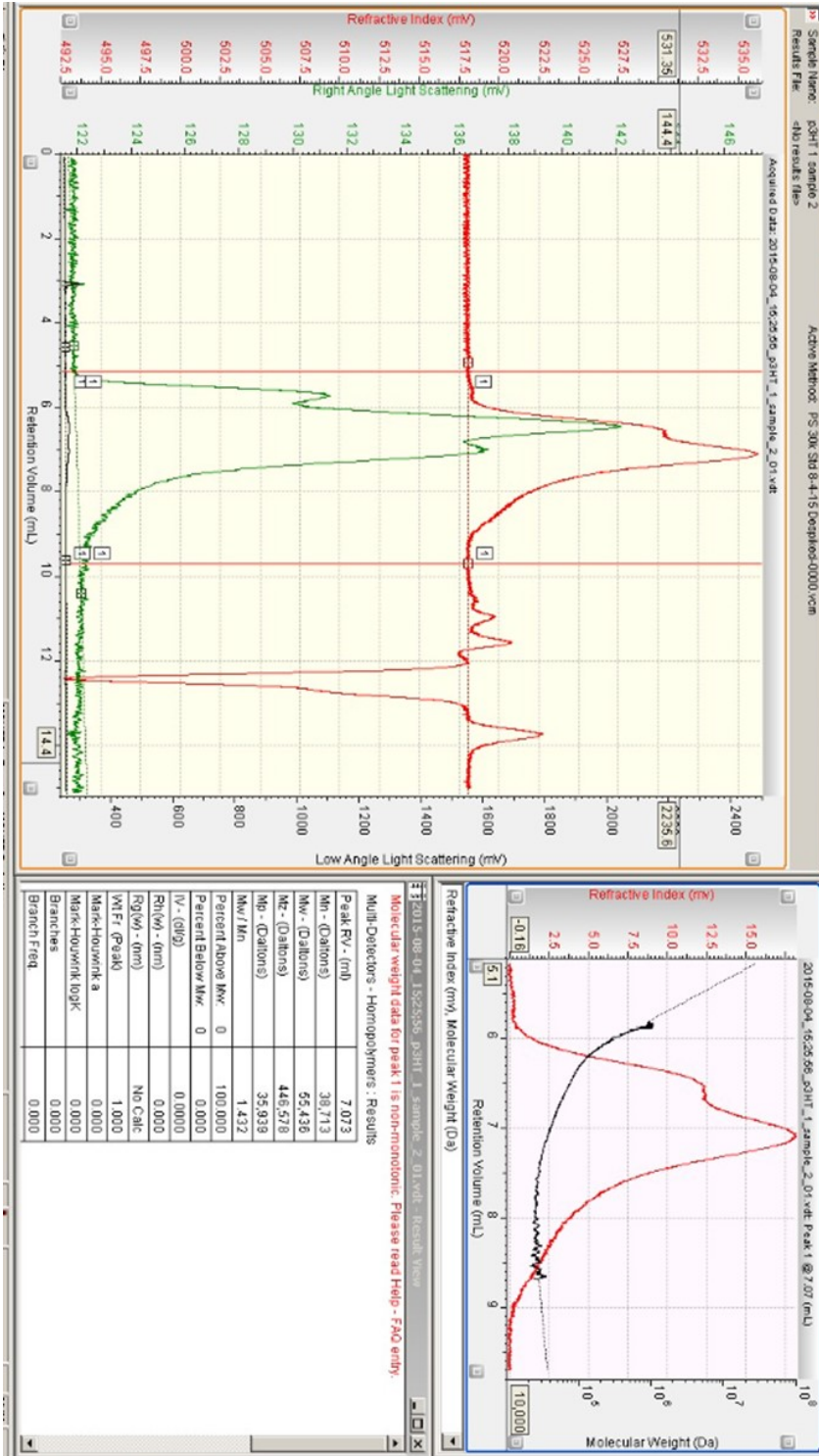
C.2 MALDI-TOF-MS poly(ProDOT-Bu<sub>2</sub>) data. Molecular weight data is presented alongside corresponding peak number in spectrum (F.1 above).

Note: conversion factor is  $\approx 34.4_8$  iu/cm (iu = intensity units)

Table 4: MALDI-TOF-MS Data (Poly(ProDOT-Bu<sub>2</sub>))

Peak #	N <sub>i</sub> (cm)	N <sub>i</sub> (iu)	M <sub>i</sub>	(M <sub>i</sub> ) <sup>2</sup>	N <sub>i</sub> M <sub>i</sub>	N <sub>i</sub> (M <sub>i</sub> ) <sup>2</sup>
1	2.85	198.2759	2475.358	6127397	490803.7	1214914968
2	5.60	293.1034	2742.258	7519979	803765.3	2204131758
3	10.7	468.9655	3009.158	9055032	1411191	4246497704
4	14.85	612.069	3276.058	10732556	2005173	6569064460
5	16.20	658.6207	3542.958	12552551	2333465	8267370053
6	15.05	618.9655	3809.855	14514995	2358169	8984281463
7	11.40	493.1034	4076.755	16619931	2010262	8195345449
8	9.70	434.4828	4343.655	18867339	1887243	8197533392
9	7.25	350.0000	4610.555	21257217	1613694	7440026093
10	5.75	298.2759	4877.455	23789567	1454827	7095853688
11	3.65	225.8621	5144.355	26464388	1161915	5977301510
12	3.60	224.1379	5411.255	29281681	1212868	6563135324
13	2.10	172.4138	5678.155	32241444	978992.2	5558869690
14	2.10	172.4138	5945.055	35343679	1025009	6093737751

C.3 P3HT GPC computer data image (P3HT molecular weight data is presented in image)

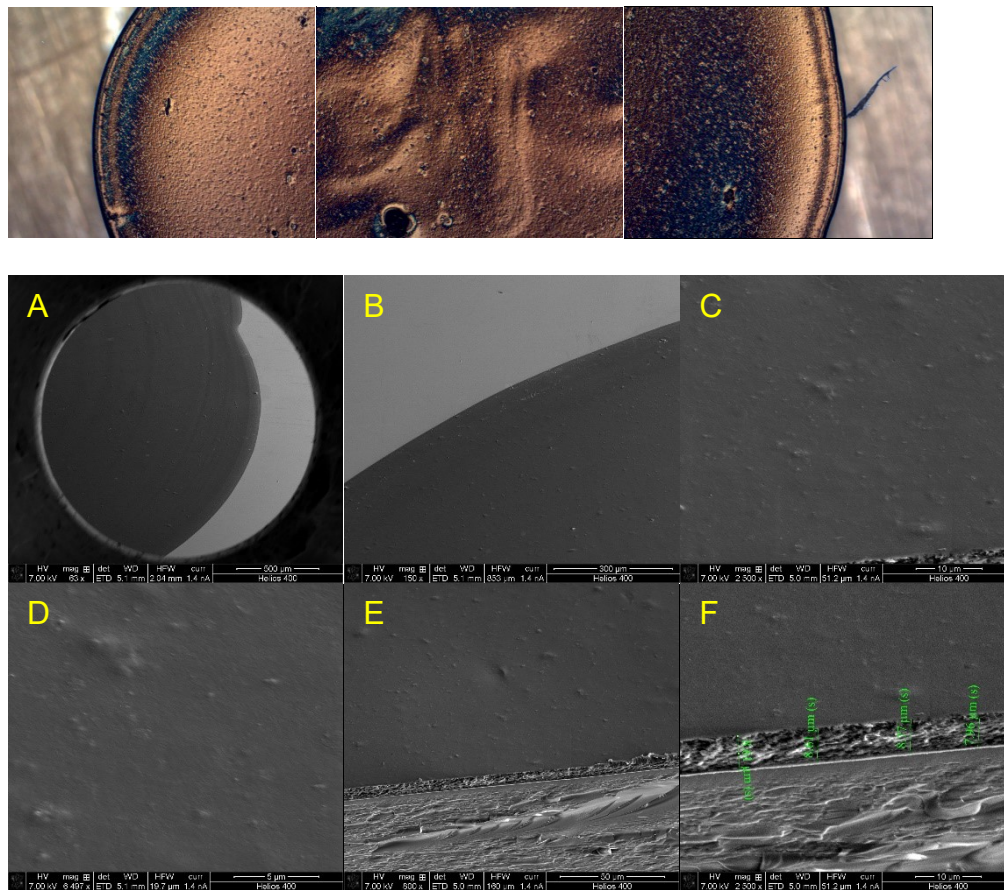


## APPENDIX D: MICROSCOPY OF TEMPLATED FILMS

Microscopy of templated films (SEM and optical microscopy) is presented with polymer name and solvent system.

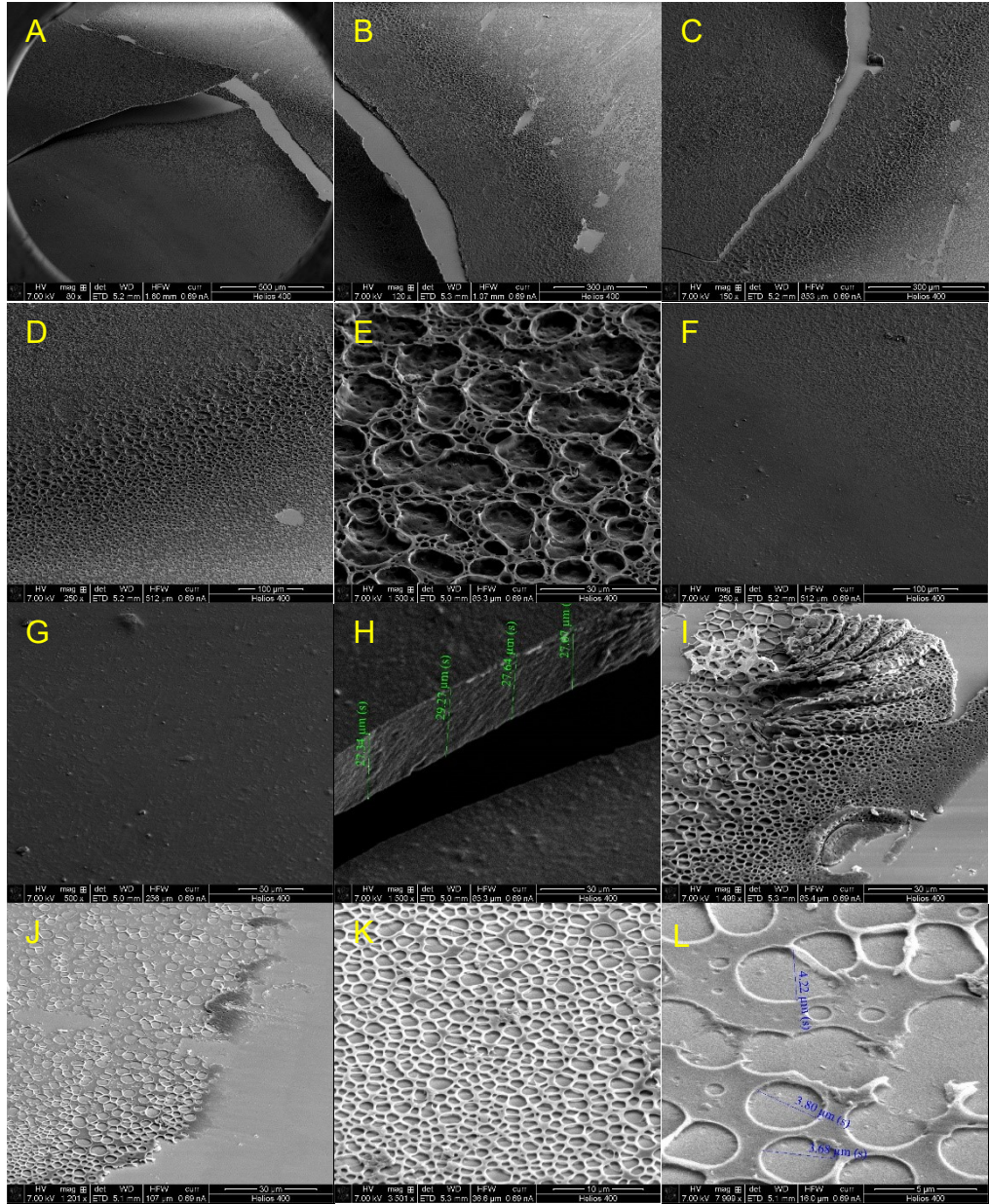
### Poly(ProDOT-Bu<sub>2</sub>)/CHCl<sub>3</sub> film

D.1 Poly(ProDOT-Bu<sub>2</sub>) film templated with no porogen using chloroform as the solvent.



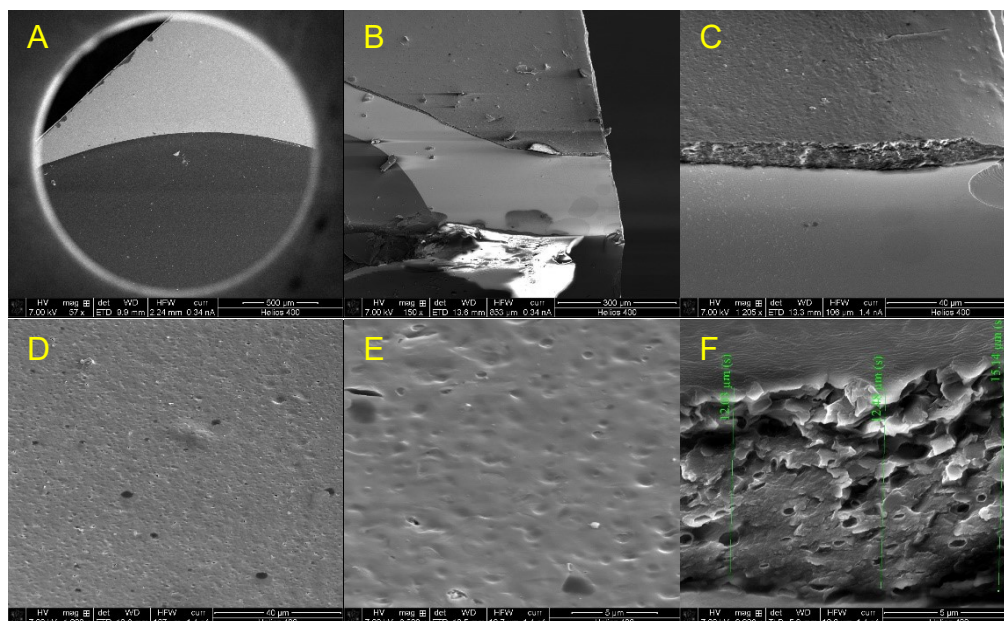
### Poly(ProDOT-Bu<sub>2</sub>)/CHCl<sub>3</sub>/28%DMSO film

D.2 Poly(ProDOT-Bu<sub>2</sub>) film templated with 28% DMSO in solution using chloroform as the solvent. (See following page)



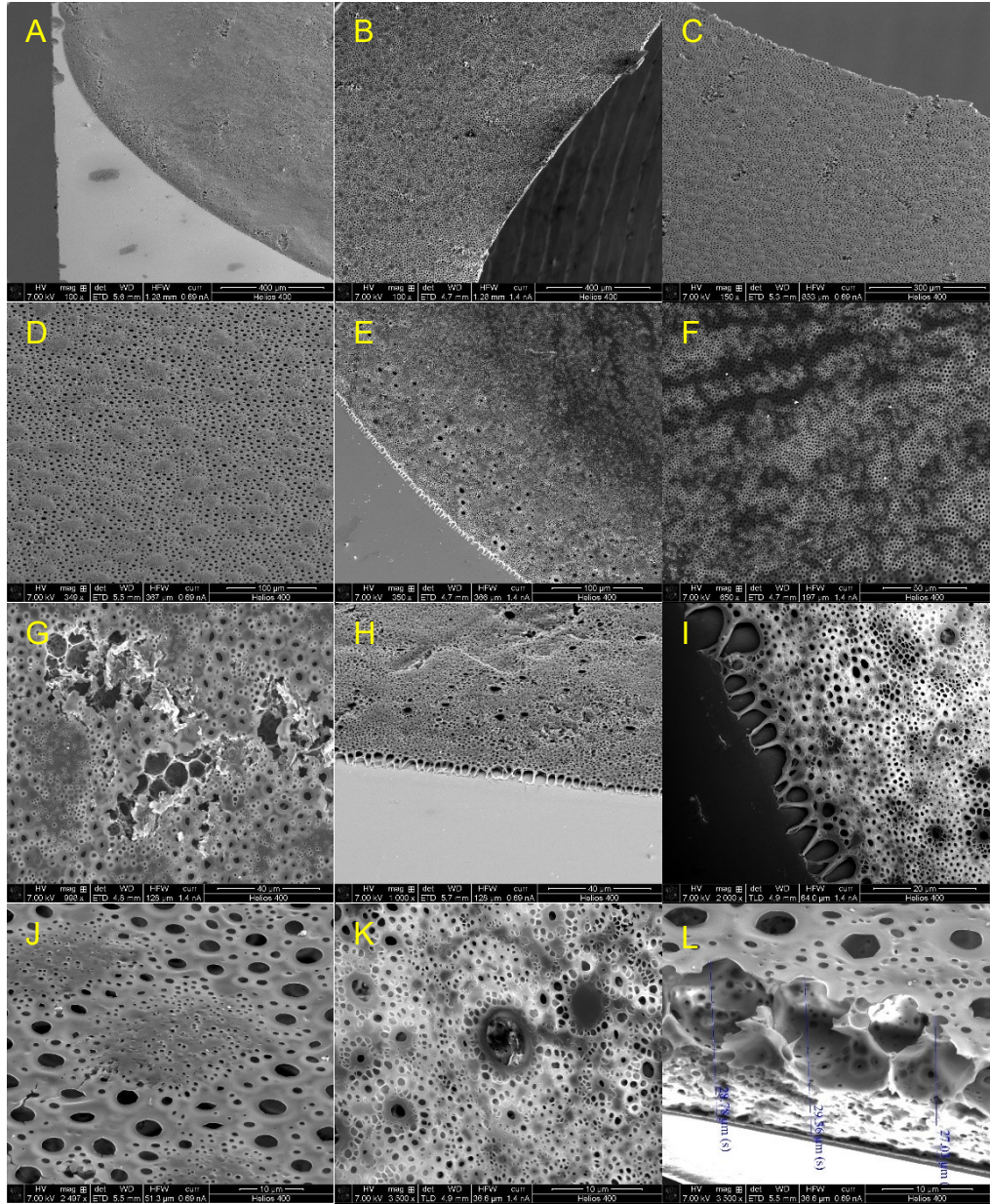
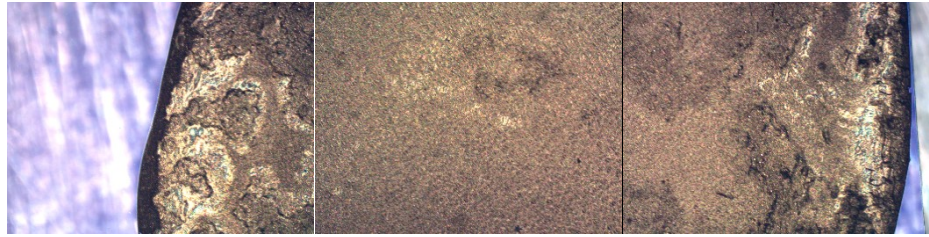
### Poly(ProDOT-Bu<sub>2</sub>)/CHCl<sub>3</sub>/28% 1,4-dioxane film

D.3 Poly(ProDOT-Bu<sub>2</sub>) film templated with 28% 1,4-dioxane using chloroform as the solvent.



### Poly(ProDOT-Bu<sub>2</sub>)/CHCl<sub>3</sub>/28% ethanolamine

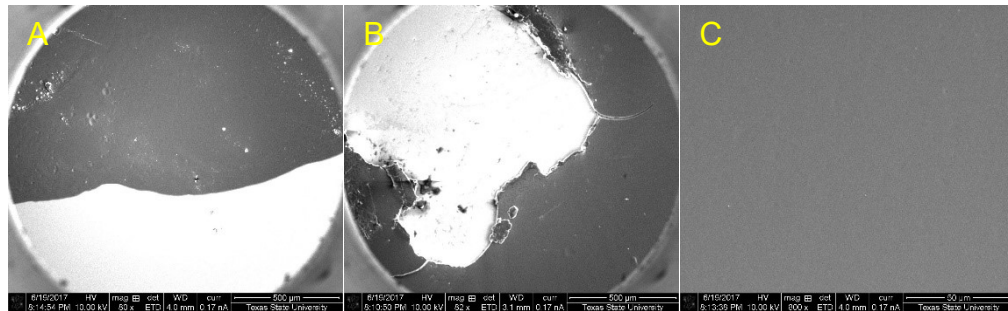
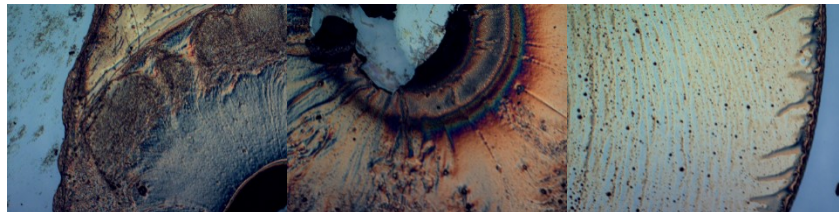
D.4 Poly(ProDOT-Bu<sub>2</sub>) film templated with 28% ethanolamine using chloroform as the solvent. (See following page)



Poly(ProDOT-Bu<sub>2</sub>)/CHCl<sub>3</sub> solvent system (0-55% DMSO)

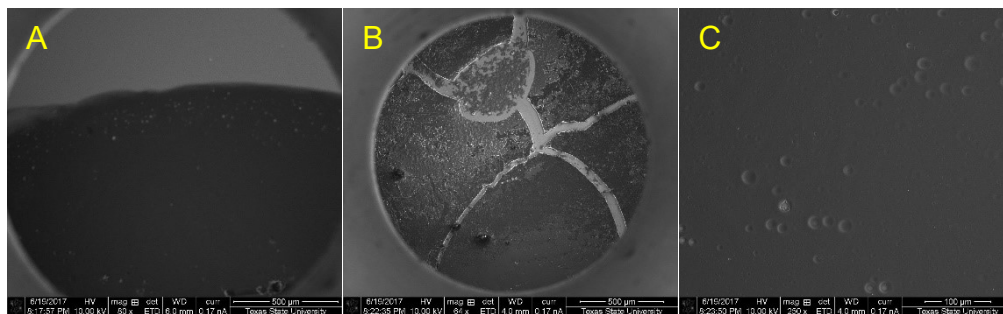
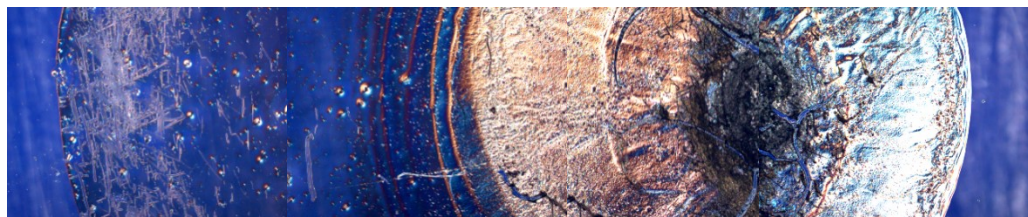
0% DMSO film

D.5 P3HT film templated with no porogen using chloroform as the solvent.



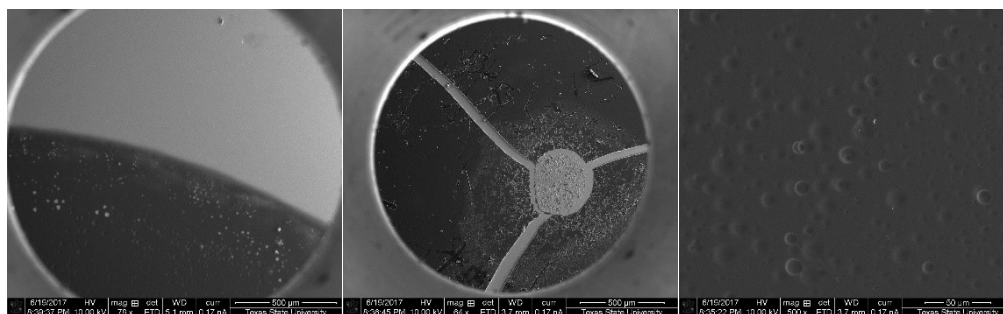
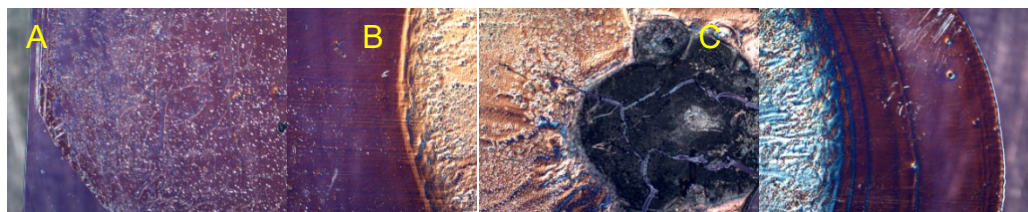
15% DMSO film

D.6 P3HT film templated with 15% DMSO using chloroform as the solvent. (See following page)



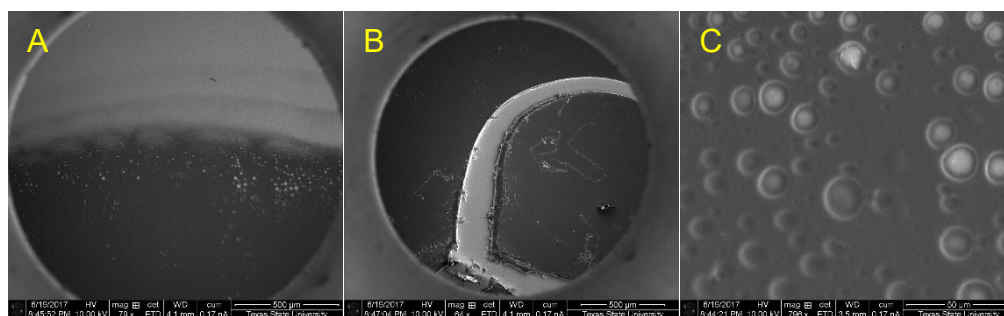
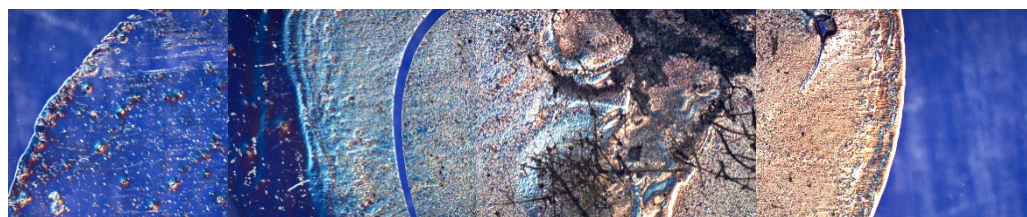
### 25% DMSO film

D.7 P3HT film templated with 25% DMSO using chloroform as the solvent.



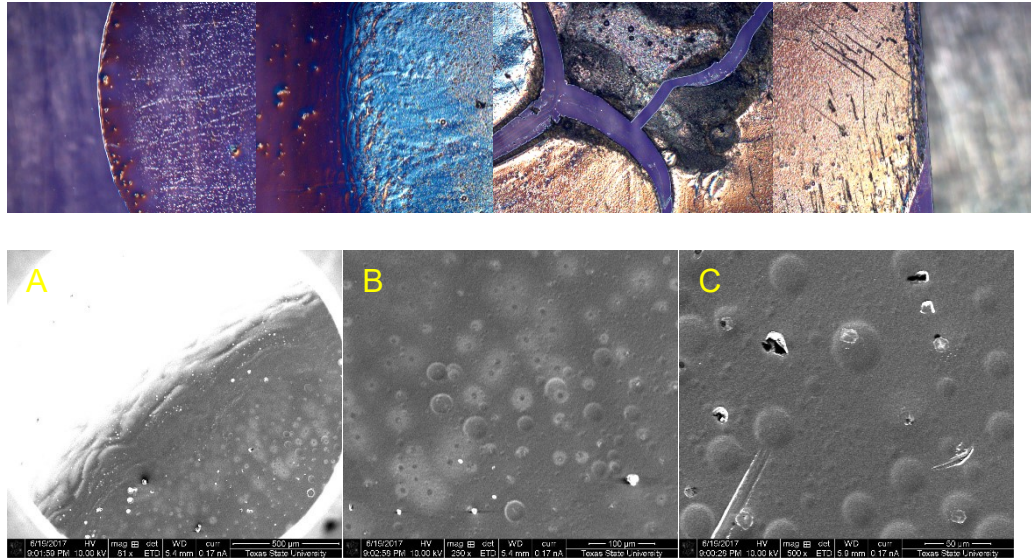
32% DMSO film

D.8 P3HT film templated with 32% DMSO using chloroform as the solvent.



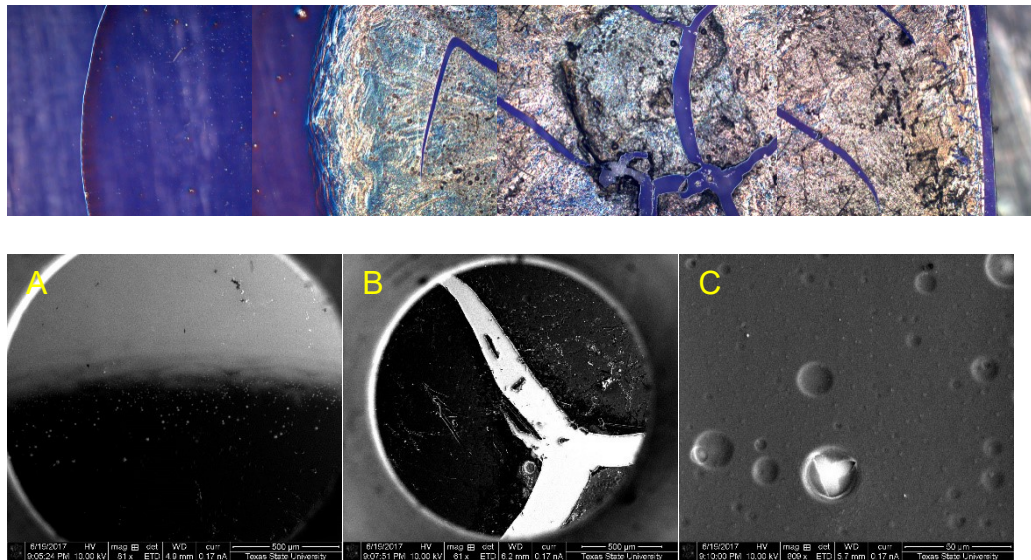
38% DMSO film

D.9 P3HT film templated with 38% DMSO using chloroform as the solvent.



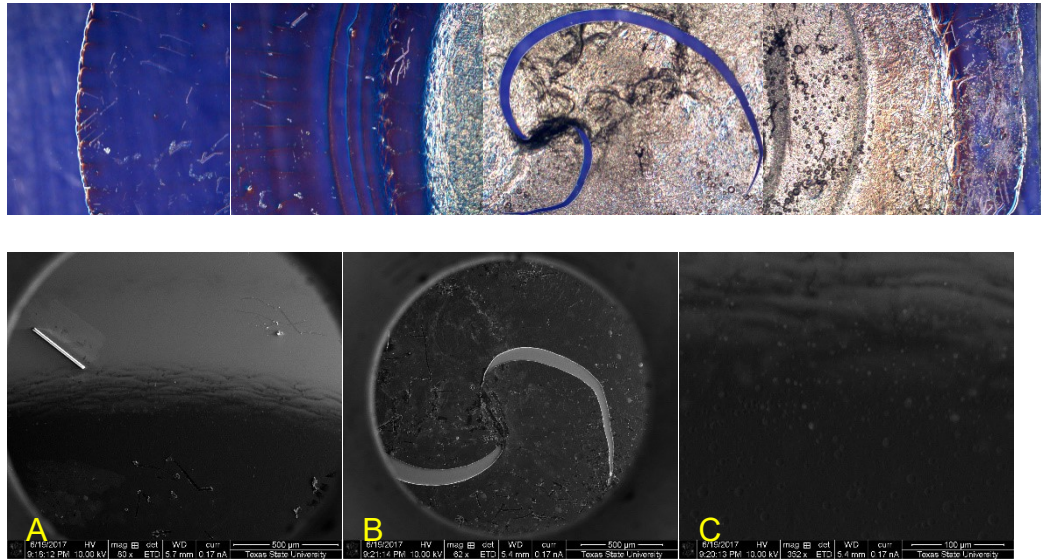
45% DMSO film

D.10 P3HT film templated with 45% DMSO using chloroform as the solvent.



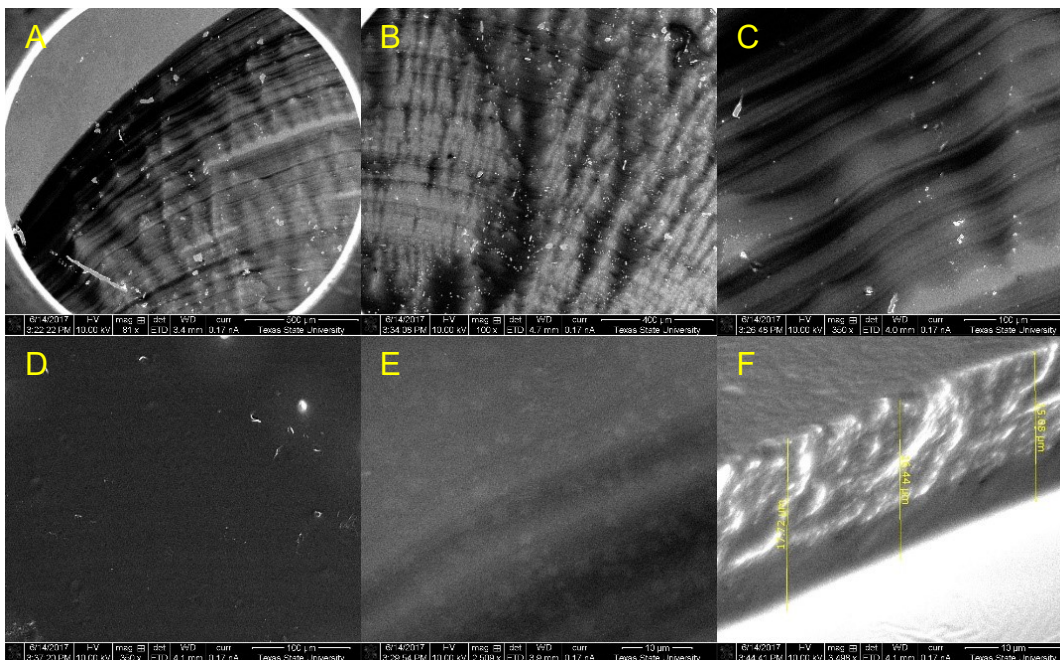
55% DMSO film

D.11 P3HT film templated with 55% DMSO using chloroform as the solvent.



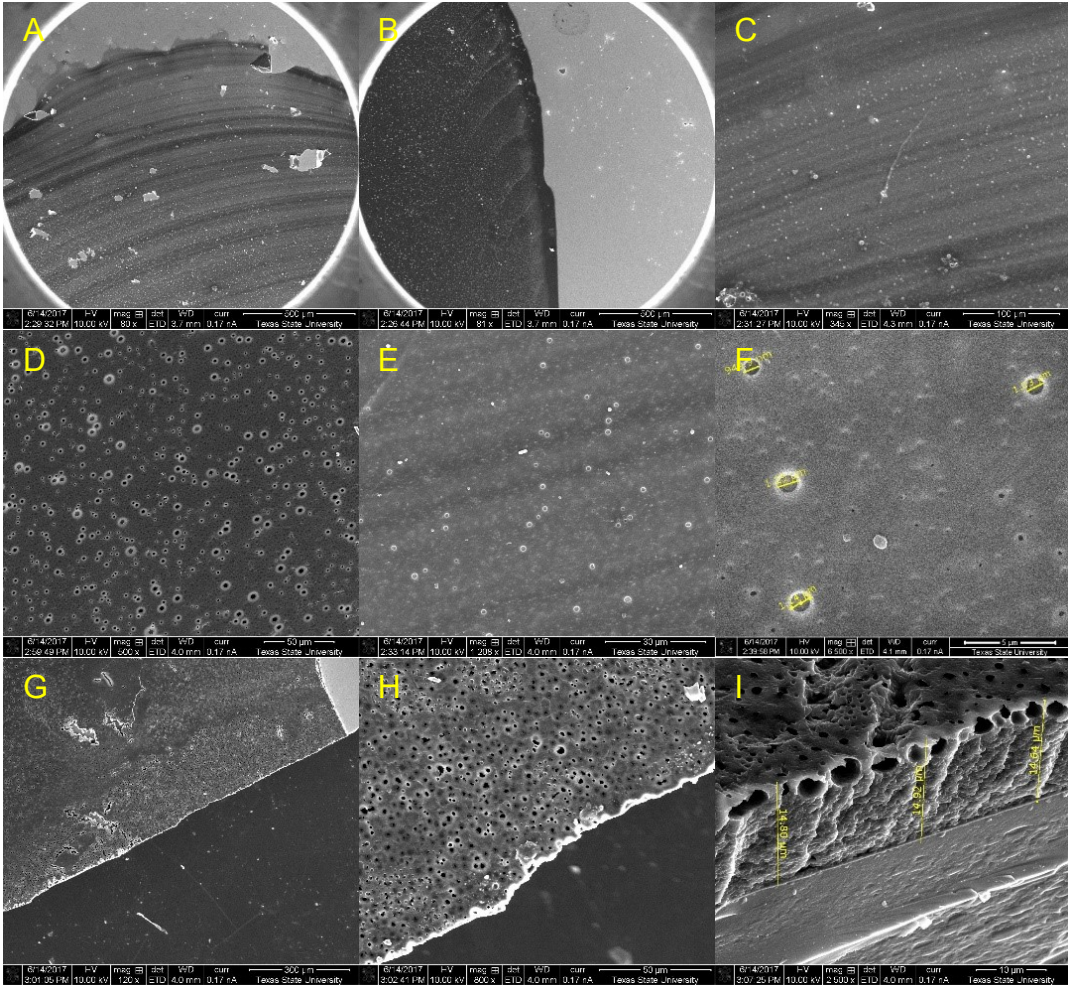
0% DMSO film

D.12 Optical images (top) presented with SEM images (bottom) of P3HT film templated (no DMSO present in solution) using chlorobenzene as the solvent. (See following page)



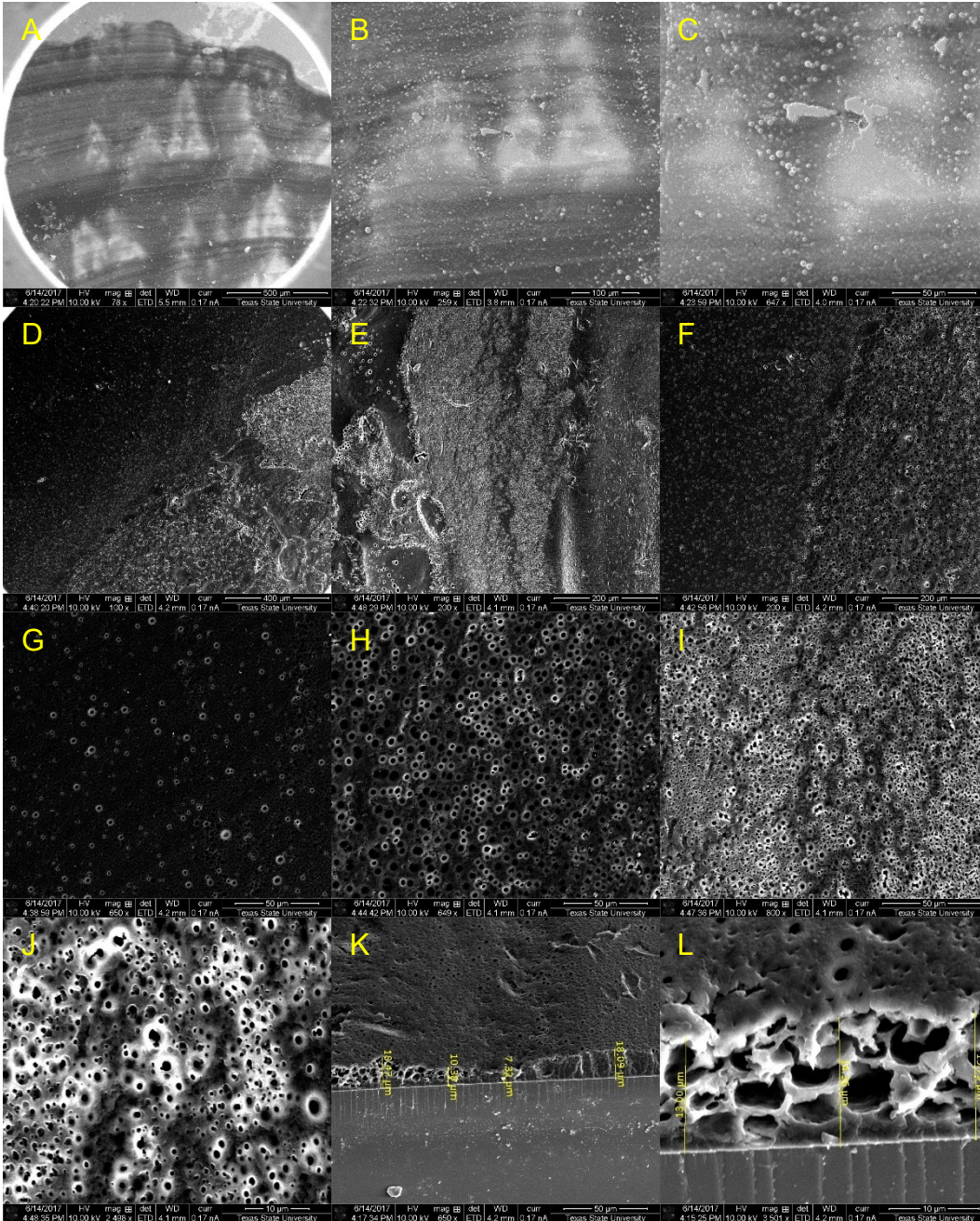
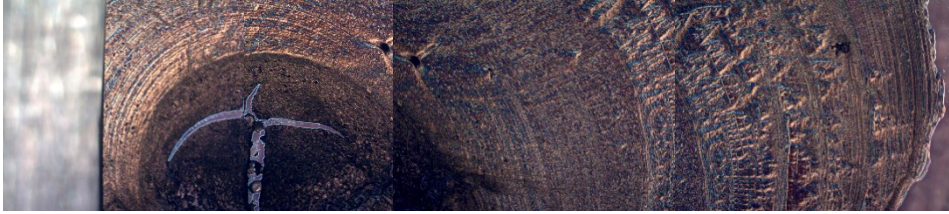
### 15% DMSO film

D.13 Optical images (top) presented with SEM images (bottom) of P3HT film templated with 15% DMSO using chlorobenzene as the solvent. (See following page)



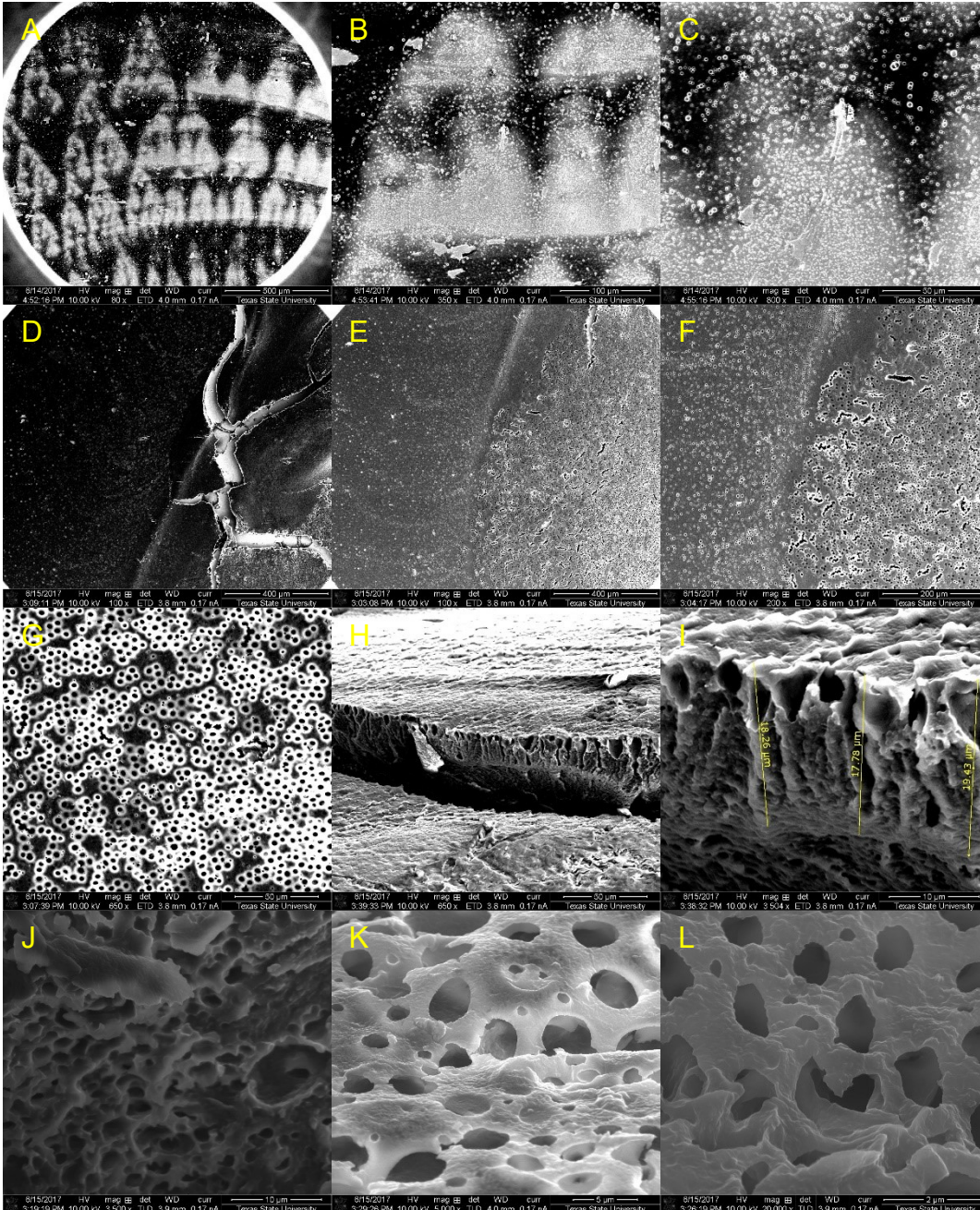
25% DMSO film

D.14 Optical images (top) presented with SEM images (bottom) of P3HT film templated with 25% DMSO using chlorobenzene as the solvent. (See following page)



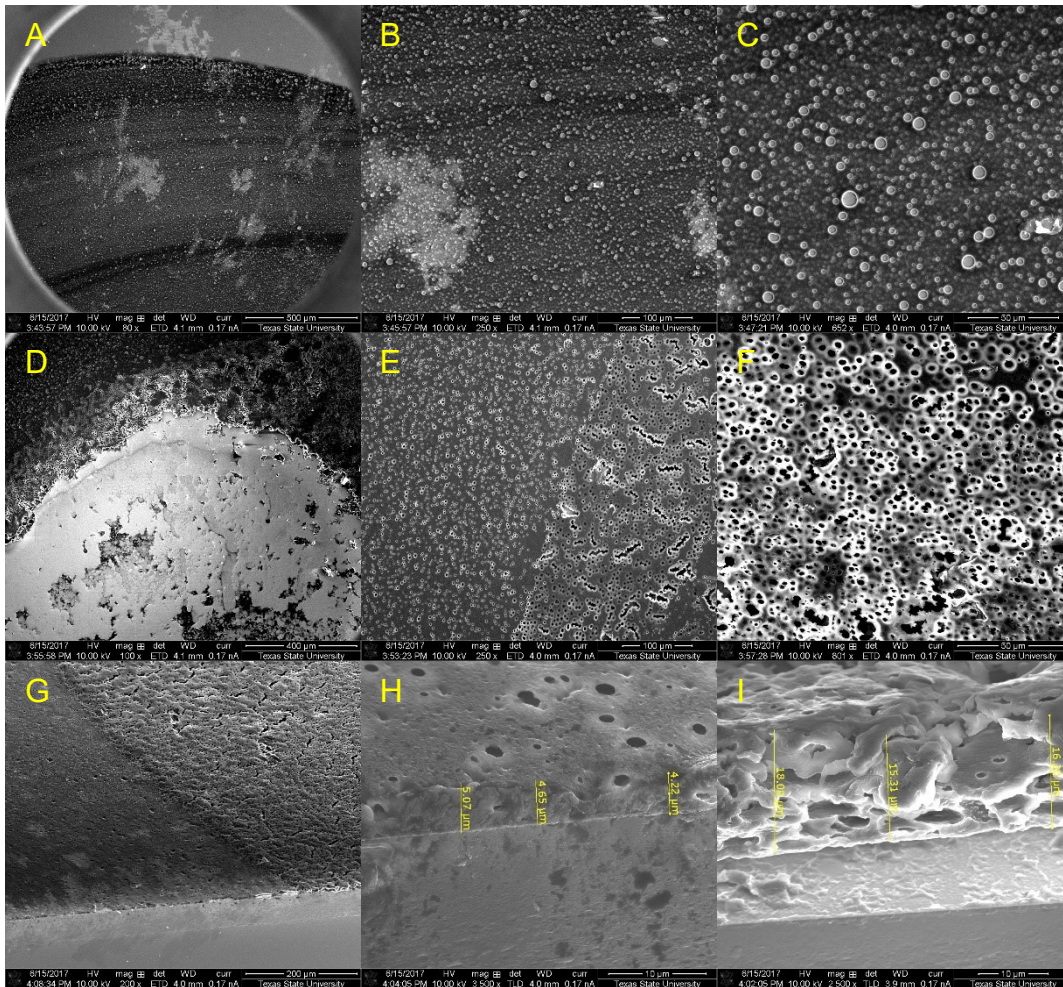
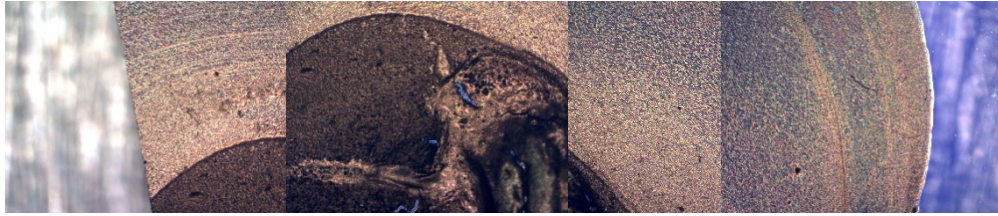
32% DMSO film

D.15 Optical images (top) presented with SEM images (bottom) of P3HT film templated with 32% DMSO using chlorobenzene as the solvent. (See following page)



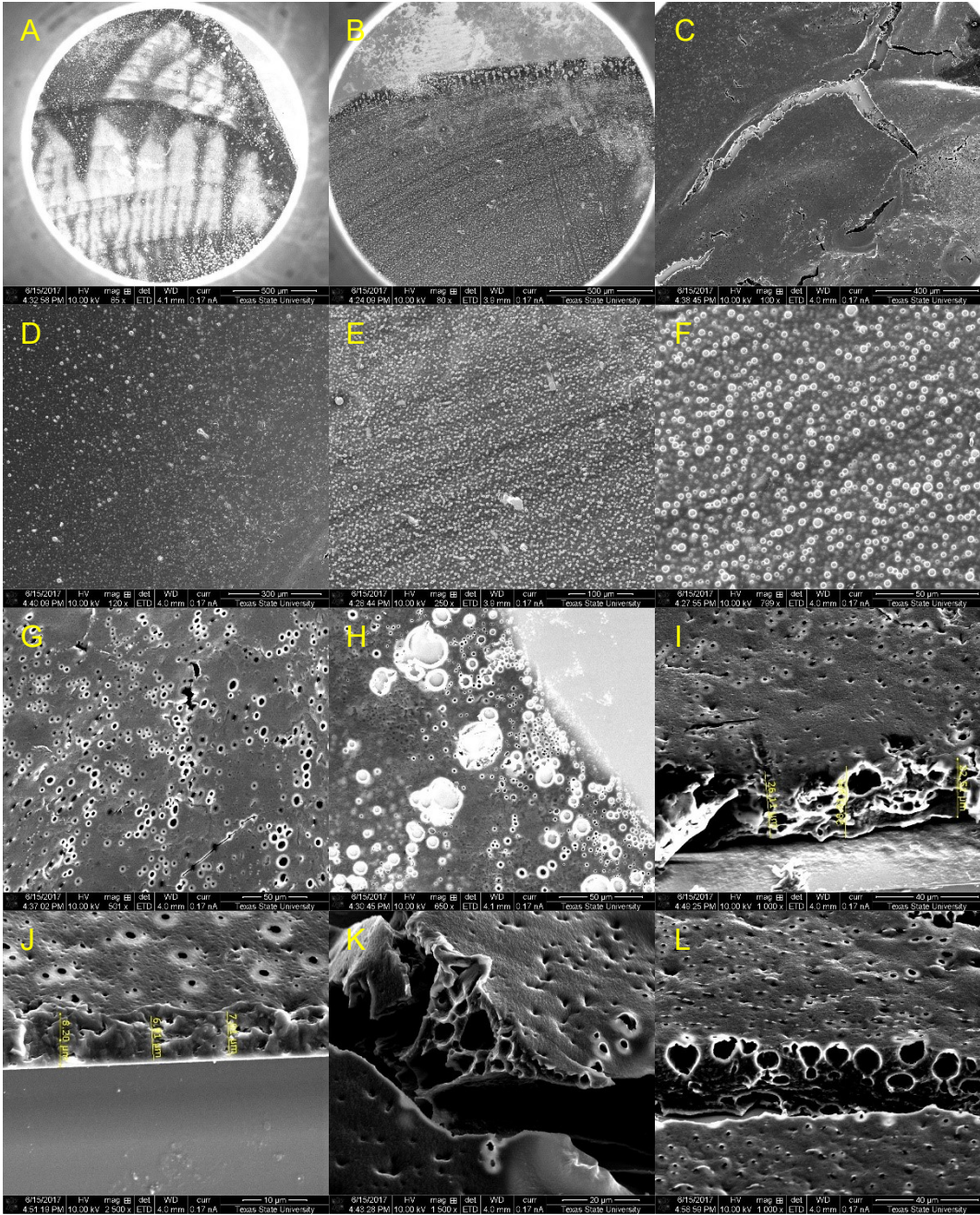
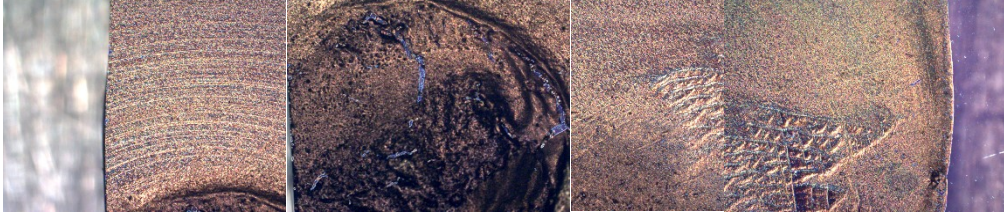
## 38% DMSO film

D.16 Optical images (top) presented with SEM images (bottom) of P3HT film templated with 38% DMSO using chlorobenzene as the solvent.



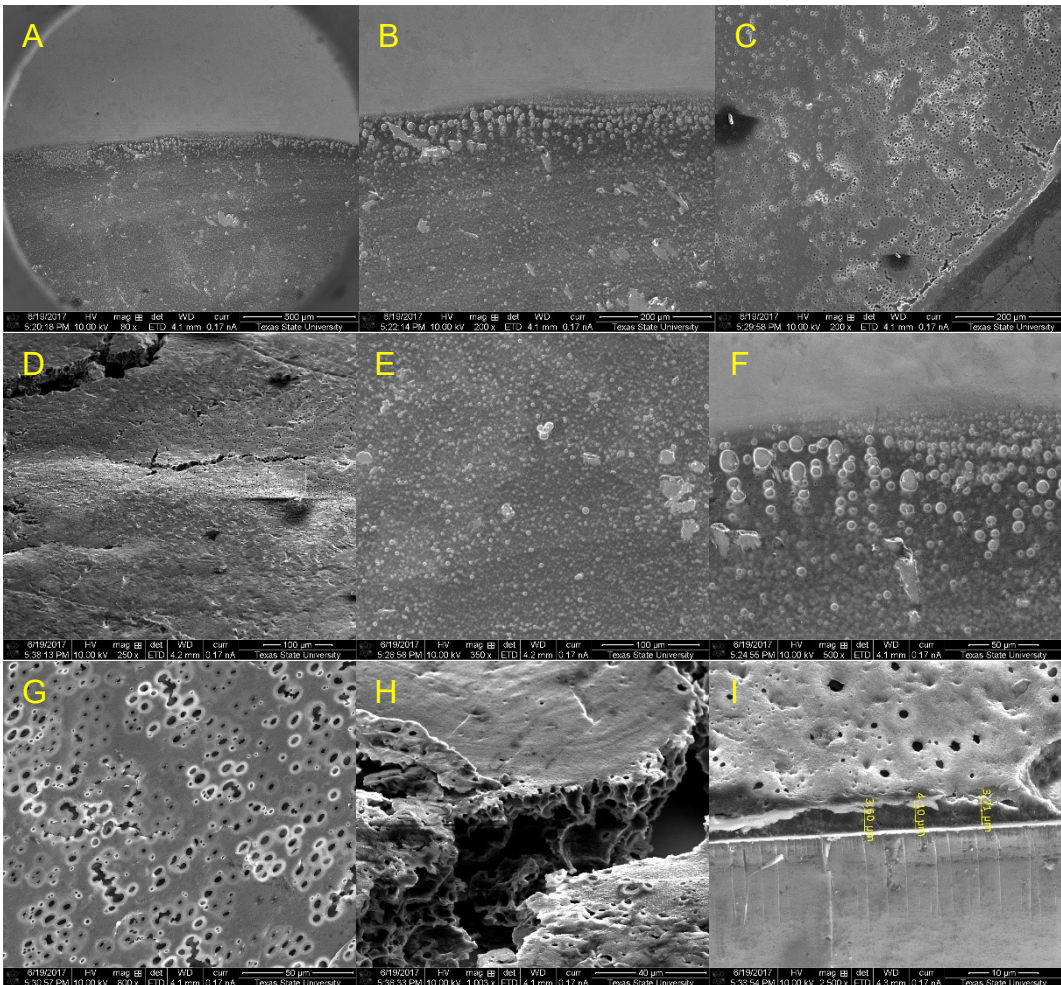
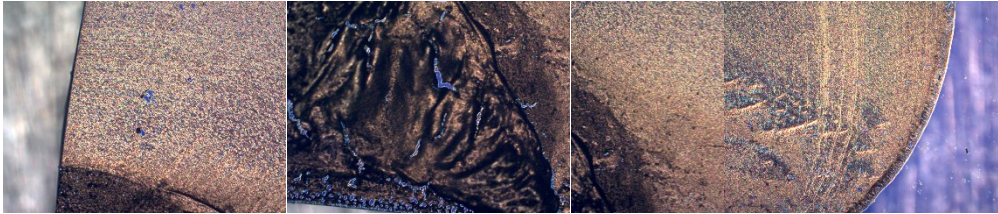
45% DMSO film

D.17 Optical images (top) presented with SEM images (bottom) of P3HT film templated with 45% DMSO using chlorobenzene as the solvent. (See following page)



55% DMSO film

D.18 Optical images (top) presented with SEM images (bottom) of P3HT film templated with 55% DMSO using chlorobenzene as the solvent.



## APPENDIX E: LINEAR REGRESSION DATA

E. Film type (with film number (#1-3) in parentheses) is presented with regression coefficient for that film. A coefficient close to unity implies proper film adhesion to ITO.

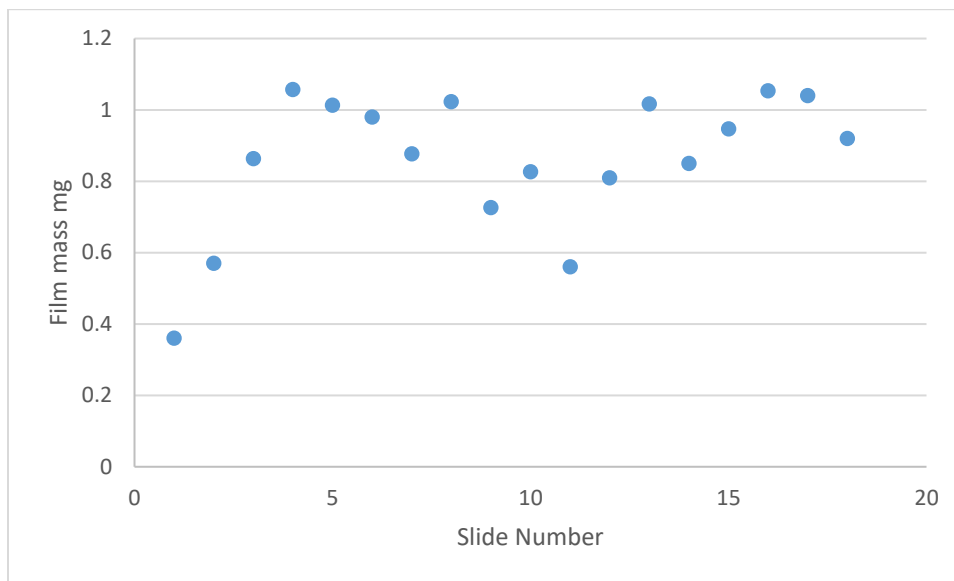
**Key:** Film = A/B/C: where A = polymer, B = solvent, C = percentage of porogen

Table 5: Linear Regression Data

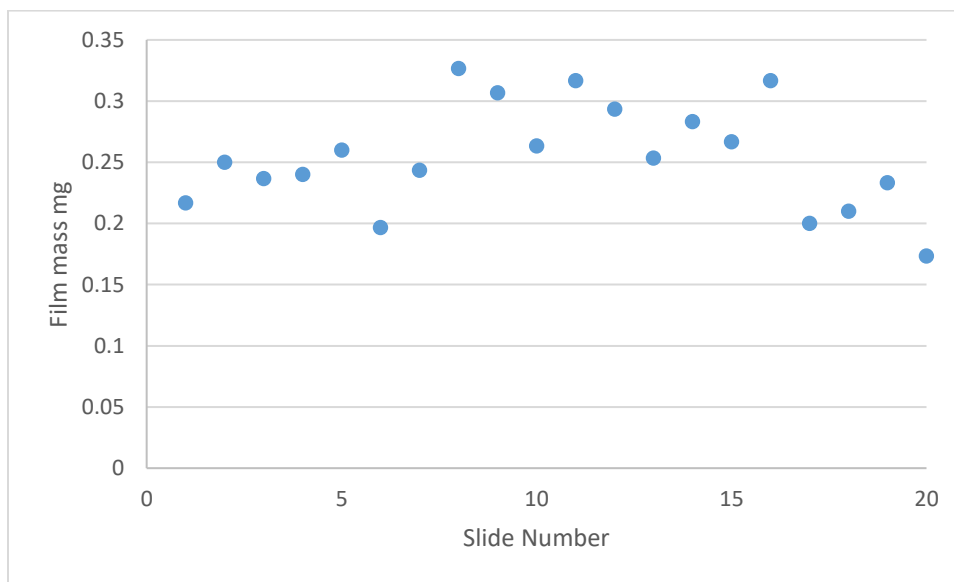
Film	poly(ProDOT-Bu <sub>2</sub> )/CHCl <sub>3</sub> (1)	poly(ProDOT-Bu <sub>2</sub> )/CHCl <sub>3</sub> (2)	poly(ProDOT-Bu <sub>2</sub> )/CHCl <sub>3</sub> /28% DMSO (1)	poly(ProDOT-Bu <sub>2</sub> )/CHCl <sub>3</sub> /28% DMSO (2)	poly(ProDOT-Bu <sub>2</sub> )/CHCl <sub>3</sub> /28% 1,4-dioxane (1)
r <sup>2</sup>	0.8774	0.9273	0.9984	0.9999	0.9874
Film	poly(ProDOT-Bu <sub>2</sub> )/CHCl <sub>3</sub> /28% 1,4-dioxane (2)	poly(ProDOT-Bu <sub>2</sub> )/CHCl <sub>3</sub> /28% ethanolamine (1)	poly(ProDOT-Bu <sub>2</sub> )/CHCl <sub>3</sub> /28% ethanolamine (2)	P3HT/CHCl <sub>3</sub> (1)	P3HT/CHCl <sub>3</sub> (2)
r <sup>2</sup>	0.9962	0.9866	0.9497	0.9985	0.9978
Film	P3HT/CHCl <sub>3</sub> (3)	P3HT/CHCl <sub>3</sub> /15% DMSO (1)	P3HT/CHCl <sub>3</sub> /15% DMSO (2)	P3HT/CHCl <sub>3</sub> /15% DMSO (3)	P3HT/CHCl <sub>3</sub> /25% DMSO (1)
r <sup>2</sup>	0.9988	0.9897	0.9936	0.9906	0.9934
Film	P3HT/CHCl <sub>3</sub> /25% DMSO (2)	P3HT/CHCl <sub>3</sub> /25% DMSO (3)	P3HT/CHCl <sub>3</sub> /32% DMSO (1)	P3HT/CHCl <sub>3</sub> /32% DMSO (2)	P3HT/CHCl <sub>3</sub> /32% DMSO (3)
r <sup>2</sup>	0.9988	0.9988	0.9989	0.9974	0.9968
Film	P3HT/CHCl <sub>3</sub> /38% DMSO (1)	P3HT/CHCl <sub>3</sub> /38% DMSO (2)	P3HT/CHCl <sub>3</sub> /38% DMSO (3)	P3HT/CHCl <sub>3</sub> /45% DMSO (1)	P3HT/CHCl <sub>3</sub> /45% DMSO (2)
r <sup>2</sup>	0.9955	0.9993	0.9956	0.9983	0.9995
Film	P3HT/CHCl <sub>3</sub> /45% DMSO (3)	P3HT/CHCl <sub>3</sub> /55% DMSO (1)	P3HT/CHCl <sub>3</sub> /55% DMSO (2)	P3HT/CB (1)	P3HT/CB (2)
r <sup>2</sup>	0.9984	0.9957	0.9972	0.9935	0.9983
Film	P3HT/CB (3)	P3HT/CB/15% DMSO (1)	P3HT/CB/15% DMSO (2)	P3HT/CB/15% DMSO (3)	P3HT/CB/25% DMSO (1)
r <sup>2</sup>	0.9903	0.9987	0.9978	0.9972	0.9984
Film	P3HT/CB/25% DMSO (2)	P3HT/CB/25% DMSO (3)	P3HT/CB/32% DMSO (1)	P3HT/CB/32% DMSO (2)	P3HT/CB/32% DMSO (3)
r <sup>2</sup>	0.9976	0.9950	0.9985	0.9988	0.9978
Film	P3HT/CB/38% DMSO (1)	P3HT/CB/38% DMSO (2)	P3HT/CB/38% DMSO (3)	P3HT/CB/45% DMSO (1)	P3HT/CB/45% DMSO (2)
r <sup>2</sup>	0.9964	0.9977	0.9957	0.9991	0.9978
Film	P3HT/CB/45% DMSO (3)	P3HT/CB/55% DMSO (1)	P3HT/CB/55% DMSO (2)	P3HT/CB/55% DMSO (3)	
r <sup>2</sup>	0.9431	0.9997	0.9989	0.9993	

## APPENDIX F: GRAVIMETRIC ANALYSIS DATA

### F.1 Mass data for templated poly(ProDOT-Bu<sub>2</sub>) films (chloroform as solvent)

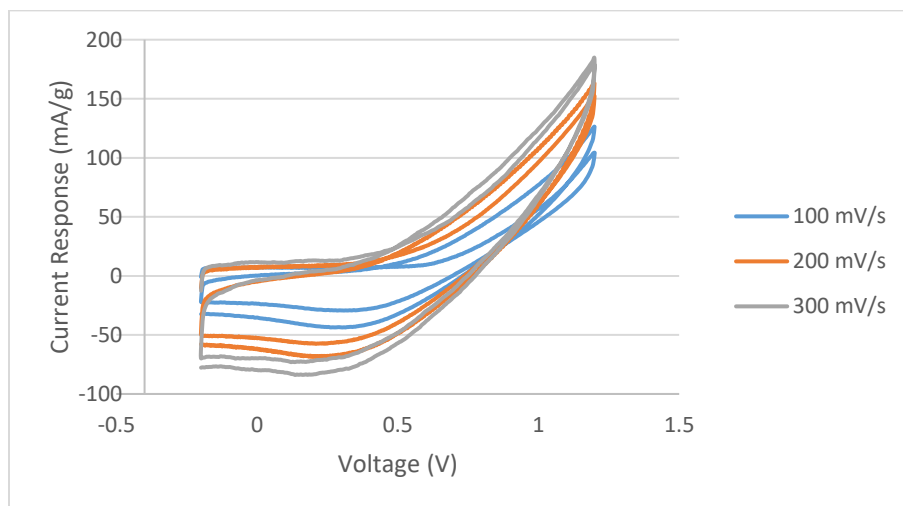


### F.2 Mass data for templated P3HT films (chloroform as solvent)

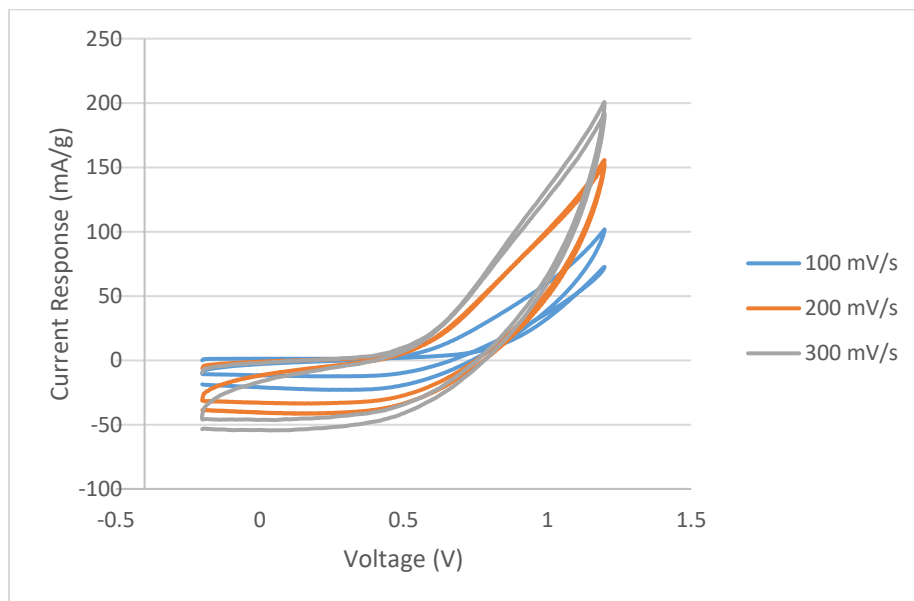


## APPENDIX G: POLY(PRODOT-BU<sub>2</sub>) EXPERIMENTAL CV DATA

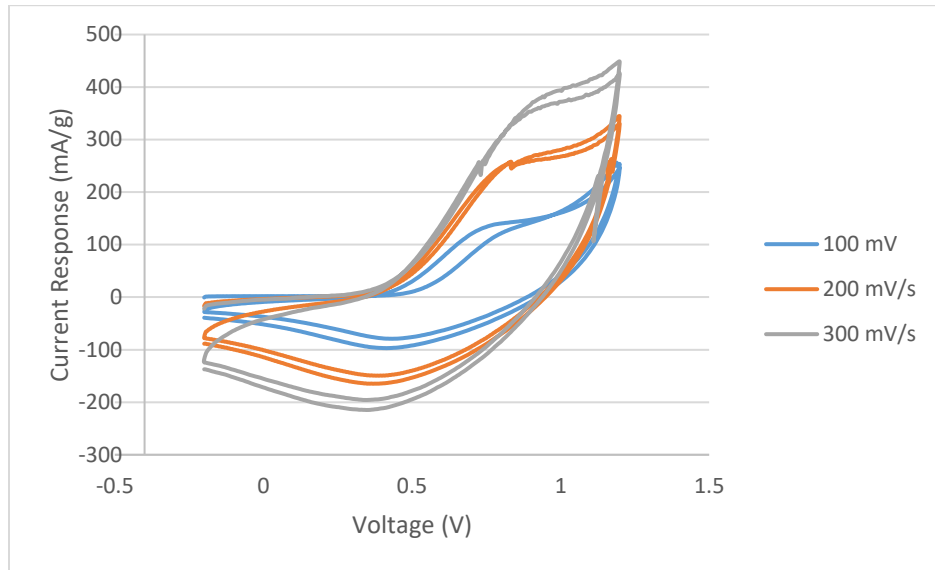
G.1 Control film CV data (poly(ProDOT-Bu<sub>2</sub>) film templated from chloroform solution with no porogen present.



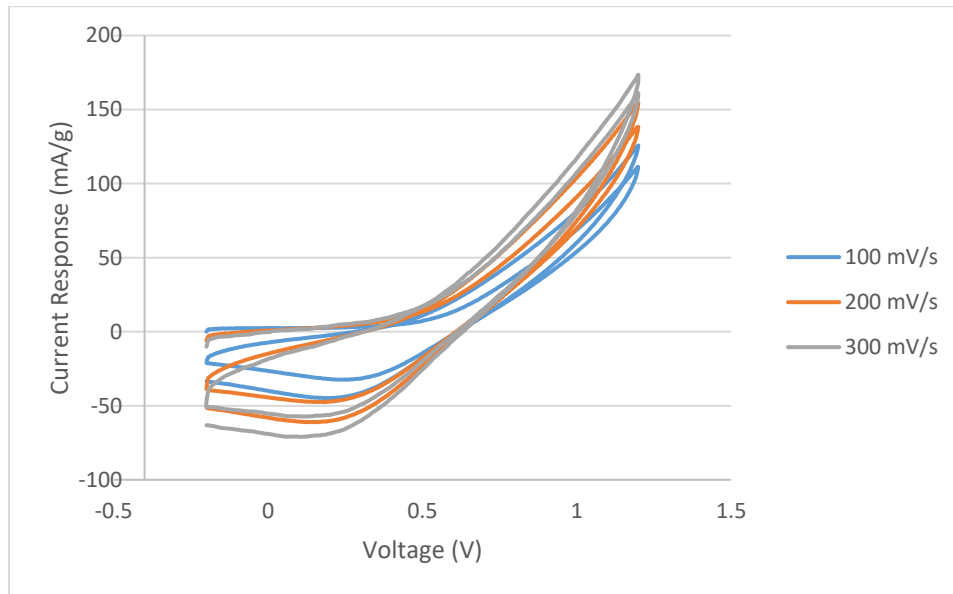
G.2 CV experimental data of poly(ProDOT-Bu<sub>2</sub>) film templated from chloroform solution with 28% 1,4-dioxane.



G.3 CV experimental data of poly(ProDOT-Bu<sub>2</sub>) film templated from chloroform solution with 28% DMSO.



G.4 CV experimental data of poly(ProDOT-Bu<sub>2</sub>) film templated from chloroform solution with 28% ethanolamine.



**APPENDIX H: NORMALIZED PEAK CURRENT RESPONSE DATA FOR P3HT**

**EXPERIMENTS**

H. Tabulated normalized current response data for two different solvent systems:

chloroform and chlorobenzene (0-55% DMSO as porogen)

Table 6: Normalized Peak Current Response Data for P3HT Experiments

Percentage DMSO	CHCl <sub>3</sub> Current Response Averages (mA/g)	Normalized Peak Current Response (mA/g)	Relative Standard Deviation (+/- %)	Chlorobenzene Current Response Averages (mA/g)	Normalized Peak Current Response (mA/g)	Relative Standard Deviation (+/- %)
0	992	1109.954	11	961	864.514	11
		902.640			938.922	
		962.916			1078.311	
15	1414	1173.583	24	1734	1707.165	5
		1262.308			1661.142	
		1806.712			1833.987	
25	1014	1137.082	27	1751	1749.192	0.2
		697.622			1748.667	
		1207.533			1754.041	
32	1319	1544.924	17	1723	1931.577	11
		1100.716			1591.414	
		1310.795			1645.337	
38	1244	1349.680	8	1950	2089.388	6
		1242.035			1892.871	
		1140.461			1868.336	
45	1218	941.905	20	1882	1576.237	16
		1323.65			1892.398	
		1389.714			2177.546	
55	1702	1476.729	19	1732	1617.098	9
		1926.635			1898.416	
					1680.889	

## REFERENCES

- 
- <sup>1</sup> Rasmussen, S. C. In *Electrically Conducting Plastics: Revising the History of Conjugated Organic Polymers*; American Chemical Society: 2011; Vol. 1080, pp 147-163
- <sup>2</sup> Nina; Hall Twenty-five years of conducting polymers. *Chem. Commun.* **2003**, 1-4
- <sup>3</sup> Deits, W.; Cukor, P.; Rubner, M.; Jopson, H. Stability and stabilization of polyacetylene, polyphenylacetylene, and acetylene/phenylacetylene copolymers. *Synthetic Metals* **1982**, *4*, 199-210
- <sup>4</sup> Zarras, P.; Irvin, J. In *Electrically Active Polymers*; John Wiley & Sons, Inc: 2002;
- <sup>5</sup> Asano, N.; Aoki, M.; Suzuki, S.; Miyatake, K.; Uchida, H.; Watanabe, M. Aliphatic/Aromatic Polyimide Ionomers as a Proton Conductive Membrane for Fuel Cell Applications. *J. Am. Chem. Soc.* **2006**, *128*, 1762-1769
- <sup>6</sup> Bhattacharyya, D.; Gleason, K. K. Single-Step Oxidative Chemical Vapor Deposition of -COOH Functional Conducting Copolymer and Immobilization of Biomolecule for Sensor Application. *Chem. Mater.* **2011**, *23*, 2600-2605
- <sup>7</sup> Wynne, K. J.; Street, G. B. Conducting polymers. A short review. *Ind. Eng. Chem. Prod. Res. Dev.* **1982**, *21*, 23-28
- <sup>8</sup> Bre´das J., L.; Marder, S. R.; Salaneck, W. R. Alan J. Heeger, Alan G. MacDiarmid, and Hideki Shirakawa. *Macromolecules* **2002**, *35*, 1137-1139
- <sup>9</sup> Van, d. W.; Chamorro, J.; Quintero, M.; Klausen, R. S. Opposites Attract: Organic Charge Transfer Salts. *J. Chem. Educ.* **2015**, *92*, 2134-2139
- <sup>10</sup> Zimmerman, H. E. Moebius-Hueckel concept in organic chemistry. Application of organic molecules and reactions. *Acc. Chem. Res.* **1971**, *4*, 272-280

- 
- <sup>11</sup> Beltrán, J. I.; Flores, F.; Martínez, J. I.; Ortega, J. Energy Level Alignment in Organic–Organic Heterojunctions: The TTF/TCNQ Interface. *J. Phys. Chem. C* **2013**, *117*, 3888-3894
- <sup>12</sup> Balian, R. In *Band Theory of Solids*; Yacobi, B. G., Ed.; Semiconductor Materials: An Introduction to Basic Principles; Springer US: Boston, MA, 2003; pp 33-58
- <sup>13</sup> Ren, F.; Zolper, J. C. *Wide Energy Bandgap Electronic Devices*; World Scientific: River Edge, N.J, 2003; , pp 485
- <sup>14</sup> Ruengsri, S.; Kaewkhao, J.; Limsuwan, P. Optical Characterization of Soda Lime Borosilicate Glass Doped with TiO<sub>2</sub>. *Procedia Engineering* **2012**, *32*, 772-779
- <sup>15</sup> Casiday, R.; Frey, R. Bonds, Bands, and Doping: How Do LEDs Work?  
<http://www.chemistry.wustl.edu/~edudev/LabTutorials/PeriodicProperties/MetalBonding/MetalBonding.html> (accessed 10/26/17)
- <sup>16</sup> Goodstein, D.; Goodstein, J. Richard Feynman and the History of Superconductivity. *Physics in Perspective* **2000**, *2*, 30-47
- <sup>17</sup> Rumble, J. R.; ed., Eds.; In *CRC Handbook of Chemistry and Physics, 98th Edition (Internet Version 2018)*; CRC Press/Taylor & Francis: Boca Raton, FL,
- <sup>18</sup> Bardeen, J.; Cooper, L. N.; Schrieffer, J. R. Theory of Superconductivity. *Phys. Rev.* **1957**, *108*, 1175-1204
- <sup>19</sup> Lebed, A. G. *The Physics of Organic Superconductors and Conductors*; Springer series in materials science; Springer: Berlin ; Heidelberg, 2008; Vol. 110, pp 3-16
- <sup>20</sup> Keller, H. J. *Low-Dimensional Cooperative Phenomena: The Possibility of High-Temperature Superconductivity*; Springer: New York, 1975;

- 
- <sup>21</sup> Coleman, L. B.; Cohen, M. J.; Sandman, D. J.; Yamagishi, F. G.; Garito, A. F.; Heeger, A. J. Superconducting fluctuations and the Peierls instability in an organic solid. *Solid State Communications* **1973**, *12*, 1125-1132
- <sup>22</sup> Eftekhari, A. *Nanostructured Conductive Polymers*; Wiley: 2011;
- <sup>23</sup> Hardinger, S. A. Conjugation. <http://www.chem.ucla.edu/~harding/IGOC/IGOC.html>
- <sup>24</sup> MacDiarmid, A. G. "Synthetic Metals": A Novel Role for Organic Polymers (Nobel Lecture). *Angewandte Chemie International Edition* **2001**, *40*, 2581-2590
- <sup>25</sup> Zigon, M. Conducting Polymers. *Chemistry International -- Newsmagazine for IUPAC* **2012**, *34*, 29-30
- <sup>26</sup> Irvin, J. Low oxidation potential electroactive polymers. University of Florida., **1998**
- <sup>27</sup> Yu, L.; Lu, Y. *Solitons and Polarons in Conducting Polymers*; Imperial College Press: Singapore, 1988;
- <sup>28</sup> Roncali, J.; Blanchard, P.; Frere, P. 3,4-Ethylenedioxythiophene (EDOT) as a versatile building block for advanced functional small pi]-conjugated systems. *J. Mater. Chem.* **2005**, *15*, 1589-1610
- <sup>29</sup> Dey, T.; Invernale, M. A.; Ding, Y.; Buyukmumcu, Z.; Sotzing, G. A. Poly(3,4-propylenedioxythiophene)s as a Single Platform for Full Color Realization. *Macromolecules* **2011**, *44*, 2415-2417
- <sup>30</sup> Ponder, J. F.; Pittelli, S. L.; Reynolds, J. R. Heteroatom Role in Polymeric Dioxyselenophene/Dioxythiophene Systems for Color and Redox Control. *ACS Macro Lett.* **2016**, *5*, 714-717

- 
- <sup>31</sup> Wei, Y.; Chan, C. C.; Tian, J.; Jang, G. W.; Hsueh, K. F. Electrochemical polymerization of thiophenes in the presence of bithiophene or terthiophene: kinetics and mechanism of the polymerization. *Chemistry of Materials* **1991**, *3*, 888-897
- <sup>32</sup> Sun, S. S.; Sariciftci, N. S. *Organic Photovoltaics: Mechanisms, Materials, and Devices*; CRC Press: 2005;
- <sup>33</sup> Roncali, J.; Blanchard, P.; Frere, P. 3,4-Ethylenedioxythiophene (EDOT) as a versatile building block for advanced functional small pi-conjugated systems. *J. Mater. Chem.* **2005**, *15*, 1589-1610
- <sup>34</sup> Dey, T.; Invernale, M. A.; Ding, Y.; Buyukmumcu, Z.; Sotzing, G. A. Poly(3,4-propylenedioxythiophene)s as a Single Platform for Full Color Realization. *Macromolecules* **2011**, *44*, 2415-2417
- <sup>35</sup> Mao, J.; Li, C.; Park, H. J.; Rouabhia, M.; Zhang, Z. Conductive Polymer Waving in Liquid Nitrogen. *ACS Nano* **2017**, *11*, 10409-10416
- <sup>36</sup> Wang, W.; Zhang, F.; Li, L.; Gao, M.; Hu, B. Improved Performance of Photomultiplication Polymer Photodetectors by Adjustment of P3HT Molecular Arrangement. *ACS Appl. Mater. Interfaces* **2015**, *7*, 22660-22668
- <sup>37</sup> Li, X.; Kang, Y.; Huang, M. Optimization of Polymerization Conditions of Furan with Aniline for Variable Conducting Polymers. *J. Comb. Chem.* **2006**, *8*, 670-678
- <sup>38</sup> Bronstein, H. A.; Luscombe, C. K. Externally Initiated Regioregular P3HT with Controlled Molecular Weight and Narrow Polydispersity. *J. Am. Chem. Soc.* **2009**, *131*, 12894-12895

- 
- <sup>39</sup> Chen, T.; Wu, X.; Rieke, R. D. Regiocontrolled Synthesis of Poly(3-alkylthiophenes) Mediated by Rieke Zinc: Their Characterization and Solid-State Properties. *J. Am. Chem. Soc.* **1995**, *117*, 233-244
- <sup>40</sup> Gutzler, R.; Perepichka, D. F.  $\pi$ -Electron Conjugation in Two Dimensions. *J. Am. Chem. Soc.* **2013**, *135*, 16585-16594
- <sup>41</sup> Kowalik, J.; Tolbert, L. M.; Narayan, S.; Abhiraman, A. S. Electrically Conducting Poly(undecylbithiophene)s. 1. Regioselective Synthesis and Primary Structure. *Macromolecules* **2001**, *34*, 5471-5479
- <sup>42</sup> Adachi, T.; Brazard, J.; Ono, R. J.; Hanson, B.; Traub, M. C.; Wu, Z.; Li, Z.; Bolinger, J. C.; Ganesan, V.; Bielawski, C. W.; Vanden Bout, D. A.; Barbara, P. F. Regioregularity and Single Polythiophene Chain Conformation. *J. Phys. Chem. Lett.* **2011**, *2*, 1400-1404
- <sup>43</sup> von Kieseritzky, F.; Allared, F.; Dahlstedt, E.; Hellberg, J. Simple one-step synthesis of 3,4-dimethoxythiophene and its conversion into 3,4-ethylenedioxythiophene (EDOT). *Tetrahedron Letters* **2004**, *45*, 6049-6050
- <sup>44</sup> Welsh, D. M.; Kumar, A.; Meijer, E. W.; Reynolds, J. R. Enhanced Contrast Ratios and Rapid Switching in Electrochromics Based on Poly(3,4-propylenedioxythiophene) Derivatives. *Adv Mater* **1999**, *11*, 1379-1382
- <sup>45</sup> Aiyar, A. R.; Hong, J.; Reichmanis, E. Regioregularity and Intrachain Ordering: Impact on the Nanostructure and Charge Transport in Two-Dimensional Assemblies of Poly(3-hexylthiophene). *Chem. Mater.* **2012**, *24*, 2845-2853
- <sup>46</sup> Poelking, C.; Andrienko, D. Effect of Polymorphism, Regioregularity and Paracrystallinity on Charge Transport in Poly(3-hexylthiophene) P3HT] Nanofibers. *Macromolecules* **2013**, *46*, 8941-8956

- 
- <sup>47</sup> Rasmussen, S. C.; Straw, B. D.; Hutchison, J. E. In *Tuning the Extent of Conjugation in Processable Polythiophenes Through Control of Side Chain Density and Regioregularity*; American Chemical Society: 1999; Vol. 735, pp 347-366
- <sup>48</sup> Gordon, M. P.; Lloyd, L. T.; Boucher, D. S. Poly(3-hexylthiophene) films prepared using binary solvent mixtures. *J. Polym. Sci. Part B: Polym. Phys.* **2015**, *54*, 624-638
- <sup>49</sup> Park, Y. D.; Lee, S. G.; Lee, H. S.; Kwak, D.; Lee, D. H.; Cho, K. Solubility-driven polythiophene nanowires and their electrical characteristics. *J. Mater. Chem.* **2011**, *21*, 2338-2343
- <sup>50</sup> Shen, X.; Hu, W.; Russell, T. P. Measuring the Degree of Crystallinity in Semicrystalline Regioregular Poly(3-hexylthiophene). *Macromolecules* **2016**, *49*, 4501-4509
- <sup>51</sup> Pascui, O. F.; Lohwasser, R.; Sommer, M.; Thelakkat, M.; Thurn-Albrecht, T.; Saalwächter, K. High Crystallinity and Nature of Crystal–Crystal Phase Transformations in Regioregular Poly(3-hexylthiophene). *Macromolecules* **2010**, *43*, 9401-9410
- <sup>52</sup> Kohn, P.; Huettner, S.; Komber, H.; Senkovskyy, V.; Tkachov, R.; Kiriya, A.; Friend, R. H.; Steiner, U.; Huck, W. T. S.; Sommer, J.; Sommer, M. On the Role of Single Regiodefects and Polydispersity in Regioregular Poly(3-hexylthiophene): Defect Distribution, Synthesis of Defect-Free Chains, and a Simple Model for the Determination of Crystallinity. *J. Am. Chem. Soc.* **2012**, *134*, 4790-4805
- <sup>53</sup> Panzer, F.; Sommer, M.; Bäessler, H.; Thelakkat, M.; Köhler, A. Spectroscopic Signature of Two Distinct H-Aggregate Species in Poly(3-hexylthiophene). *Macromolecules* **2015**, *48*, 1543-1553

- 
- <sup>54</sup> Chu, P.; Kleinhenz, N.; Persson, N.; McBride, M.; Hernandez, J. L.; Fu, B.; Zhang, G.; Reichmanis, E. Toward Precision Control of Nanofiber Orientation in Conjugated Polymer Thin Films: Impact on Charge Transport. *Chem. Mater.* **2016**, *28*, 9099-9109
- <sup>55</sup> Gao, Y.; Martin, T. P.; Thomas, A. K.; Grey, J. K. Resonance Raman Spectroscopic and Photocurrent Imaging of Polythiophene/Fullerene Solar Cells. *J. Phys. Chem. Lett.* **2010**, *1*, 178-182
- <sup>56</sup> Park, Y. D.; Lee, H. S.; Choi, Y. J.; Kwak, D.; Cho, J. H.; Lee, S.; Cho, K. Solubility-Induced Ordered Polythiophene Precursors for High-Performance Organic Thin-Film Transistors. *Adv. Funct. Mater.* **2009**, *19*, 1200-1206
- <sup>57</sup> Na, J. Y.; Kim, M.; Park, Y. D. Solution Processing with a Good Solvent Additive for Highly Reliable Organic Thin-Film Transistors. *J. Phys. Chem. C* **2017**, *121*, 13930-13937
- <sup>58</sup> Brandrup, J.; Burg, K. H.; Cherdron, H. In *Morphology of Polymers: Some Industrial Aspects*; American Chemical Society: 1981; Vol. 175, pp 289-306
- <sup>59</sup> Li, J.; Kleintschek, T.; Rieder, A.; Cheng, Y.; Baumbach, T.; Obst, U.; Schwartz, T.; Levkin, P. A. Hydrophobic Liquid-Infused Porous Polymer Surfaces for Antibacterial Applications. *ACS Appl. Mater. Interfaces* **2013**, *5*, 6704-6711
- <sup>60</sup> Lu, W.; Yuan, D.; Zhao, D.; Schilling, C. I.; Plietzsch, O.; Muller, T.; Bräse, S.; Guenther, J.; Blümel, J.; Krishna, R.; Li, Z.; Zhou, H. Porous Polymer Networks: Synthesis, Porosity, and Applications in Gas Storage/Separation. *Chem. Mater.* **2010**, *22*, 5964-5972
- <sup>61</sup> Zhang, Y.; Ionov, L. Actuating Porous Polyimide Films. *ACS Appl. Mater. Interfaces* **2014**, *6*, 10072-10077

- 
- <sup>62</sup> Tiemann, M. Repeated Templating. *Chem. Mater.* **2008**, *20*, 961-971
- <sup>63</sup> Thomas, A.; Goettmann, F.; Antonietti, M. Hard Templates for Soft Materials: Creating Nanostructured Organic Materials. *Chem. Mater.* **2008**, *20*, 738-755
- <sup>64</sup> Schuster, J.; Köhn, R.; Keilbach, A.; Döblinger, M.; Amenitsch, H.; Bein, T. Two-Dimensional-Hexagonal Periodic Mesoporous Polymer Resin Thin Films by Soft Templating. *Chem. Mater.* **2009**, *21*, 5754-5762
- <sup>65</sup> O'Neil, K. D.; Forristal, T. A.; Semenikhin, O. A. The effect of electropolymerization method on the nanoscale properties and redox behavior of poly[2,2'-bithiophene] thin film electrodes. *Electrochimica Acta* **2012**, *78*, 160-170
- <sup>66</sup> Heeger, A. J. Semiconducting and Metallic Polymers: The Fourth Generation of Polymeric Materials. *J Phys Chem B* **2001**, *105*, 8475-8491
- <sup>67</sup> Zhao, F.; Shi, Y.; Pan, L.; Yu, G. Multifunctional Nanostructured Conductive Polymer Gels: Synthesis, Properties, and Applications. *Acc. Chem. Res.* **2017**, *50*, 1734-1743
- <sup>68</sup> Shi, Y.; Yu, G. Designing Hierarchically Nanostructured Conductive Polymer Gels for Electrochemical Energy Storage and Conversion. *Chem. Mater.* **2016**, *28*, 2466-2477
- <sup>69</sup> Pernaut, J.; Reynolds, J. R. Use of Conducting Electroactive Polymers for Drug Delivery and Sensing of Bioactive Molecules. A Redox Chemistry Approach. *J Phys Chem B* **2000**, *104*, 4080-4090
- <sup>70</sup> Arns, C. H.; Knackstedt, M. A.; Roberts, A. P.; Pinczewski, V. W. Morphology, Cocontinuity, and Conductive Properties of Anisotropic Polymer Blends. *Macromolecules* **1999**, *32*, 5964-5966
- <sup>71</sup> Ionov, L. Polymeric Actuators. *Langmuir* **2015**, *31*, 5015-5024

- 
- <sup>72</sup> Pappenfus, T. M.; Hermanson, D. L.; Kohl, S. G.; Melby, J. H.; Thoma, L. M.; Carpenter, N. E.; da, S. F.; Bredas, J. Regiochemistry of Poly(3-hexylthiophene): Synthesis and Investigation of a Conducting Polymer. *J. Chem. Educ.* **2010**, *87*, 522-525
- <sup>73</sup> Bhatt, M. P.; Magurudeniya, H. D.; Sista, P.; Sheina, E. E.; Jeffries-EL, M.; Janesko, B. G.; McCullough, R. D.; Stefan, M. C. Role of the transition metal in Grignard metathesis polymerization (GRIM) of 3-hexylthiophene. *J. Mater. Chem. A* **2013**, *1*, 12841-12849
- <sup>74</sup> Zen, A.; Saphiannikova, M.; Neher, D.; Grenzer, J.; Grigorian, S.; Pietsch, U.; Asawapirom, U.; Janietz, S.; Scherf, U.; Lieberwirth, I.; Wegner, G. Effect of Molecular Weight on the Structure and Crystallinity of Poly(3-hexylthiophene). *Macromolecules* **2006**, *39*, 2162-2171
- <sup>75</sup> Mao, H.; Xu, B.; Holdcroft, S. Synthesis and structure-property relationships of regioirregular poly(3-hexylthiophenes). *Macromolecules* **1993**, *26*, 1163-1169
- <sup>76</sup> Jacobs, I. E.; Li, J.; Burg, S. L.; Bilsky, D. J.; Rotondo, B. T.; Augustine, M. P.; Stroeve, P.; Moulé, A. J. Reversible Optical Control of Conjugated Polymer Solubility with Sub-micrometer Resolution. *ACS Nano* **2015**, *9*, 1905-1912
- <sup>77</sup> Gao, J.; Niles, E. T.; Grey, J. K. Aggregates Promote Efficient Charge Transfer Doping of Poly(3-hexylthiophene). *J. Phys. Chem. Lett.* **2013**, *4*, 2953-2957
- <sup>78</sup> Fleming Ian; Trost Barry, M. In *2.3 Coupling Reactions between sp<sup>2</sup> Carbon Centers*; Comprehensive Organic Synthesis - Selectivity, Strategy and Efficiency in Modern Organic Chemistry, Volumes 1 - 9; Elsevier: 1991; pp 1

- 
- <sup>79</sup> Loewe, R. S.; Ewbank, P. C.; Liu, J.; Zhai, L.; McCullough, R. D. Regioregular, Head-to-Tail Coupled Poly(3-alkylthiophenes) Made Easy by the GRIM Method: Investigation of the Reaction and the Origin of Regioselectivity. *Macromolecules* **2001**, *34*, 4324-4333
- <sup>80</sup> Atwood, J. D.; Wovkulich, M. J.; Sonnenberger, D. C. Ligand effects on organometallic substitution reactions. *Acc. Chem. Res.* **1983**, *16*, 350-355
- <sup>81</sup> Tamba, S.; Fuji, K.; Nakamura, K.; Mori, A. Nickel(II)-Catalyzed Cross-Coupling Polycondensation of Thiophenes via C–S Bond Cleavage. *Organometallics* **2014**, *33*, 12-15
- <sup>82</sup> Loewe, R. S.; Khersonsky, S. M.; McCullough, R. D. A Simple Method to Prepare Head-to-Tail Coupled, Regioregular Poly(3-alkylthiophenes) Using Grignard Metathesis. *Adv Mater* **1999**, *11*, 250-253
- <sup>83</sup> Welsh, D. M.; Kloeppner, L. J.; Madrigal, L.; Pinto, M. R.; Thompson, B. C.; Schanze, K. S.; Abboud, K. A.; Powell, D.; Reynolds, J. R. Regiosymmetric Dibutyl-Substituted Poly(3,4-propylenedioxythiophene)s as Highly Electron-Rich Electroactive and Luminescent Polymers. *Macromolecules* **2002**, *35*, 6517-6525
- <sup>84</sup> Wei, H.; Scudiero, L.; Eilers, H. Infrared and photoelectron spectroscopy study of vapor phase deposited poly (3-hexylthiophene). *Applied Surface Science* **2009**, *255*, 8593-8597
- <sup>85</sup> Roesing, M.; Howell, J.; Boucher, D. Solubility characteristics of poly(3-hexylthiophene). *J. Polym. Sci. Part B: Polym. Phys.* **2017**, *55*, 1075-1087
- <sup>86</sup> Xu, S Pd- and Ni-catalyzed cross-coupling reactions in the synthesis of organic electronic materials. *Science and Technology of Advanced Materials* **2014**, *15*, 044201

- 
- <sup>87</sup> D'Arcy, J. M.; Tran, H. D.; Tung, V. C.; Tucker-Schwartz, A.; Wong, R. P.; Yang, Y.; Kaner, R. B. Versatile solution for growing thin films of conducting polymers. *Proceedings of the National Academy of Sciences* **2010**, *107*, 19673-19678
- <sup>88</sup> Crossland, E. J. W.; Rahimi, K.; Reiter, G.; Steiner, U.; Ludwigs, S. Systematic Control of Nucleation Density in Poly(3-Hexylthiophene) Thin Films. *Adv. Funct. Mater.* **2011**, *21*, 518-524
- <sup>89</sup> Pringle, J. M.; Efthimiadis, J.; Howlett, P. C.; Efthimiadis, J.; MacFarlane, D. R.; Chaplin, A. B.; Hall, S. B.; Officer, D. L.; Wallace, G. G.; Forsyth, M. Electrochemical synthesis of polypyrrole in ionic liquids. *Polymer* **2004**, *45*, 1447-1453
- <sup>90</sup> Irvin, D. J.; Stenger-Smith, J.; Yandek, G. R.; Carberry, J. R.; Currie, D. A.; Theodoropoulou, N.; Irvin, J. A. Enhanced electrochemical response of solution-deposited n-doping polymer via cocasting with ionic liquid. *J. Polym. Sci. B Polym. Phys.* **2012**, *50*, 1145-1150
- <sup>91</sup> BATES, F. S. Polymer-Polymer Phase Behavior. *Science* **1991**, *251*, 898
- <sup>92</sup> Anonymous Application Notes Delta Technologies. <http://www.deltatechnologies.com/downloads/applicationnotes.pdf?C=8>
- <sup>93</sup> Biswas, N.; Datta, A. "Coffee-ring" Patterns of Polymer Droplets; 2013; Vol. 1512
- <sup>94</sup> Damman, C Poulard and P Control of spreading and drying of a polymer solution from Marangoni flows. *EPL (Europhysics Letters)* **2007**, *80*, 64001
- <sup>95</sup> Caddeo, C.; Mattoni, A. Atomistic Investigation of the Solubility of 3-Alkylthiophene Polymers in Tetrahydrofuran Solvent. *Macromolecules* **2013**, *46*, 8003-8008
- <sup>96</sup> Biswas, N.; Datta, A. "Coffee-ring" Patterns of Polymer Droplets; 2013; Vol. 1512

- 
- <sup>97</sup> Gupta, S. K.; Jindal, R.; Garg, A. Microscopic Investigations into the Effect of Surface Treatment of Cathode and Electron Transport Layer on the Performance of Inverted Organic Solar Cells. *ACS Appl. Mater. Interfaces* **2015**, *7*, 16418-16427
- <sup>98</sup> Allain, L Pauchard and C Buckling instability induced by polymer solution drying. *EPL (Europhysics Letters)* **2003**, *62*, 897
- <sup>99</sup> Mackay, D. *Handbook of Physical-Chemical Properties and Environmental Fate for Organic Chemicals*; CRC Press: Boca Raton, FL, 2006
- <sup>100</sup> Eales, A. D.; Routh, A. F.; Dartnell, N.; Simon, G. Evaporation of pinned droplets containing polymer – an examination of the important groups controlling final shape. *AIChE J.* **2015**, *61*, 1759-1767
- <sup>101</sup> Gileadi, E. *Electrode kinetics for chemists, chemical engineers, and materials scientists*; VCH: New York, NY, 1993
- <sup>102</sup> Scharsich, C.; Lohwasser, R. H.; Sommer, M.; Asawapirom, U.; Scherf, U.; Thelakkat, M.; Neher, D.; Köhler, A. Control of aggregate formation in poly(3-hexylthiophene) by solvent, molecular weight, and synthetic method. *J. Polym. Sci. B Polym. Phys.* **2012**, *50*, 442-453